Dissertation

Zum Erwerb des Doctor of Philosophy

(Ph.D.)

an der Medizinischen Fakultät der

Ludwig-Maximilians-Universität zu München

An *in vivo* inflammatory loop potentiates KRAS blockade

vorgelegt von

Kristina Anna Maria Arendt

aus München, Deutschland

eingereicht 2019

verteidigt 2020

Kristina Anna Maria Arendt
CPC Munich

Helmholtz Center Munich
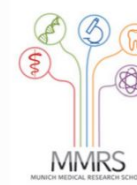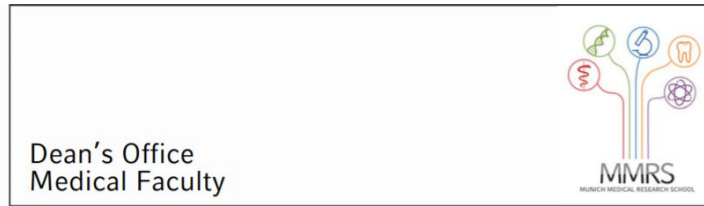

München

2019

<u>Erklärung</u>

Diese Dissertation wurde im Sinne von § 7 der Promotionsordnung vom 28. November 2011 von Herrn

Prof. Dr. Georgios Stathopoulos betreut.

1. Gutachter: Prof. Dr. med. Rudolf Hatz

2. Gutachter: PD Dr. med. Sebastian Kobold

Dissertation eingereicht am   23.08.2019

Mündliche Prüfung am   19.05.2020

Affidavit

Arendt, Kristina Anna Maria
Surname, first name

Max-Lebsche-Platz 31, 81377 Munich
Address

Germany
Country

I hereby declare, that the submitted thesis entitled

"An in vivo inflammatory loop potentiates KRAS blockade"

is my own work. I have only used the sources indicated and have not made unauthorized use of services of a third party. Where the work of others has been quoted or reproduced, the source is always given.

I further declare that the submitted thesis or parts thereof have not been presented as part of an examination degree to any other university.

Munich, 25.5.2020   Kristina Anna Maria Arendt

Place, Date   Signature doctoral candidate

LUDWIG-
MAXIMILIANS-
UNIVERSITÄT
MÜNCHEN

Dean's Office
Medical Faculty

MMRS
MUNICH MEDICAL RESEARCH SCHOOL

Confirmation of congruency between printed and electronic version of

the doctoral thesis

Doctoral Candidate: Kristina Anna Maria Arendt

Address: Max-Lebsche-Platz 31, 81377 Munich

I hereby declare that the electronic version of the submitted thesis, entitled

"An in vivo inflammatory loop potentiates KRAS blockade"

is congruent with the printed version both in content and format.

Munich, 25.5.2020   Kristina Anna Maria Arendt

Place, Date   Signature doctoral candidate

"Everything is going to be fine in the end. If it's not fine, it's not the end."

Oscar Wilde

Table of Contents

1. Summary

Inhibitors targeting *KRAS* proto-oncogene GTPase do not compare favorably with other drugs and have so far failed in clinical trials. Based on these facts, KRAS is seen as undruggable. However, with a mutation incidence of 30-40% of all human cancers, KRAS is still considered an attractive pan-cancer target. To shed light on this major clinical problem, we treated a panel of murine and human tumor cells with KRAS drugs deltarasin (inhibiting transport protein phosphodiesterase-δ), cysmethynil (inhibiting isoprenylcysteine carboxylmethyltransferase), and AA12 (allosterically inhibiting mutant KRAS^{G12C} isoform). Additionally, we overexpressed or silenced mutant KRAS using gene modification techniques. We show an exclusively *in vivo* effect of *Kras/KRAS* mutant cancer cells to genetic and pharmacologic KRAS blockade. We demonstrate that the hyperactive GTPase uses host myeloid cells via a C-C motif chemokine ligand 2 (CCL2)/ interleukin-1β (IL-1β)-mediated signaling loop for constant tumorigenicity. Certainly, tumors harboring mutated *Kras/KRAS* did respond less to daily deltarasin treatment in *Ccr2* and *Il1b* gene-deficient mice while being drug-sensitive in wild-type (WT) mice. Similar findings were achieved with adoptive bone marrow transplant (BMT) experiments of *Ccr2*-deficient mice receiving WT bone marrow. Deltarasin treatment suppressed interleukin-1 receptor 1 (IL1R1) expression and myeloid IL-1β-initiated pro-growth effects *in vivo*. With this we provide a novel mechanism of how mutant KRAS functions to promote tumorigenesis beyond the confines of the cancer cell. Our murine KRAS dependent pro-inflammatory gene expression signature showed strong parallels with *KRAS* mutant human cancers and predicted poor survival. This work highlights the possibility that CCL2 and IL-1β, as well as their respective receptors are important targets to consider in the search for treating *KRAS* mutant cancer patients. In particular, IL-1β blockade can be a strategy suitable for this therapy which might provide mechanistic insights on recent findings on IL-1β blockade and lung cancer incidence in the CANTOS (Canakinumab anti-inflammatory thrombosis outcome study) trial. In addition, the findings imply that traditional methods employed for drug screens are inaccurate for the development of anti-KRAS compound screens since the essential drug function needs to address the inflammatory tumor microenvironment. This is in line with others, believing in a discrepancy between *in vitro* and *in vivo* findings related to *KRAS* inhibition.

2. Zusammenfassung

KRAS (Proto-Oncogene GTPase) ist eines der häufigsten Onkogene und kommt in soliden Tumoren vor, allen voran Pankreas-, Darm- und Lungenkrebs. Obwohl es eine extrem wichtige Stellung hat, gibt es noch keine zielgerichteten Therapeutika. Bis jetzt stellt die Mutation maximal einen indirekten Angriffspunkt für Medikamente dar und einen Biomarker für Primär- und Sekundärresistenzen von klinischen EGFR-Inhibitoren. Eine Vielzahl von Versuchen wurde unternommen, um KRAS Inhibitoren zu entwickeln, teilweise auch in klinischen Studien, ohne Erfolg. Um dieses medizinische Problem besser zu verstehen, wurden hier *in vitro* und *in vivo* Versuche in humanen und murinen Zelllinien mit den KRAS Inhibitoren Deltarasin, Cysmethynil und AA12 verglichen und entscheidende Unterschiede festgestellt. Diese zeigten uns, dass deren Wirkung *in vitro* unabhängig von dem Vorliegen der Mutation eintritt. Im Vergleich dazu zeigte der KRAS Inhibitor Deltarasin in Mausmodellen eine spezifisch wirksame Verlangsamung des Tumorwachstums. Das Gleiche wurde parallel an genetisch veränderten Zelllinien durchgeführt mit entsprechendem Ergebnis. Im weiteren Verlauf konnten wir diese Unterschiede einer KRAS regulierten Immunantwort zuordnen, bei der CCR2+ myeloide Zellen durch C-C Motif Chemokine Ligand 2 (CCL2) - Sekretion rekrutiert werden und diese Interleukin-1β (IL-1β) ausschütten. Die Interleukin-Sekretion bewirkt ein aggressiveres Wachstum KRAS mutierter Tumore. Diese Signalkaskade konnte mit geeigneten Knockout- sowie Knochenmark-Transplantations- Mausmodellen bewiesen werden. Der KRAS Inhibitor Deltarasin greift in diesen Mechanismus ein. Wir konnten zeigen, dass der Wirkstoff die Expression von IL-1R1 minimiert. Durch Transkriptomanalyse filterten wir eine *Kras*-spezifische Liste von Genen heraus, die inflammatorische Mediatoren enthält, unter anderem *Il1r1* und *Ccl2*. Diese Daten spielten auch im humanen, molekularen Krankheitsprofil eine Rolle. So präsentiert diese Arbeit innovative, klinisch relevante Angriffspunkte für die Behandlung von Lungenkrebs mit vorliegender *KRAS* Mutation: Die Mediatoren CCL2 und IL-1β, sowie deren Rezeptoren. Außerdem wird deutlich, dass konservative Screening-Methoden nicht das Mittel der Wahl sind, um KRAS Inhibitoren zu entwickeln, da die Immunantwort dabei außer Acht gelassen wird.

3. Introduction

3.1 Lung cancer – an overview

3.1.1 Epidemiology

Cancer is the second reason for death nowadays behind cardiovascular diseases (Fig. 1A). Lung cancer (LC) is the global number one occurring cancer type with increasing incidence rates and an estimation of 2.09 Mio new cases in 2018[1]. It is also the leading cause of cancer related deaths gender independent and worldwide (Fig. 1B)[1,2]. A geographical difference is evident depending on smoking habits, indoor and outdoor air pollution, tobacco taxes, and anti-smoking policies of countries like USA or Europe in contrast to China and Asia. In South Africa, price per package had quadrupled over ten years and consumption thereby has halved[3]. On the other side, China with increasing smoker numbers, consuming one-third of all cigarettes smoked globally and with China the world's main tobacco producer[1]. This will increase in the next years and visualizes a shift in the worldwide lung cancer burden from high-income to low- and middle-income countries, predominantly Asia[4]. General incidence and mortality rates are still similar (Fig. 1B) since early diagnosis is not given yet and therapy options are limited. Men have a higher risk of developing lung cancer then women (Fig. 1B). Main risk factor is smoking being the reason for over 90% of new lung cancer cases. This includes exposure to passive cigarette smoking. Other harmful factors are agents like asbestos, arsenic, nickel, and chromium, radiation, and outdoor and indoor air pollution[5]. The presence of other lung disorders are affecting the incidence rate of lung cancer as well, such as fibrotic disorders or COPD[1,2].
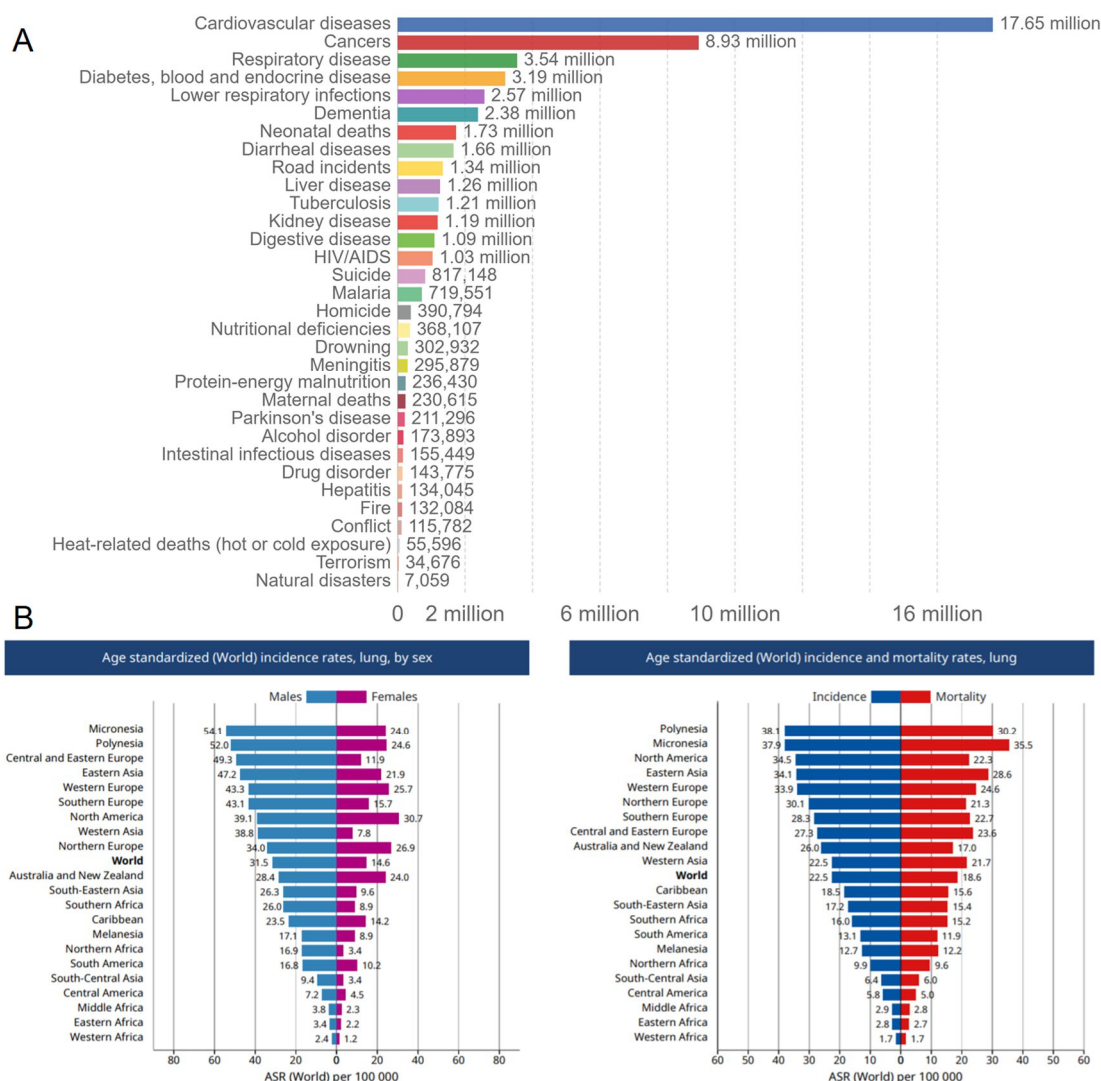
Figure 1: Incidence and mortality of diseases and lung cancer. (A) Worldwide causes of death, 2016. Figure produced based on numbers of the global burden of disease (GBD) database and available online at: https://ourworldindata.org/causes-of-death. Last accessed July 26, 2019. (B) Worldwide lung cancer incidence and mortality stratified by sex. Figure from GLOBOCAN made by the International Agency for Research on Cancer (IARC) for 2018. Online available at: http://gco.iarc.fr/today/data/factsheets/cancers/15-Lung-fact-sheet.pdf. Last accessed July 26, 2019.

3.1.2   Histology and mutational landscape

LC is classified according to the world health organization (WHO) into two main types, 15% of all cases are small cell lung carcinoma (SCLC) and non-SCLC (NSCLC) accounting for the rest (85%). NSCLC can be subdivided into aggressive large cell carcinoma (15%), squamous cell carcinoma (30%), and lung adenocarcinoma (LADC; 40%) making LADC the most

common type. It is further divided depending on invasiveness, in detail i*n situ* as preinvasive tumor, minimal invasive adenocarcinoma, lepidic predominant adenocarcinoma, or invasive adenocarcinoma classified by size. LADC appears often in the cells lining the alveoli, while squamous cell carcinoma appears in the flat cells of the airways near the bronchi. In 2015 the WHO established a new category of invasive, neuroendocrine tumors comprising three subtypes: large cell neuroendocrine carcinoma (LCNEC), SCLC, and typical or atypical carcinoid tumor[6].

The Cancer Genome Atlas (TCGA) is working on identification of genomic and molecular alterations for different types of cancer. For LADC a high mutation burden is proven [8.9 mutations per one million nucleotides (one megabase, Mb)] and common mutations are: TP53 (46%), KRAS (33%), STK11 (17%), KEAP1 (17%), EGFR (14%), NF1 (11%), BRAF (10%), ARID1A (7%), MET (7%), PIK3CA (7%), SMARCA4 (6%), and CDKN2A (4%, see full gene names under 9. abbreviations)[7]. Epidermal growth factor receptor (EGFR), B-Raf proto-oncogene (BRAF), the rare anaplastic lymphoma kinase (ALK; 1.3%), and ROS proto-oncogene (ROS1) fusions (1.7%) are clinically used biomarkers. EGFR and KRAS proto-oncogene GTPase (KRAS) mutations are mutually exclusive, but serine/threonine kinase 11 (STK11) or tumor protein P53 (TP53) mutations are positively correlated with mutations in KRAS[8]. Moreover, 75% of LADC genetic alterations promote the RTK/RAS/RAF signaling pathway, due to driver mutations promoting this signaling pathway. These include KRAS, EGFR, and BRAF. Driver mutations are crucial for initiation and progression of tumor growth, same in all patients of a specific cancer, and support the cell with a clonal selective advantage. Passenger mutations are more random and occur often through drug resistance development, but mainly prior to the driver mutation. They can also transform into drivers, then called latent driver mutations[9]. Both loss-of-function mutations in tumorsupressors and gain-of-function mutations in oncogenes work together to change the normal growth of cells to an abnormal pathological network effecting cell proliferation, cell cycle, repair mechanisms, control of transcription and protein expression, etc. (Fig. 2)[7].
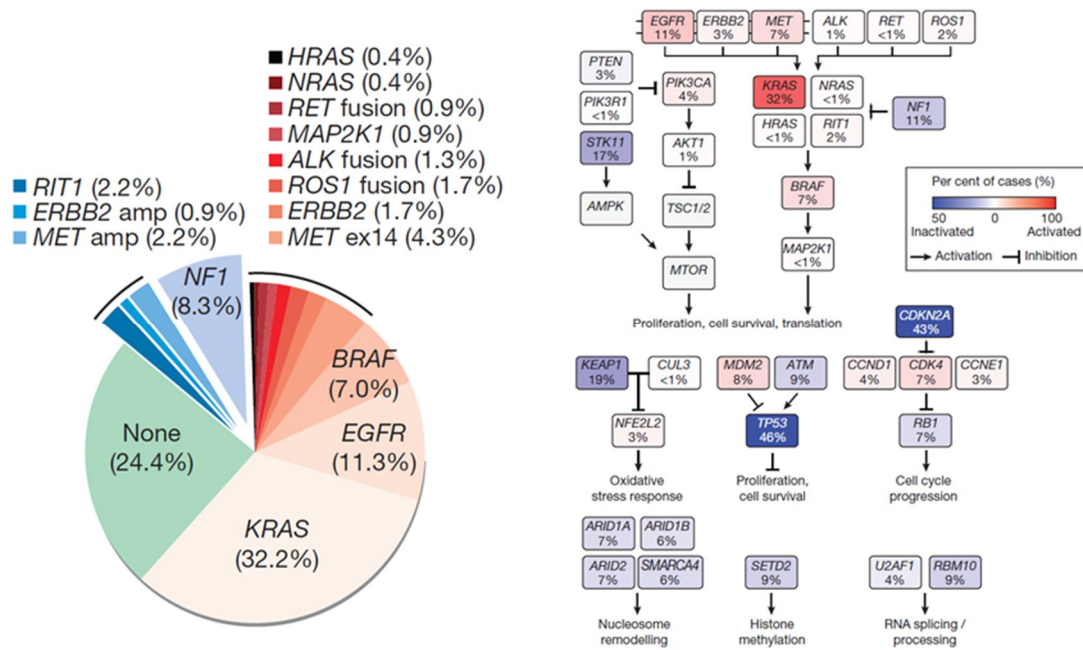
Figure 2: The cancer genome atlas research network (TCGA) analyzed the molecular profile of lung tumor and matched healthy tissue of 230 lung cancer patients. (Left) Main driver mutations are found to be involved in RTK/RAS/RAF signaling to 75%. (Right) Main tumorsupressors (blue) and oncogenes (red) of LADC are involved in variant signaling pathways such as proliferation, cell survival, cell cycle progression, oxidative stress response, and nucleosome remodeling. Figures from TCGA publication 2014 analyzing 230 LADC patient samples on DNA, RNA, and protein level[7].

3.1.3 Current staging and treatment

General age of diagnosis is 68 to 70 years and usually too late, since early diagnosis via computer-tomography (CT) is no routine yet and could help especially the at-risk group of smokers. Nowadays patient groups will be classified by multiple variants like genotype, age, sex, histology, stage, comorbidity, and fitness. Therapy options depend on progression of cancer and are surgery, chemotherapy, radiation, and targeted therapy. The latter improved therapy in the last years, especially with identification of biomarkers, and the use of immune checkpoint- and kinase- inhibitors[10].

Lung cancer is classified via TNM staging, T for primary tumor extent, N for involvement of lymph nodes, and M for metastasis. Tumors will be detected via CT, while N and M staging is done via CT and PET-CT (positron emission tomography). T is subclassified in $T_0 - T_4$,

dependent on tumor size and invasiveness. T_{is} is defined as carcinoma *in situ*, is a non-invasive tumor in early development and can be fully resected. N_1-N_3 staging is done dependent on locality of cancer cells in lymph nodes. M staging is from M_0-M_{1c} and classifies the existence of metastasis and if they are regional or extra thoracic[11].

Treatment possibilities are dependent on the staging. Surgery will be done in early stages and tumor sizes < 4 cm. The 5-year survival rate is then between 75 – 80%. In patients with more advanced primary tumor surgery is followed by adjuvant chemotherapy or irradiation. If the tumor size limits the success of surgery a preoperative neoadjuvant chemotherapy (e.g., Cisplatin) can be a choice. When metastases are present in lymph nodes survival rates and treatment options are strongly dependent on localization and number of lymph node metastasis, but will be a combination of irradiation, chemotherapy, and surgery. Patients with multiple metastasis will be treated palliative. Positive results are also achieved with targeted therapy, with which survival can be prolonged for years in patients with advanced NSCLC[12]. This possibility is achieved by tremendous efforts to generate genetic profiles of the disease, like The Cancer Genome Atlas (TCGA) is doing[7]. Since now, common drug targets are ALK translocation (e.g., Alectinib), ROS1 translocation (e.g., Crizotinib), EGFR (e.g., Osimertinib for exon 19 deletion, L858R, T790M, and other mutations), and BRAF V600E mutations (e.g., Dabrafenib)[13,14]. Targeted therapy has the advantage of less side effects, oral application, and better life quality for the patient. Often secondary resistance appears in the first months of treatment and the drug needs to be changed, so is the T790M mutation the most common secondary resistance mutation in patients with an EGFR abnormality[14]. Besides tremendous efforts, the most commonly mutated oncogene in lung adenocarcinoma, KRAS is still a not druggable target[15]. In case of no detection of targets in the genetic profile of the lung tumor such as ROS-1, ALK, or EGFR and in higher progressed stages, patients can be given immune checkpoint inhibitors, such as against Programmed Cell Death-Ligand 1 (PD-L1). The treatment is based on manipulation of the tumor-host interaction. When T-cell are recruited in an area of inflammation or cancer growth, they secrete interferon-γ, which stimulates the

production of PD-L1 by tumor cells. The subsequent binding of the ligand to its receptor PD-1 on the surface of T-cells leads to T-cell death, thereby stopping the immune response against the tumor. If PD-L1 is expressed in > 50% tumor cells, a monotherapy with PD-L1 inhibitor (e.g., Nivolumab, Pembrolizumab) can be started. By antagonizing the PD-1 receptor, the suppression of the immune attack can be prevented, and tumor cells can be recognized and cleared[16].

3.2 The KRAS oncogene

3.2.1 The oncogenic RAS family

The family of rat sarcoma (RAS) proto-oncogenes includes three members (*HRAS, KRAS*, and *NRAS*) encoding 4 proteins: HRAS, KRAS4A, KRAS4B, and NRAS, sharing 80 – 90% sequence identity[15]. The KRAS isoform is one of the most common mutated oncogenes in human cancers and related to poor prognosis[17]. All forms play a central role in various human cancers. They first were identified 1964 (KRAS) and 1967 (HRAS) in viruses being responsible for the malignant changes in bladder and lung carcinoma cells, later their human homologs were discovered and with this their importance in cancer biology. KRAS and HRAS were named after their ability to cause sarcomas in rat, adding their discovers names Kirsten and Harvey. First, they were understood as virus proteins, causing the transformation of a normal gene into an oncogene. Ten years later the human cellular counterparts were found for HRAS and KRAS. NRAS was discovered 1983 in the DNA of a neuroblastoma patient sample and named thereafter[18].

Figure 3: HRAS NRAS, and KRAS share 90% homolog sequence and only differ in the HVR (hypervariable region). Within the G domain lies the binding motif for GTP/GDP binding (switch I/II). Location of most common point mutation are in the G domain and highlighted as stars. In the HVR is the CAAX motif important for posttranslational modification and transportation. CAAX- tetrapeptide motif, cysteine, aliphatic residue, and X for any amino acid. Figure from Ryan *et al*.[19].

The 21 kD small GTPase proteins, attached at the cell membrane, translate extracellular signals, such as EGFR activation, to intracellular signaling cascades and beyond. G-proteins use an on or off conformation regulated by nucleotide binding via Switch I and II domains (Fig. 3), with the GTP-bound form as active signaling state[15,17]. Receptor tyrosine kinases (RTK) such as epidermal growth factor receptor (EGFR) bind extracellular signals and undergo intracellular autophosphorylation, thereby recruiting adapter protein complex GRB2 (growth factor receptor bound 2) and SOS (son of sevenless, GEF protein), in that way binding RAS proteins (Fig. 4)[20]. The GTP to GDP hydrolysis is catalyzed by GTPase-activating proteins (GAP) like neurofibromin-1 (NF1), while guanine nucleotide exchange factors (GEF) direct GTP dissociation and new binding of GTP will follow due to its high cellular concentration[21]. Before Kras4B and other RAS isoforms become active, they perform multiple posttranslational modification steps (Fig. 4). First, a farnesyl group (F) is added to the carboxy terminus (CAAX tetrapeptide motif, cysteine, aliphatic residue, and X any amino acid) by farnesyltransferase enzymes. As a second step, the AAX tetrapeptide termini of the prenylated RAS is cleaved by the protease RCE1 (Ras-converting enzyme 1), leaving only a cysteine residue. This will be carboxymethylated (M) by isoprenylcysteine carboxylmethyltransferase (ICMT) and finally KRAS4B is integrated into the cell membrane by adding lysine residues and being transported

by phosphodiesterase δ (PDEδ). The other RAS isoforms get palmitoylated at the SH group of the amino acid cysteine[22]. All proteins share same highly conserved catalytic G-domains of 165 amino acids (aa), but differ in the 25 aa long hypervariable region (HVR), changing posttranslational modification, localization, and interaction with effector proteins[23]. In there lies KRAS4B's higher oncogenic potential, therefore representing the most interesting drug target[15]. Regardless of their high degree of sequence homology, Ras proteins are not functionally comparable. For instance, knockout of the KRAS gene in mouse embryos is lethal, while deletion of either HRAS or NRAS is not[15,24]. Unique to KRAS4B is its ability to bind calmodulin and fully activate PI3K/AKT/mTOR signaling, making KRAS4B signaling more effective[23]. While NRAS and KRAS4A are farnesylated and palmitoylated, KRAS4B is only farnesylated and HRAS is double palmitoylated and farnesylated. Whereas farnesylation is a permanent PTM, palmitoylation can be reversed. This also implies different binding capabilities to chaperons, PDE transport proteins, and scaffolding proteins like galectin-1[25]. Activating KRAS point-mutations, a single amino acid substitution, occur most frequent in codon 12 (accounting for 90% of entire mutations in the KRAS gene) and 13, mainly G12C, G12D and G12V, while NRAS point mutations are predominantly in codon 61 (60%), and HRAS both in codon 12 and 61 (30%)[17,21,23]. The KRAS mutations are found in 25-30% smokers (mainly G12C) versus 5% in nonsmokers (mainly G12D)[8]. The KRAS mutation *per se* is more frequently mutated in smokers than non-smokers[26,27]. Hyperactive KRAS affects various hallmarks of cancer, cell proliferation, migration, metastasis, angiogenesis, inflammation, and apoptosis evasion and is exclusive among its family members since KRAS has a considerably higher mutation frequency in human cancer[23]. NRAS is mainly mutated in hematopoietic malignancies, HRAS in skin and head and neck cancer, while KRAS mutations appear in pancreatic (86 – 96%), colon (40 – 54%), and lung adenocarcinoma (27 – 39%)[24,28].
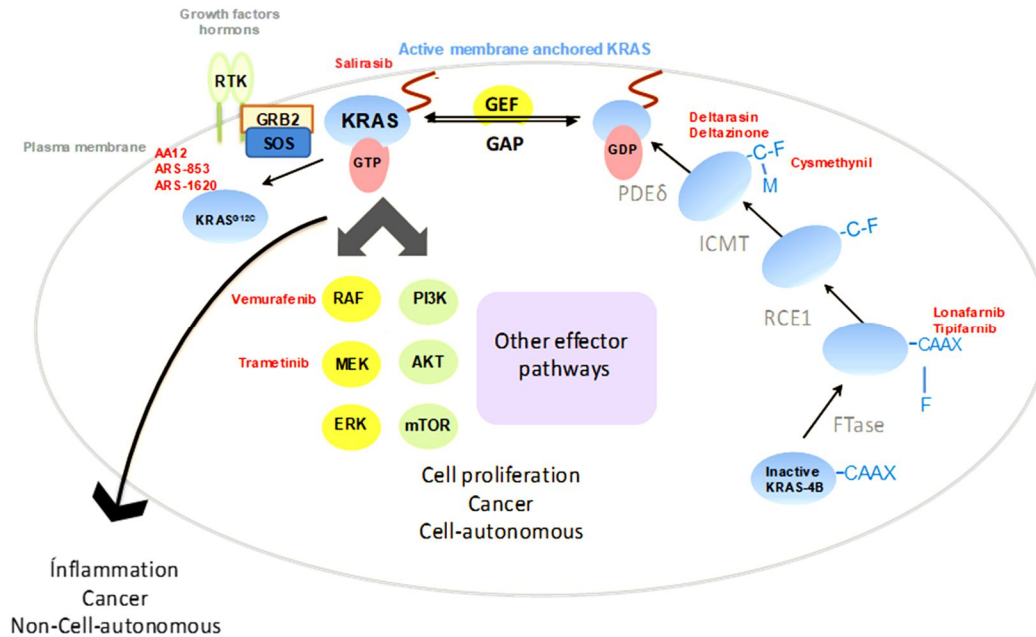
Figure 4: Overview of the KRAS life. The KRAS protein needs posttranslational modification steps for full activation and integration in the plasma membrane. GTP binding leads to full KRAS activation and of multiple effector pathways like RAF/MAPK or PI3K/AKT/mTOR. This affects cell-autonomous and non-cell-autonomous processes. KRAS can be inhibited at multiple steps with different preclinical drugs (named in red) targeting different proteins (in grey, or KRAS[G12C], or downstream proteins such as RAF or MEK). -CAAX tetrapeptide motif, cysteine, aliphatic residue, and X for any amino acid; -F, farnesyl-tail; -M, methylgroup; RTK, receptor tyrosin kinase; GRB2, growth factor receptor bound 2; SOS, son of sevenless; GEF, guanine nucleotide exchange factor; GAP, GTPase-activating protein; PDEδ, phosphodiesterase δ; ICMT, isoprenylcysteine carboxylmethyltransferase; RCE1, Ras-converting enzyme 1; FTase, farnesytransferase.

Why the isoforms are predominant expressed in different cancer types and why they arise from different germ layers are questions still unsolved (Fig. 5A, B). Experiments with F9 mouse embryonal carcinoma stem cells have shown that only hyperactive KRAS, but not HRAS or NRAS can sustain cell proliferation and stem cell characteristics, and thereby promote tumorigenesis of these endodermal progenitor cells, while mutant HRAS initiated cell differentiation. A possible explanation could be the differences in the HVR region, leading to different RAS localization and effector binding, and downstream signaling[29]. Another interesting experiment showed that the tissue-specific expression of isoforms is predominantly regulated via regulatory elements in the promotor regions. When expressing mutant HRAS under the control of the KRAS promotor, lung tumorigenesis was inducible in these genetic

modified mice[24]. Additional topic of interest is why specific point mutations are in context with disease progression. So is the *KRAS*[G12V] mutation in NSCLC and colon cancer more harmful than *KRAS*[G12D], and only one dissimilar amino acid can make a difference in the transformation of the KRAS protein[24]. Also when testing different mutant forms of KRAS the codon 12 allele had the highest transformation capability when expressed in murine fibroblasts[17].
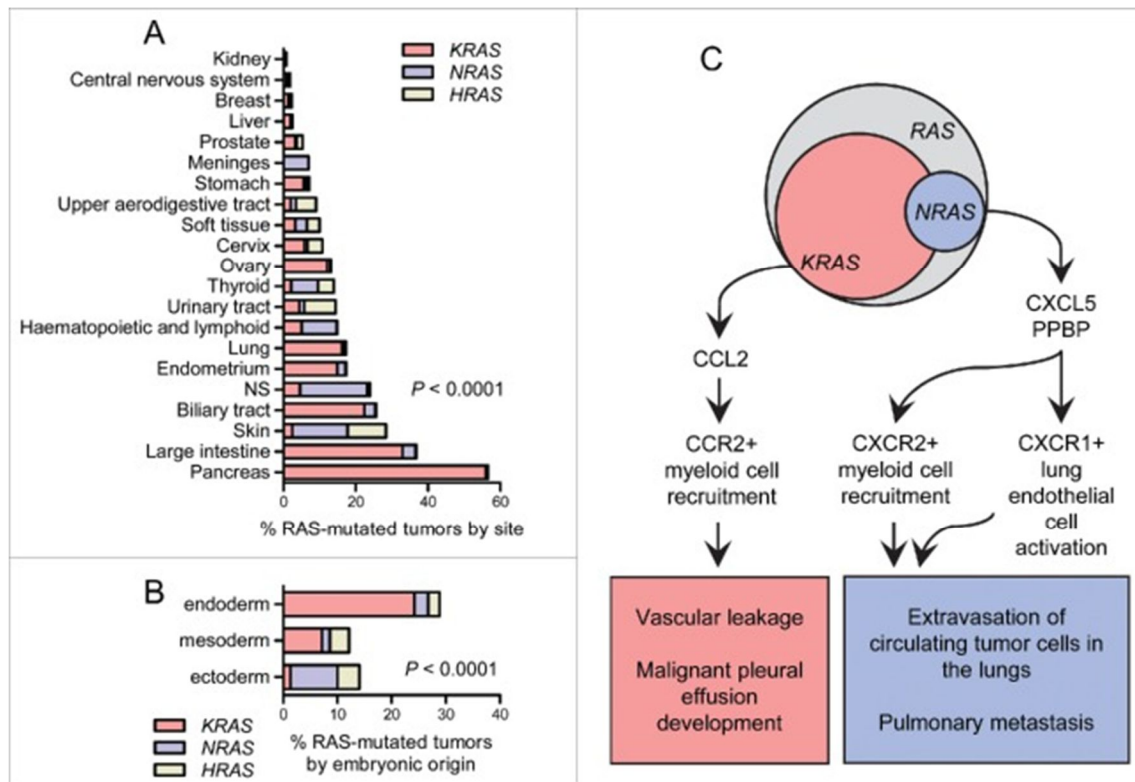
Figure 5: Differences in the RAS isoforms KRAS, NRAS, and HRAS. (A) Tissue expression of the three isoforms. (B) Three embryonic layers give rise to specific RAS isoforms. (C) KRAS is secreting CCL2, while NRAS is acting via CXCL5, resulting in different pathological profiles. Figure from Spella *et al*.[30].

3.2.2 KRAS downstream signaling and beyond

KRAS is an important, multitasking mediator of a huge signaling network and its dysregulation affects all hallmarks of cancer (cell proliferation, migration, apoptosis evasion, metastasis, angiogenesis, and inflammation). The two most well studied downstream effector pathways are mitogen-activated protein kinase (MAPK) and phosphoinositide 3-kinase (PI3K)/ serine/threonine kinase 1 (AKT)/ mammalian target of rapamycin (mTOR). Active KRAS

recruits rapidly accelerated fibrosarcoma (RAF) protein kinases to the plasma membrane including BRAF and CRAF, both potent oncogenes themselves. Dimerization activates mitogen-activated protein kinase kinase 1/2 (MAPKK/MEK 1/2) and extracellular-signal-regulated kinase 1/2 (ERK 1/2) via phosphorylation[20]. This stimulates downstream factors including variant transcription factors for expression of cell cycle progression like cyclin D1[31,32]. The MAPK pathway is thought to be the most important signaling cascade for the oncogene and KRAS mutations are mutually exclusive with other molecules of this pathway like EGFR and BRAF[33]. KRAS also interacts with PI3K, which phosphorylates PIP_2 to PIP_3 (phosphatidylinositol-4,5-bisphosphate to -3,4,5-trisphosphate) and subsequently recruits AKT to the plasma membrane. AKT phosphorylates and activates multiple targets, such as pyruvate dehydrogenase kinase 1 (PDK1) and mTOR. The tumor suppressor phosphatase and tensin homolog (PTEN) can inactivate this cascade[34]. PI3K/AKT/mTOR signaling has numerous targets including nuclear factor-kappaB (NF-κB), pro-survival mediators, and regulators of protein translation and cell growth. The NF-κB pathway itself is tightly linked to inflammation and cancer progression, but in particular to KRAS mutant cancer types like lung and pancreatic cancers[35,36]. Since NF-κB activation is controlled via its activating IκB kinases IKKα/β, and the degradation of the inhibitors of κB, called IκBs or the non-canonical IκB kinase TBK1, these regulators are seen as possible new targets[37–39]. One out of many effects of this signaling is the regulation of apoptosis suppression through upregulation of IAP's (inhibitor of apoptosis protein) or pro-apoptotic B-cell lymphoma 2 (BCL-2) family members like Bcl-2-Antagonist of Cell Death (BAD)[15,24]. If the upstream activator EGFR is absent, calcium-bound calmodulin (CaM/Ca^{2+}) can close this gap and fully stimulate KRAS signaling, a mechanism often hyperactive in oncogenic signaling and unique to KRAS4B[32]. Different downstream pathways are tissue-specific, signaling via PI3K/AKT/PDK1 is crucial for PDAC development, while CRAF/MAPK is essential for NSCLC development. This makes it necessary to distinguish the tissue-specific efficacy of drugs targeting KRAS downstream effectors[33,29].

KRAS is a potent oncogene acting cell-autonomous, but it also has huge control over non-cell-autonomous mechanisms. This is presented by its ability to change the heterocellular tumor microenvironment by extracellular matrix (ECM) remodeling, metabolic reprogramming, inflammatory cell infiltration, endothelial cell recruitment, and fibroblast modulation[15,31,40–43]. The remodulation of the ECM by hyperactive KRAS was already published 1988, and is possible through upregulation of matrix metalloproteases (MMP) degrading type IV collagen[40]. Furthermore, oncogenic KRAS controls angiogenesis, the building of new blood vessels, by increasing vascular endothelial growth factor A (VEGFA) expression. In context to malignant pleural effusion (MPE), that KRAS[MUT] tumor cells need paracrine C-C motif chemokine ligand 2 (CCL2) signaling to surrounding myeloid cells such as mononuclear and mast cells (Fig. 5C). In turn, myeloid-derived interleukin-1β (IL-1β) can selectively trigger NF-κB activation in KRAS[MUT] cancer cells via high expression levels of IL1R1 and inhibitor of NF-κB kinase alpha (IKKα), by this presenting a noticeable therapeutic target for *KRAS*[MUT] lung cancer[36,41]. In addition KRAS driven PI3K/AKT signaling can promote vascularization through NF-κB mediated interleukin-8 (IL-8) expression[44]. These non-cell autonomous mechanisms are of high importance for survival and evasion of tumor cells and basis of aggressive KRAS mutant cancer types[24]. It presents a topic of huge interest in KRAS research: KRAS dependent regulation of the inflammatory response and recruitment of inflammatory mediators to the tumor microenvironment. Oncogenic KRAS is proven to recruit immune cells to the tumor environment via secretion of chemokines including IL-8, IL-1, IL-6, CXCL-1, CCL2 and CCL-5 leading to control multiple favorable mechanism for cancer progression[24,36,43].

3.2.3   Drug targets of oncogenic KRAS

So far, efforts to drug the oncoprotein were unfruitful, although research is ongoing for over 30 years. Compared to the successes of FDA approved small molecules for other oncogenes, the development for the most important cancer driver KRAS is lacking tremendously behind. The scientific community is pushing research forward (see the National Cancer Institute (NCI)-

supported RAS Initiative, https://www.cancer.gov/research/key-initiatives/ras) to develop KRAS inhibitors, a game changing finding with tremendous impact in cancer therapy and patient survival[45]. One of the first indirect attempts in the 1990s was inhibiting RAS farnesylation, a mandatory posttranslational lipid modification for full activation and localization, which were proven unsuccessful in phase III clinical trials (Lonafarnib, Tipifarnib) due to compensatory enzymes like geranylgeranyl transferases (GGT, Fig. 4)[42]. In the first years of RAS research, studies were conducted with HRAS models, assuming same functions for all RAS isoforms. This was the main pitfall for FTIs in clinical trials[46]. Another attempt was targeting the PTM step of methylation by inhibiting ICMT with the molecule cysmethynil resulting in mislocalization of KRAS and showing significant tumor growth reduction in severe combined immunodeficient (SCID) mice harboring PC-3 (prostate cancer-3) cell line derived flank tumors (treatment with 100 mg/Kg drug ip every 48 h)[47,48]. More recent studies focused on blocking the KRAS transport protein phosphodiesterase δ (PDEδ) and thereby interfering with the shuttling and plasma membrane integration of KRAS[49]. One such drug, deltarasin, is competing with KRAS for the binding pocket of PDEδ. In nude mice models with pancreatic xenografts daily ip injection of 15 mg/Kg deltarasin was successful in decreasing tumor growth. A similar inhibitor is salirasib, which removes the farnesylated and attached KRAS protein from the membrane by mimicking active KRAS[50]. The KRAS[G12C] point mutation can be blocked with the compound AA12, harboring a thiol (SH) group[51]. With this the molecule binds via disulphide (S-S) bonds to the cysteine residue at the specific pocket of mutant KRAS, but the S-S bonds are degraded rapidly in the cells. Since direct allosteric inhibition of mutation specific sites would be the most specific option, multiple studies of drug structure optimization are ongoing[52,53]. The biotechnology company AMGEN has just presented their outcome of a clinical trial I study with the KRAS[G12C] inhibitor AMG510 with promising results at multiple oncology meetings (https://clinicaltrials.gov/ct2/show/NCT03600883)[54]. Not feasible is targeting the GTP binding pocket for GDP/GTP. Picomolar concentrations of GTP are sufficient for KRAS activation, but micromolar concentrations of GTP are present in the cell[20].

Alternatively, researchers search for synthetic lethality partners of mutant KRAS, since oncogene addiction makes cancer cells vulnerable and would be exclusive to the cancerogenic state of the cells. Examples for this approach are Serine/threonine Kinase 11 (STK11/LKB1), TANK Binding Kinase 1 (TBK1), and Cyclin Dependent Kinase 4 (CDK4), which drive cell survival selectively in KRAS-dependent cancer cells[37,55,56]. Scholl *et al.* identified STK11 through high-throughput screenings using RNA interference against a huge library of targets. The protein is involved in cancer-specific mechanisms to evade apoptosis. In particular, STK11 can suppress BAD, a proapoptotic protein of the BCL-2 family[55]. With the same method and RNA libraries of the Broad Institute RNAi Consortium (TRC) Barbie *et al*. found TBK1 as promising synthetic lethality partner of KRAS. By inhibiting TKB1 and subsequent NF-κB signaling pro-survival responses were suppressed[37].

In addition to studies focusing on processing and structural features of KRAS itself, downstream proteins of RAS signaling, RAF, MEK or PI3K, are studied intensively. Many inhibitors are in clinical test phases, some already food and drug administration (FDA) approved and in use for other diseases. They are still predominantly not clinically relevant for RAS mutated cancers due to countervailing pathways and feedback loops[46,57]. Vemurafenib is in use for Raf mutant tumors such as melanoma (Fig. 4). Unfortunately, RAF inhibitors upregulate MAPK signaling when KRAS is mutant by activating a positive feedback loop. A more promising option are various MEK inhibitors like Trametinib[31]. However, KRAS can affect multiple pathways and therefore drugging only one target might be useless. MEK inhibitors tested could not show clinically relevant effects in NSCLC patients, evaluated as monotherapy or in combination with chemotherapeutics like Pemetrexed or Docetaxel[58]. Combination therapies to attack hyperactive KRAS could be therapeutically more interesting, but this option is proven to be significantly toxic for the patients[59]. A dual treatment with MEK and PI3K inhibitors showed efficacy in mice models, but in clinical trials tolerable doses were not successful and dose increase would be too toxic for the patients[19].

Why is the search for KRAS inhibitors still unfruitful? One fundamental error could be the use of conventional *in vitro* and cell-based assays for drug screenings, which cannot reproduce the very complex nature of a target like KRAS. Just recently Janes *et al.* reported different KRAS dependencies *in vitro* versus *in vivo*[53]. Chen *et al.* showed how different pancreatic cell lines behave after shRNA induced KRAS downregulation[60]. They and others describe the differential sensitivity to KRAS inhibition in *in vivo* systems compared to cellular models. In comparison to that, mouse models of mutant KRAS are a highly reliable source in cancer studies[57,61]. Findings like that get more and more accepted as KRAS-specific un-druggability *in vitro.* The role of the oncogene beyond the cancer cell itself is huge with the inflammatory response playing an important role for tumor development and cancer treatment.

3.3 Immune system in Cancer progression and treatment

The immune system (IS) has tremendous impact on cancer development and progression and was therefore integrated in the original 6 hallmarks of cancer postulated 2000 by Weinberg and Hanahan. They enlarged their proposal 2011 to 10 hallmarks of cancer including tumor-promoting inflammation as one big new point to consider (Fig. 6)[62,63]. Rudolf Virchow was one of the first linking inflammation and abnormal cell proliferation even before a microscope was invented[64]. The immune system has a dual role in cancer progression since it recognizes and destroys cancer cells, but by this it can select the fittest cancer cells to survive. The immune cells surrounding the tumor create an environment which can as well be positive for tumor outgrowth[65]. Host-derived cytokines can defeat tumor development, but cancer cells can also exploit these cytokines to promote tumor growth, angiogenesis, and increase resistance to apoptosis[66].
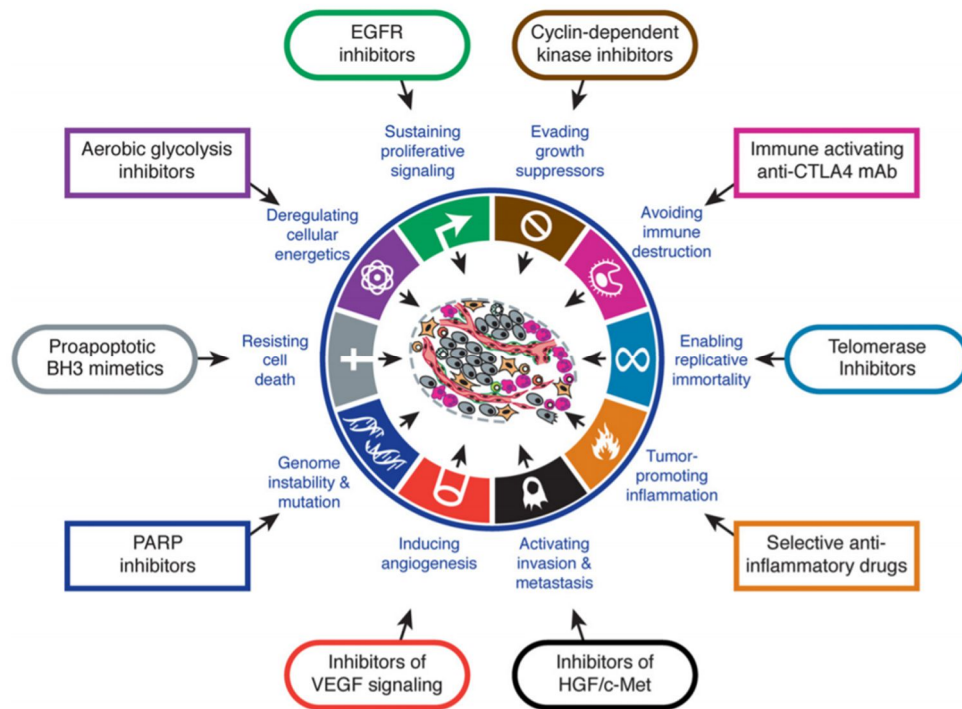
Figure 6: The former 6 hallmarks of cancer from 2000 and the new version from 2011. The authors re-evaluated and supplemented them with the new hallmarks avoiding immune destruction, tumor-promoting inflammation, genome instability & mutation, and deregulating cellular energetics. For each capability are inhibtors in clinical development or in clinical use. Figure from Hanahan *et al.*[63].

The IS is the defense system against any toxic, harmful particle, and within this system, the innate IS represents widely first-line defense mechanisms, while the adaptive IS produces specific antigens for pathogens[66]. Both have their own task force, a panel of cell types specialized for either acute or long-term defense. The cells of origin are leukocytes (white blood cells) from hematopoietic stem cells found in bone marrow, placenta, and peripheral blood[67]. Leukocytes can amount up to 50% of full tumor mass[68]. These cells differentiate into myeloid or lymphoid progenitors. The latter divides in B-, T-, and NK cells, which belong in most parts to the adaptive IS. Myeloid progenitors divide further in granulocytes (monocytes, macrophages, mast cells, neutrophils, basophils, and eosinophils), platelets, and erythrocytes[67]. The adaptive IS acts slow, but produces specific antibodies and remembers its response for future action via antigen-specific receptors on the surface of T- and B- cells to foster targeted effector responses[69].
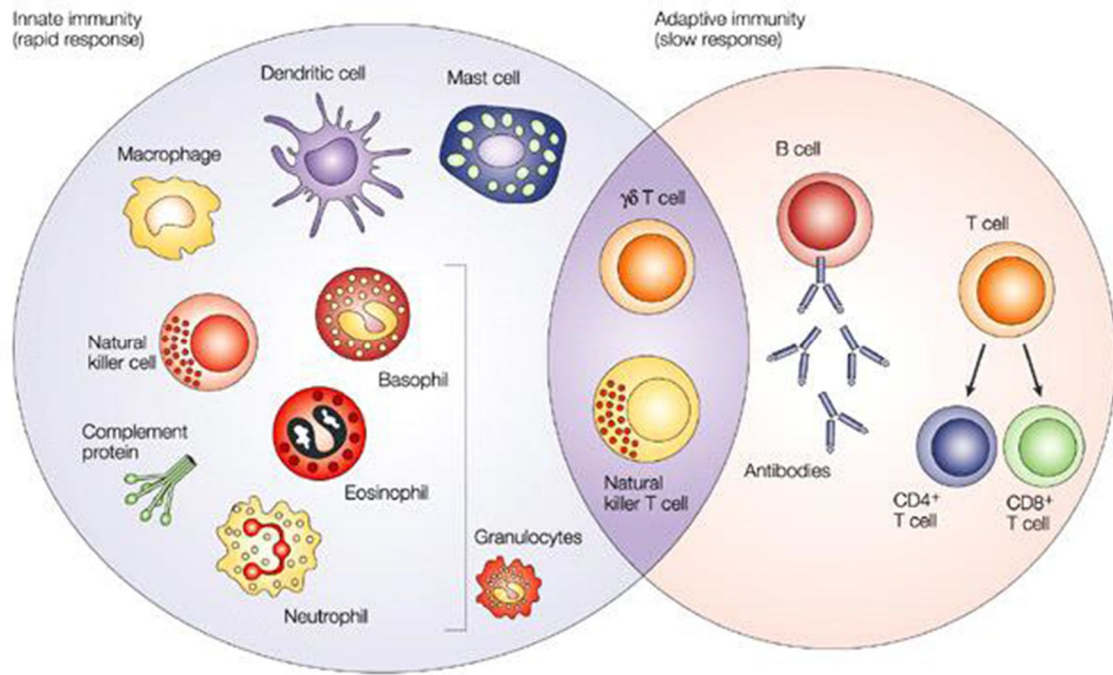
Figure 7: Adaptive and innate immune system and their main cells of action. For rapid defense the innate immune response with its cellular components is in charge, granulocytes (basophils, eosinophils, and neutrophils), natural killer cells, macrophages, dendritic cells and mast cells. The slower defense is the adaptive immunity, but it has increased antigenic specificity and memory. It involves antibodies, B cells, CD4^{+} and CD8^{+} T lymphocytes. At the interface of both immune responses are natural killer T cells and γδ T cells, cytotoxic lymphocytes. Figure from Dranoff *et al*. [66].

The innate IS recognizes a large group of harmful microorganisms expressing pathogen-associated molecular patterns (PAMP) like bacterial lipopolysaccharide, peptidoglycan, bacterial DNA, double-stranded RNA) via their pattern-recognition receptors (PRR). In case of recognition the immune cell immediately reacts without further proliferation. By the recognition of PAMPs inflammatory cells such as macrophages and mast cells get activated and produce and release cytokines (tumor necrosis factor TNFα, IL-1β, IL-6) and proinflammatory chemokines (IL-8, CCL2), which stimulate recruitment of more immune cells to the site of inflammation[68]. One subset of PRR are the toll-like receptors (TLR), which activate multiple downstream signaling cascades after PAMP binding. Among those the NF-κB activation leads to transcription of many inflammatory mediators as mentioned above[70]. The innate IS and its role in chronic inflammation is a well-studied subject and tightly linked to cancer. "Wounds that

never heal" are thereby a huge risk factor for cancer development causing approximately 25% of all cancers[68,71]. They share common pathways, such as constant tissue damage and their need to proliferate, increased cell survival, migration, and enhanced angiogenesis[68]. Extrinsic factors can cause constant irritation which can lead to tumor development, such as tobacco smoking as main reason for NSCLC, *helicobacter pylori* infection triggering chronic gastritis, in turn causing 75% of stomach cancers, pancreatitis as main risk factor for pancreatic cancer, and Crohn's disease causing a tenfold higher colon cancer risk[26,68,72]. The general mechanism connecting inflammation and cancer is that both extrinsic factors (inflammation) and intrinsic pathways (genetic events such as MYC, RAS, RET mutation) promote activation of transcription factors (fe NF-κB, STAT3), transcribing cytokines (IL-6, IL-22, IL-1, CCL2, and more), which attract immune cell populations and in turn infiltrating tumor tissue. They again activate transcription of pro-tumorigenic cytokines ending in a positive feedback loop for tumor progression[73]. In KRAS mutant cancer it was shown that by expressing high amounts of cytokines like CCL2, myeloid cells get recruited to the tumor environment thereby promoting further tumor growth as well as malignant pleural effusion[41]. The strong involved NF-kB pathway supports this interplay of KRAS mutant cancer cells and inflammatory response[36].

3.4   Outlook

Here we show that *KRAS* inhibition through genetic manipulation or 3 inhibitors (deltarasin, AA12, cysmethynil) show primary resistance *in vitro* in lung cancer cell lines, proven with different assays. However, they do have mutation specific effects *in vivo* in immunocompetent flank mouse models of lung cancer. This led us to assume that non-cell autonomous effects of KRAS are of much higher importance than KRAS-controlled cell intrinsic signaling. By analyzing the gene expression profile of a panel of murine cell lines we teased out a *Kras*-mutant specific gene-set which was highly similar to a human *KRAS*-signature, as well as inflammatory response signaling. Consistent with similar expression profiles and their validation used to study mast cell recruitment and *Kras*-induced MPE formation done by

Giannou *et al.*, Marazioti *et al*., and Agalioti *et al*. we found the inflammatory mediators *Il1r1* and *Ccl2* highly upregulated[36,41,43]. The authors were able to show a KRAS-regulated expression of CCL2 which resulted in CCR+ myeloid cell recruitment to the tumor microenvironment. By this, host cell secreted IL-1β supported MPE formation and tumor growth. In this piece of work, we further analyzed the role of both inflammatory mediators in response to KRAS inhibition. We show that the KRAS-specific drug deltarasin inhibits the IL-1R1 expression of *KRAS*-mutant tumor cells and so stopping the cascade initiated by recruitment of myeloid cells to the tumor environment. Consequently, CCL2/IL-1β signaling is significantly lesser and *KRAS*-mutant tumor cells are not fueled anymore with this growth-promoting mechanism. We propose that the KRAS/CCL2/IL-1β axis is not just responsible for MPE formation, but also plays a crucial role in effective inhibition of *KRAS*-mutant lung adenocarcinoma. For this reason, study design for KRAS drug development needs a shift towards *in vivo* screenings.

3.5   Aim of this dissertation

Background:

- KRAS is one of the most mutated oncogenes in various cancer types and predicts decreased patient survival.
- KRAS drug development is on-going, but so far failed in preclinical or clinical stages.
- The immune system influences cancer progression and development.
- *KRAS* mutant cancers are strongly dependent on their tumour microenvironment and inflammatory signalling offering new possibilities for treatment.

Study highlights contributed by this work are:

- Evaluation of different preclinical KRAS inhibitors *in vitro* with multiple assays and a large panel of human and murine cell lines.
- Proof of a huge discrepancy between *in vitro* and *in vivo* findings related to KRAS inhibition.
- Identification and validation of a mechanism for the *in vivo*-restricted efficacy of KRAS inhibitor deltarasin.
- Determination of the requirement for the KRAS/CCL2/IL-1β axis to successfully inhibit KRAS.
- Proof-of-concept human data supporting the existence of the proposed mechanism in human cancer.
- KRAS drug development can be improved by an *in vivo* setting.

4. Materials

4.1 Antibodies

Table 1. Antibodies

Method[a]	Target protein	Providers	Catalog number	Dilution
WB	p-ERK	Santa Cruz Biotechnology	sc-7383	1:1000
WB	t-ERK	Santa Cruz Biotechnology	sc-514302	1:1000
WB	GAPDH	Cell Signaling	#2118	1:2000
WB	rat anti-mouse IgG	Abcam	ab131368	1:10000
WB	anti-rabbit IgG VHH	Abcam	ab191866	1:10000
IF	IL-1β-Alexa488	Santa Cruz Biotechnology	sc-515598 AF488	1:50
IF	CCR2	Thermo Fisher Scientific	PA5-23043	1:50
IF	DAPI Staining Solution	Abcam	ab228549	300 nM
IF	donkey anti-rabbit IgG AlexaFluor647	Abcam	ab150075	1:500
IF	normal mouse IgG2a Alexa Fluor488	Santa Cruz Biotechnology	sc-3891	1:50

4.2 Assays & Kits

BCA assay	Pierce™ Rapid gold BCA protein assay; Thermo Fisher Scientific; Waltham, USA
cDNA synthesis	iScript Advanced cDNA synthesis kit for RT-qPCR; Bio-rad Laboratories; Hercules, USA
DNA purification	NucleoSpin® Gel and PCR Clean-up; Macherey-Nagel; Düren, Germany
ELISA	human MCP-1(CCL2); murine JE/MCP-1 (CCL2); ABTS ELISA buffer kit; Peprotech; London, UK
Mycoplasma Detection	MycoAlert; LONZA; Verviers, Belgium
Plasmid purification	NucleoSpin® Plasmid easyPure; Macherey-Nagel; Düren, Germany
qPCR	Lightcycler 480 Sybr Green I Master; Roche Diagnostics; Mannheim, Germany
RNA isolation	Trizol LS reagent; Thermo Fisher Scientific; Waltham, USA
RNA purification	RNAeasy mini kit; Qiagen; Hilden, Germany
Cell viability assay	WST-8/ CCK-8 (cell counting kit 8) assay; Bimake; Munich, Germany

4.3 Buffers

PBS	NaCl	8 g
	Na_2HPO_4	1.15 g
	KH_2PO_4	0.2 g
	H_2O	to 1 L

10x SDS Running buffer	Tris-base	30 g
	Glycerin	144 g
	SDS	10 g
	H_2O	to 1 L

10x Transfer buffer pH 8.3	Tris	30 g
	Glycine	144 g
	SDS	5 g
	H_2O	to 1 L

1x Transfer buffer (TB)	10x TB	100 ml
	Methanol	100 ml
	H_2O	to 1 L

| Citrate buffer pH 6.0 | Citric acid | 2.1 g |
| | H_2O | to 1 L |

50x TAE buffer	Tris	242 g
	0.5 M EDTA pH 8.0	100 ml
	Acetic acid	57.1 ml
	H_2O	to 1 L

6x Protein loading dye	1 M Tris HCL	3 ml
	Glycerol	1.5 ml
	SDS	0.6 g
	Bromophenol blue	1 mg
	H_2O	to 20 ml

GdmCl buffer 6 M	10 M GdmCl stock	12 ml (6 M final)
	0.5 M TCEP stock	0.4 ml (10 mM final)
	0.5 M CAA stock	1.6 ml (40 mM final)
	1.5 M Tris pH 8.5	1.3 ml (100 mM final)
	H_2O	to 20 ml

4.4   Cell lines

Table 2. Cell lines

Organism	Cell line	Tissue origin	KRAS mutation status
C57BL/6 mouse	LLC	Lewis lung carcinoma	G12C
C57BL/6 mouse	MC38	Colon adenocarcinoma	G13R

C57BL/6 mouse	AE17	Malignant pleural mesothelioma	G12C
C57BL/6 mouse	B16F10	Malignant skin melanoma	none
C57BL/6 mouse	PANO2	Pancreatic adenocarcinoma	none
C57BL/6 mouse	CULA	Urethane-induced lung adenocarcinoma	none
FVB mouse	FULA	Urethane-induced lung adenocarcinoma	Q61R
Human	A549	Lung adenocarcinoma	G12S
Human	H460	Lung large cell carcinoma	Q61H
Human	H358	NSCLC	G12C
Human	H358M	Bronchiolo-alveolar carcinoma	G12D
Human	H1944	NSCLC	G13D
Human	HOP-62	Lung adenocarcinoma	G12C
Human	H520	Squamous cell carcinoma	none
Human	EKVX	Lung adenocarcinoma	none
Human	H1299	NSCLC	none
Human	H3122	NSCLC	none

4.5   Drugs

AA12   CAS 1469337-95-8; Selleckchem #S7331; Houston, TX, USA

Cysmethynil   CAS 851636-83-4; Cayman Chemicals #14745; Ann Arbor, MI, USA

Deltarasin   CAS 1440898-82-7; Tocris Bio-Techne #5424; Wiesbaden-

Nordenstadt, Germany

BV6   CAS 1001600-56-1; BioVision Incorporated # B1332-5; Milpitas, CA,

USA

Z-DEVD-FMK   CAS 210344-95-9; Cayman Chemicals #T6005; Ann Arbor, MI, USA

4.6   E. coli bacterial strains

DH5α   Genotype: F– Φ80*lacZ*ΔM15 Δ(*lac*ZYA-*arg*F) U169 *rec*A1 *end*A1
                 *hsd*R17 (rK-, mK+) *pho*A *sup*E44 λ– *thi*-1 *gyr*A96 *rel*A1
                 Source: #18265017; Thermo Fisher Scientific; Waltham, USA

4.7   Lab equipment

ABI2000 Bioanalyzer   Agilent, Santa Clara, CA

Autoclave   Varioklav, H+P Labortechnik, Oberschleissheim, Germany

Balances   PM 4800 Delta Range, Mettler-Toledo, Columbus, OH, USA

2001 MP2, Sartorius, Göttingen, Germany

Bioruptor   Bioruptor Plus sonication device, Liège, Belgium

Centrifuges   Mikro 200R, Hettich, Tuttlingen, Germany

Rotanta 460R, Hettich, Tuttlingen, Germany

Decloaking chamber   Medical decloaking chamber, Biocare Medical, Pacheco, USA

Electrophoresis	Mini Protean-Tetra Cell System, Bio-Rad Laboratories Inc., Hercules, CA, USA
Gel imaging system	Chemidoc XRS+ System, Bio-Rad Laboratories Inc., Hercules, CA, USA
Incubation shaker	HT Multitron, Infors, Bottmingen, Switzerland
Incubator	BBD6220, Heraeus, Thermo Scientific, Waltham, MA, USA
Ice machine	Ziegra, Isernhagen, Germany
Laminar flow	LaminAir HB 2472S, Heraeus, Hanau, Germany
Lightcycler 480 II	Roche Diagnostics, Basel, Switzerland
Magnetic stirrer	MR3003, Heidolph, Kelheim, Germany
	KMO2 basic, IKA, Staufen, Germany
Microplate reader	TECAN Sunrise microplate reader; Männedorf, Switzerland
Microscope, inverted	Axiovert 40 C; Zeiss; Jena, Germany
Microscope, light	AxioImager.M2; Zeiss; Jena, Germany
Microtome	Hyrax M55 cool-cut; Zeiss; Jena, Germany
pH-meter	Inolab pH Level 1, WTW, Weilheim, Germany
PCR cycler	Mastercycler gradient, Eppendorf AG, Hamburg, Germany
Shaker	Duomax 1030, Heidolph, Schwabach, Germany
Spectrophotometer	ND-1000, peqlab, Erlangen, Germany
Thermoblock	Thermomixer 5436, Eppendorf AG, Hamburg, Germany

Water bath incubator   MA6, Lauda, Lauda-Königshofen, Germany

Water preparation   Milli Q Advantage, Millipore, Billerica, MA, USA

Western Blotting   Mini Trans-Blot Cell System, Bio-Rad Laboratories Inc., Hercules, CA, USA

4.8 Plasmids

The shRNA plasmids are pools of 3-5 lentiviral vector plasmids, which are coding for 19-25 nucleotide (nt) long shRNA. They, the Kras^{G12C} plasmid, and appropriate control plasmids can be transfected with common protocols and selected with puromycin for stable expression.

Table 3. Plasmids

Plasmid	Insert	Provider	Catalog number
GFP-KrasG12C_2B_puro* (pKras^{G12C})	mouse Kras 2B (G12C mutant)	Addgene	64372
Bicistronic_GFP_ires_puro* (pC)	GFP fluorescent protein	Addgene	64336
murine shKras	Pool of 3 shRNA constructs against mKras	Santa Cruz Biotechnology	sc-43876-V
murine shCcl2	Pool of 3 shRNA constructs against mCcl2	Santa Cruz Biotechnology	sc-43914-SH
random negative control shRNA (shC)	Scrambled shRNA	Santa Cruz Biotechnology	sc-108080-V

*Vector maps can be found in the Appendix and online at addgene.org

4.9 Primers

Oligonucleotides for qPCR were synthesized by Eurofins Genomics (Ebersberg, Germany).

Table 4. Primers

Primer	Sequence	Amplicon (bp)
Murine *Il1r*F	GCTGACTTGAGGCAGTT	200
Murine *Il1r*R	CATACGTCAATCTCCAGCGAC	
Human *IL1R1*F	AGGTAGACGCACCCTCTGAA	154
Human *IL1R1*R	GCATTTATCAGCCTCCAGAGAAG	
Murine *Gapdh*F	CCCTTAAGAGGGATGCTGCC	124
Murine *Gapdh*R	TACGGCCAAATCCGTTCACA	
Human *GAPDH*F	TTAGGAAAGCCTGCCGGTGA	157
Human *GAPDH*R	GGCGCCCAATACGACCAAA	

F forward, R reverse

4.10 Mice strains

The table below shows mice strains used for this study. The genetically engineered mice strain names are given by the mixed backgrounds (B6, C57BL/6; 129, 129 strain including subtype), followed by target gene and superscripted abbreviation "tm" for targeted mutation, allele number, creator's lab code, and lab code of provider ("J", Jackson laboratory).

Table 5. Mice strains

Strain	Background	Provider	Catalog number
FVB/NJ	FVB	Jackson Laboratory (Bar Harbor, ME)	001800
C57BL/6J	C57BL/6	Jackson Laboratory	000664

B6(Cg)-Rag2^{tm1.1Cgn/J}	Rag2	Jackson Laboratory	008449
B6.129P2-Cxcr1^{tm1Dgen/J}	C57BL/6	Jackson Laboratory	005820
B6.129S2(C)-Cxcr2^{tm1Mwm/J}	C57BL/6	Jackson Laboratory	006848
B6.129S4-Ccr2^{tm1Ifc/J}	C57BL/6 or FVB	Jackson Laboratory	004999
Il1b^{tm1Yiw} mice	C57BL/6 or FVB	Dr. Yoichiro Iwakura (Tokyo University of Sciences, Japan)	2157396 (MGI)

4.11 Reagents

Agarose   Thermo Fisher Scientific, Waltham, USA

BSA   Santa Cruz Biotechnology, Dallas, USA

Crystal Violet   Sigma-Aldrich, St. Louis, USA

DMSO   Sigma-Aldrich, St. Louis, USA

DNA Loading dye, 6x   Thermo Fisher Scientific, Waltham, USA

DNA ladder, 1 kb   Thermo Fisher Scientific, Waltham, USA

FBS   Thermo Fisher Scientific, Waltham, USA

GeneJuice Transfection   Merck KGaA, Darmstadt, Germany
Reagent

LB- Agar   AppliChem GmbH, Darmstadt, Germany

LB- Medium   AppliChem GmbH, Darmstadt, Germany

Midori green DNA Stain   Nippon Genetics Europe GmbH, Düren, Germany

Mounting medium	Fluorescence mounting medium, DAKO North America Inc., Carpinteria, USA
Paraformaldehyde	Sigma-Aldrich, St. Louis, USA
Trizol x 100	Thermo Fisher Scientific, Waltham, USA
Trypsin	Thermo Fisher Scientific, Waltham, USA
Pen/Strp	Thermo Fisher Scientific, Waltham, USA
Phosphatase/- Protease- Inhibitor Cocktail	Thermo Fisher Scientific, Waltham, USA
Protein loading dye	SERVA Electrophoresis GmbH, Heidelberg, Germany
Protein marker	SERVA Electrophoresis GmbH, Heidelberg, Germany
Puromycin	Abcam, Cambridge, UK
RIPA	Thermo Fisher Scientific, Waltham, USA
Xfect	Takarabio Inc, Kusatsu, Japan

4.12   Software

Table 6: Software

Software	Use	Link and Reference	Provider
Transcriptome Analysis Console Software (TAC)	Analysis of transcriptional expression differences of microarray data	https://www.thermofisher.com/de/de/home/life-science/microarray-analysis/microarray-analysis-instruments-software-services/microarray-analysis-software/affymetrix-transcriptome-analysis-console-software.html	Thermo Fisher Scientific, Waltham, USA
Broad Institute pre-ranked	Computational method to find differences	http://software.broadinstitute.org/gsea/index.jsp[74]	Broad Institute, Massachus

Gene Set Enrichment Analysis (GSEA)	within a gene set fe. between $Kras^{MUT}$ and $Kras^{WT}$ phenotypes or identification of signaling pathway members		etts Institute of Technology (MIT), CA, USA
Wikipathway y analysis	database of biological pathways	https://www.wikipathways.org/index.php/Wiki Pathways[75]	National Institute for General Medical Sciences, Bethesda, MD, USA
QuantaSoft	Analysis of qPCR runs	http://www.bio-rad.com/en-gr/sku/1864011-quantasoft-software-regulatory-edition?ID=1864011	Bio-Rad Laboratorie s Inc., Hercules, CA, USA
ImageJ	Immunoblotting processing and lane intensity quantification	http://www.bio-rad.com/en-us/sku/1709690-image-lab-software	Bio-Rad Laboratorie s Inc., Hercules, CA, USA
G*Power	Statistical program to calculate number of mice	http://www.gpower.hhu.de/[76]	Heinrich-Heine-Universität Düsseldorf, GER
GraphPad Prism	Data analysis, production of graphs, and statistical computation	http://www.graphpad.com/	GraphPad Software, San Diego, CA, USA
Fiji	Immunofluoresc ence processing	http://fiji.sc	National institute of health (NIH),

			Bethesda, MD, USA
OrthoDB v10	Transcription of murine gene list to human orthologs	https://www.orthodb.org/[77]	E. Zdobnov, University of Geneva, CHE
Kaplan-Meier plotter	Cancer survival curve creation depending on expression of genes of interest	http://www.kmplot.com[78]	B. Gyorffy MD PhD, Hungarian Academy of Sciences, Budapest, HUN

5.Methods

5.1 Chemicals and solutions

AA12, BV6, cysmethynil, deltarasin, and Z-DEVD-FMK were dissolved in DMSO to a stock concentration of 10 mM, and stored at −80 °C. Further dilutions for *in vitro* assays were done in the right media. For *in vivo* injections deltarasin was dissolved to a final concentration of 15 mg/kg in 100 µl PBS.

Chemicals were obtained from different companies, among others Bio-Rad Laboratories (Hercules, CA, USA), Merck (Darmstadt, Germany), Biozym (Hessisch Oldendorf, Germany), Life Technologies (Carlsbad, CA, USA), GE Healthcare (Little Chalfont, Buckinghamshire, UK), Qiagen (Hilden, Deutschland), Roth (Karlsruhe, Germany), and Sigma-Aldrich (St Louis, MO, USA). Consumables were ordered from Corning (Corning, NY, USA), Eppendorf (Hamburg, Germany), Biozym (Hessisch Oldendorf, Germany), BD Biosciences, Nunc/Thermo Fisher Scientific (Waltham, MA, USA), and others.

5.2 Cell culture

All murine and human cancer cell lines were chosen according to their *Kras/KRAS* mutation presence (table 2, supplementary figure S1). NCI-H460, -H358, -H358M, -H1944, -H1299, -H3122, -H460, -H520, -HOP-62 (omitting NCI- from now on), EKVX, A549, LLC, B16F10, and PANO2 were ordered from the National Cancer Institute (Frederick, MD); MC38 cells were received as a gift from Dr. Timothy S. Blackwell (Vanderbilt University, Nashville, TN) and AE17 cells from Dr. YC Gary Lee (University of Western Australia, Perth, Australia)[36,41,79,80]. FULA1 and CULA cell lines were generated from *C57BL/6* or *FVB* mice harboring primary lung adenocarcinoma developed after urethane exposure[26]. Benign samples including tracheal epithelial cells (TEC; cultured out from murine tracheas), whole murine lungs, bone marrow-derived macrophages (BMDM; isolated from murine bone marrow and differentiated *in vitro* in

DMEM with 10% FBS and 20 ng/mL M-CSF), and mast cells (BMMC; murine bone marrow isolation followed by culturing in DMEM containing 10% FBS and monthly incubation with 100 ng/mL IL-3 plus KITL) were prepared as described elsewhere[26,36,43]. Human cell lines were cultured in RPMI-1640, murine cell lines in DMEM supplemented with 10% FBS and 100 IU/ml penicillin/streptomycin. They were kept in a humidified incubator at 37 °C with 5% CO_2. All cell lines included in this study were negative for mycoplasma *Mycoplasma Spp* and regularly checked via MycoAlert Mycoplasma Detection Kit.

For passaging and splitting, confluent cells were washed once with 1x PBS and trypsinized for 2-5 min. For sub-culturing, a splitting ratio of 1:2 to 1:10 was applied, or cells were seeded in dishes or multiwell-plates for experiments. Counting of cells was performed using a hemocytometer (Neubauer improved), after 10 min centrifugation (400 rpm) of trypsinized cells in full growth media following dilution of the cell pellet in fresh growth media. Following formula for calculating total cell number/ ml was used: $cell\ number/ml = average\ cell\ number \times 10.000$. For final dilution calculation the equation $C_1 \times V_1 = C_2 \times V_2$ was used.

For freezing and thawing, cells were collected and centrifuged as described, and cell number was determined using the hemocytometer. Cell pellets were resuspended in freezing media containing FBS and 10% DMSO for cryoprotection. Vials were frozen at -80 °C overnight and moved to liquid nitrogen. Thawing was performed by letting cryovials carefully defrost in the 37 °C water bath and then plated in fresh prewarmed full growth media.

5.3   Constructs

Knockdown gene expression experiments were done using shRNA against *Kras* or *Ccl2*. Protein overexpression was performed using custom-made plasmids encoding mutant *Kras*[G12C] oncogene. *Kras* silencing was induced in LLC, AE17 and MC38, *Ccl2* silencing in FULA1, and *Kras*[G12C] overexpressing in B16F10, PANO2, EKVX, and H3122. LLC, AE17 and MC38 sh*Kras* were produced as described elsewhere[41]. A similar strategy was applied for FULA1 sh*Ccl2*. For stable shRNA transfection, 10^5 tumor cells in 6-well culture vessels were

transfected with 5 µg DNA using Xfect reagent (Takara) and clones were selected by puromycin (2-10 µg/mL). After primary harsh selection, clones were picked, most efficient ones identified via ELISA assay and pooled. Puromycin treatment was reduced to 1 µg/ml for further cultivation to guarantee stable transfection with sh*Ccl2*. For negative and positive controls lentiviral plasmids expressing random scrambled shRNA were used. H3122 and EKVX cells were stably transfected with p*Kras*^{G12C} or its homologous GFP backbone plasmid without *Kras*^{G12C}. For this, 60% confluent cells were starved for 4 hours before transfection with GeneJuice reagent in a ratio of transfection reagent to DNA of 3 µl reagent to 1 µg DNA. After 48 hours, media was replaced by media containing 0.5-15 µg/mL puromycin. Stable clones were selected and subcultured under constant antibiotic pressure. Validation was done with an inverted fluorescence microscope (Axiovert 40 C; Zeiss) and GFP expression. All plasmids for overexpression were made inhouse, deposited, confirmed, and repurchased from Addgene (Watertown, MA, supplementary figure S2 for plasmid maps). After receiving the plasmids as transformed bacteria in stab culture, bacteria were streaked out on a LB agar plate and incubated at 37°C overnight. A single colony was picked and inoculated overnight in LB media at 37°C. Plasmids were purified using the NucleoSpin® Plasmid easyPure kit, test digested with appropriate restriction enzymes according to company instructions (Promega GmbH, Mannheim) and controlled on an agarose gel (1% agarose in PBS-T (0,05%); 1 h, 100 V).

5.4   *In vitro* cell culture assays

5.4.1   Cell viability assay

In vitro cell proliferation of various cell lines (see 4.3) was determined using WST-8 assay (tetrazolium-1[2-(4-iodophenyl)-3-(4-nitrophenyl)-5-(2,4-disulphophenyl)-2H-tetrazolium, WST-8 monosodium salt, Bimake) assay. The assays mechanism is hereby based on the activity of mitochondrial succinate dehydrogenases exclusively active in living cells. By adding the tetrazolium salt to cells and in presence of 1-Methoxy PMS, an electron carrier, reduction by these enzymes will take place and an orange, water-soluble formazan dye develops, directly proportional to the number of living cells and detectable at a specific wavelength (while cellular cofactors NADH/NADPH are oxidized). The water solubility of the dye is one of multiple improvements to former used MTT reagents[81]. 3000 cells/ well were plated in triplicates in 96-well plates in media containing 5% FBS and allowed to adhere overnight. Cells were treated with different concentrations of drugs the next day (between 0 – 100 µM). 72 hours later 1:10 solution and measured after 1- 4 hours incubation time on a TECAN Sunrise microplate reader at 450 nm. The plates were incubated at 37 °C in a 5% CO_2 humidified incubator. For controls the maximal dosage of DMSO was used, in correlation to the highest drug concentration (2% of full sample volume), labeling DMSO control samples as controls (CTRL) subsequently. For drug combinations, different concentrations of deltarasin were combined with IC_{25} concentrations of either BV6 or Z-DEVD-FMK or DMSO controls and incubated for 72 hours before measurement.
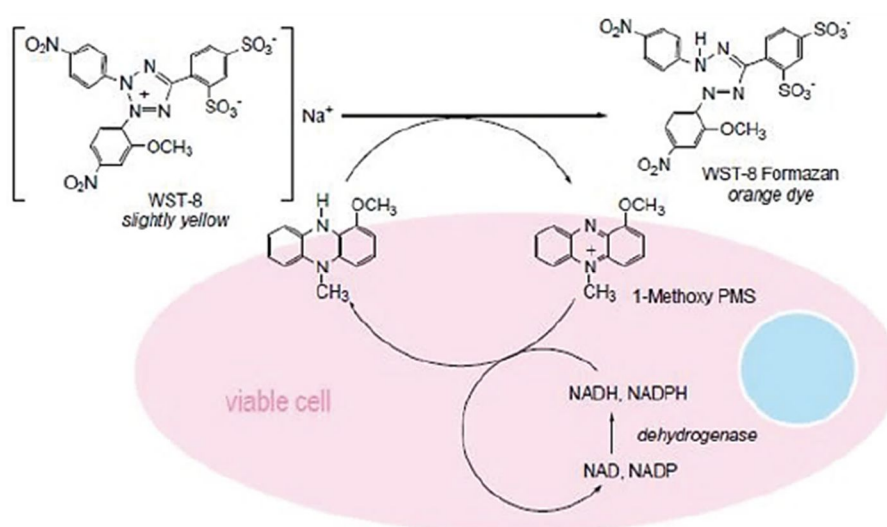
Figure 8: Mechanism of WST-8 assay. The tetrazolium salt is reduced to an orange formazan salt via intact cellular enzymes. This colour development is direct proportional to the viable cells and measurable at 450 nm. NAD/NADH, Nicotinamide adenine dinucleotide; NADP/NADPH, nicotinamide adenine dinucleotide phosphate; PMS, 5-methylphenazinium methyl sulfate; WST, tetrazolium-1[2-(4-iodophenyl)-3-(4-nitrophenyl)-5-(2,4-disulphophenyl)-2H-teterazolium. Description of cell counting kit-8, online available at: https://www.bimake.com/product/vita-orange-cell-viability-reagent.html (accessed 13 May 2019).

5.4.2 Colony formation assay

For detection of colony formation, 300 cells were plated in triplicates in 6-well plates in 5% FBS-containing media. 24 hours later murine cell lines were treated with 1 µM deltarasin, human cell lines with 2 µM deltarasin. Media was replaced with drug-free media 72 hours later. Incubation kept going until ≤ 50 colonies were formed. Cell colonies were fixed with 80% ethanol, stained with 0.5% crystal-violet diluted in distilled H_2O, and counted. Pictures were taken with an AxioImager.M2. Colonies were counted in each well and all cellular experiments were independently repeated at least three times[80].

5.5 Immunological methods

5.5.1 Western blot analysis

Protein lysates were prepared as following: Adherent cells were cultivated in FBS-free medium 4 hours prior to cell lysis, then washed with PBS and scraped off for collection in Eppendorf

tubes. After centrifugation to remove debris (1000 rpm, 10 min), cell pellets were lysed using RIPA buffer containing phosphatase/protease inhibitor cocktail. Lysis took place for 30 min on ice. To determine protein concentration a bicinchoninic acid assay (BCA) was done according to manufactures protocol and a standard curve was produced to calculate protein amount in experimental samples. The BCA assay uses the reduction of Cu^{2+} to Cu^{1+} by proteins in an alkaline medium which result in a colored reaction with an absorbance at 480 nm. Protein lysates were diluted in 1x SDS sample buffer to a final concentration of 1 µg/µl and heated up at 95 °C for 5 min before storage at -20 °C. Protein samples were separated by mass using SDS- PAGE (80 V, 20 min followed by 100 V, 40 min) and transferred to nitrocellulose membranes following standard protocols, using the 10x transfer buffer, 10% methanol and VE-H_2O. Briefly, electrophoretic transfer of proteins was achieved using wet transfer techniques and nitrocellulose membrane (100 V, 60 min). After blocking in 5% BSA solution in PBS-T for 1 h, immunostaining was performed over night with antibody dilutions in PBS-T and 1% BSA at 4°C shaking (see 4.1, table 1. antibodies). Anti-t-ERK, anti-p-ERK, and anti-GAPDH antibodies were obtained from Santa Cruz Biotechnology. Secondary antibodies were applied next day in a 1:10000 dilution in PBS-T for 1 h after 3x washing for 10 min with PBS-T.

5.5.2   Immunofluorescence

Murine tumor tissue samples were fixed in paraformaldehyde overnight, embedded in paraffin, and shipped from Patras, Greece, to Munich, Germany. Paraffin blocks were cut into 3 µM sections with a Hyrax M55 cool-cut microtome (Zeiss). After overnight incubation at 60°C, tissue sections were deparaffinized with xylene 2x 5 min, rehydrated with 100% ethanol 2x 3 min, 90% ethanol 3 min, 80 % ethanol 3 min, 70% ethanol 3 min, and stored in H_2O. Antigen retrieval was done in citrate buffer pH 6,0 in a medical decloaking chamber (Biocare medical). Slides were rinsed in TRIS buffer pH 7.6 2x 10 min. Before staining, slides were post-fixed with 4% paraformaldehyde, rinsed with 0.1% PBS-T 2x 10 min, and permeabilized with 0.3% Triton-X100 in PBS for 5min. Slides were washed 3x with PBS-T and blocking of unspecific

binding sites was performed using 3% BSA, 10% FBS for 30 min. First antibody was diluted in 1% BSA solution together with 300 nM DAPI, added in right dilution (see 4.1, table 1. antibodies) and incubated overnight at 4°C in the dark. After 3x PBS-T washing steps for 5 min each, secondary antibody was added and incubated for 2 hours. Slides were mounted after a final 3x washing step on coverslips using fluorescence mounting medium. For control staining's, secondary antibody only (donkey anti-rabbit IgG AlexaFluor647) and normal mouse IgG2a Alexa Fluor488 isotype control were added instead of reactive antibodies. Pictures were taken on an inverted microscope (Axiovert 40 C; Zeiss; Jena, Germany).

5.5.3 ELISA assays

Cell culture supernatants to measure CCL2 were collected from murine and human cell lines after incubation with IC_{60} deltarasin for 72 hours, or without treatment for validation of efficient knockdown of CCL2 in FULA1 cells. Quantitative measurement of natural CCL2 was done using sandwich ELISA kits from the Peprotech GmbH company. With this technique an antibody pair, capture and detection, is used to bind the antigen from test samples by creating the so-called sandwich. The amount of bound biotinylated detection antibody can be quantified by adding binding partner avidin, which is conjugated to horseradish peroxidase (HRP)-enzymes. By adding ABTS (2,2'-Azinobis [3-ethylbenzothiazoline-6-sulfonic acid]-diammonium salt) substrate and its oxidation a green colour change is formed and absorbance can be measured which is directly proportional to the amount of protein. For this, 96 well ELISA microplates were coated with capture antibody (0.25 µg/ml) overnight. Samples were loaded next day undiluted and a standard dilution series. For detection, 0.5 µg/ml detection antibody was used. Then Avidin-HRP-conjugate was added for 30 min before ABTS liquid substrate was incubated until color development and signal intensity measurement at 405 nm (650 nm for background-subtraction) on a microplate reader (TECAN). For normalization of CCL2 levels to total cellular protein, whole cellular lysates of same sample as supernatants were prepared as described previously using RIPA buffer and quantified using BCA assay kit.
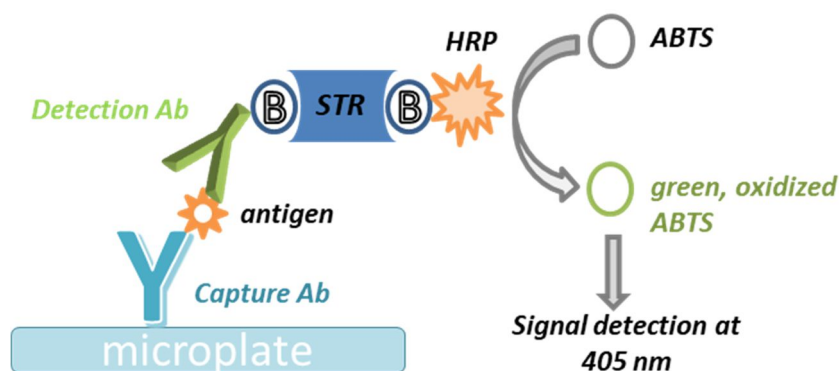
Figure 9: Mechanism of sandwich ELISA using the biotin-streptavidin bond and enzymatic reaction of HRP and ABTS substrate. Ab, antibody; ABTS, 2,2'-Azinobis [3-ethylbenzothiazoline-6-sulfonic acid]-diammonium salt; B, biotin; HRP, horseradish peroxidase; STR, streptavidin.

5.6   Molecular biology methods

5.6.1   Proteomics analysis

For proteomics analysis samples were prepared as following: Either cells or tumor tissue was used, 3 biological samples were prepared and then pooled for proteome analysis. The tumor tissue was minced into small pieces. The cell lines LLC, FULA1 and PANO2 were either treated or not treated with deltarasin IC_{60} concentrations or 2% DMSO/saline controls for 72 h before washing with PBS once. Cells were scraped off in PBS, collected and centrifuged (400G, 10 min). The tumor tissue or cell pellet was resuspended in 150 µl 6 M GdmCL buffer, sonicated for 10min at 4°C with a bioruptor sonication machine (10 cycles à 30 sec sonication, 30 sec pause), stored on ice for another 10 min before final centrifugation. A BCA assay was performed determining protein concentration and 20 µg/ sample was used for proteome analysis conducted by the core facility proteomics of the Helmholtz center Munich. Liquid chromatography with tandem mass spectrometry (LC-MSMS) analysis was done on an Ultimate3000 nano HPLC system (Dionex, Sunnyvale, CA) online coupled to LTQ OrbitrapXL mass spectrometer (Thermo Fisher Scientific). Raw abundances were normalized for factors resulting from experimental disparity. A normalization factor is automatically calculated in all

samples and over all features correcting all samples in a similar way[82]. The normalized data was used for further analysis. The ratios of treated/ untreated samples, and the ratios of $Kras^{MUT}/Kras^{WT}$ samples were produced and final results were compared for finding differently expressed proteins in *in vitro* versus *in vivo* samples (ratios <0.5 and >2 were considered as relevant different expression; fold changes in protein abundance ΔPE).

5.6.2 RNA isolation and purification (column and/or ethanol purification)

Cellular RNA was isolated using Trizol reagent following the manufacturer's instruction. Further purification was done by RNAeasy column kit and genomic DNA removal. Additional ethanol purification was used if RNA quality was low. For this 0.1 volume of 3 M sodium-acetate and 3 volumes of ice-cold 100% ethanol were added to the sample before storing at -80°C overnight. After 30 min centrifugation (4°C at 13000 rpm) the day after the pellet was washed twice with 75% ethanol, air dried and resuspended in water.

5.6.3 cDNA synthesis and qPCR

cDNA synthesis was performed using 1 µg RNA, oligo(dT)$_{18}$ and iScript Advanced cDNA synthesis kit for RT-qPCR in separate tubes. Specific primers for human and murine *Gapdh/GAPDH* and murine and human *Il1r1/IL1R1* are listed in table 4. Quantitative PCR (qPCR) was performed using Lightcycler 480 Sybr Green I Master in a Lightcycler 480 II. Following setting was used to run qPCR:

Preheating	95°C
300 sec	95°C
10 sec	95°C
20 sec	57°C } 45 cycles
10 sec	72°C
60 sec	95°C
∞	4°C

Ct values from triplicate reactions were analyzed with the $2^{-\Delta CT}$ method. mRNA abundance was determined compared to *Gapdh/GAPDH* (ΔCT= Ct (*Il1r1/IL1R1*) – Ct (*Gapdh/GAPDH*)) and is given as $2^{-\Delta CT}$.

5.6.4 Microarray analysis

RNA extraction was performed as described above in triplicate cultures of 10^6 cells. Five µg of pooled total RNA were tested for RNA quality on an ABI2000 Bioanalyzer labelled and hybridized to GeneChip Mouse Gene 1.0 or 2.0 ST arrays (Affymetrix; Santa Clara, CA). For statistical analysis of differential gene expression (ΔGE), unsupervised hierarchical clustering, and WikiPathway analysis, Affymetrix Expression/Transcriptome Analysis Console (TAC) was used to normalize all arrays together using Lowess multi-array algorithm and intensity-dependent estimation of noise (Thermo Fisher Scientific), and finally profile transcriptional changes of *Kras*^{MUT} and *Kras*^{WT} cell lines normalized to benign cells (whole murine lungs, tracheal epithelial cells (TEC), bone marrow-derived macrophages (BMDM), and mast cells (BMMC). Microarray data is stored online and available at the GEO (http://www.ncbi.nlm.nih.gov/geo/; Accession IDs: GSE130624).

5.6.5 GSEA and Kaplan-Meier Analysis

Gene set enrichment analysis (GSEA) was performed using a free available software provided by the Broad Institute (Fig. 10). The following datasets were used for further analysis: GSE31852 with gene expression profiles of 121 biopsies from patients with non-small cell lung cancer including *EGFR*^{MUT} (n = 17), *KRAS*^{MUT} (n = 21) or double wildtype control samples (n = 83; Biomarker-integrated Approaches of Targeted Therapy for Lung Cancer Elimination (BATTLE) trial, GEO data portal, https://www.ncbi.nlm.nih.gov/geo/)[83]. Another comparison was made using a subset of the molecular signature database (MSigDB), the 50 hallmarks gene set (Broad Institute, see supplementary list 12.3).
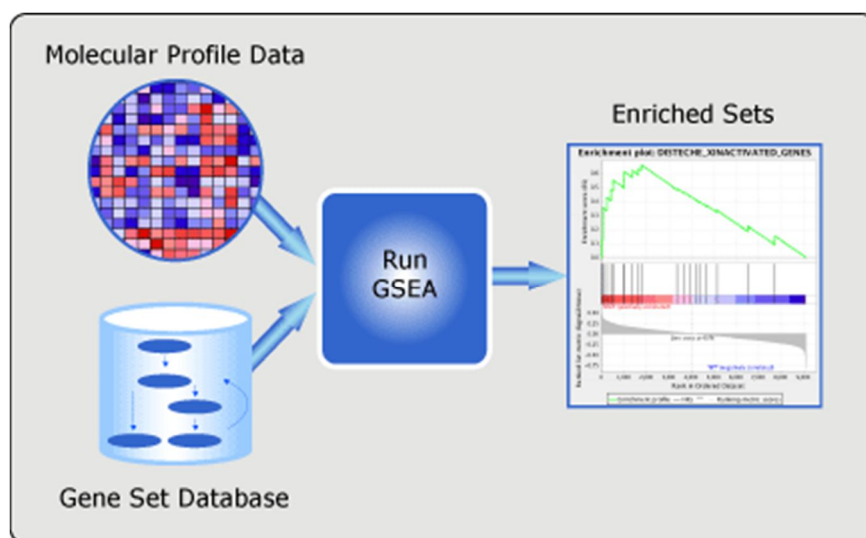
Figure 10: GSEA analysis overview. GSEA is performed by applying online available datasets to the gene list of interest to create enrichment plots. Online available at: http://software.broadinstitute.org/gsea/index.jsp (accessed 12 July 2019).

Further downloaded and reanalyzed with the TAC software (Thermofisher Scientific) was following dataset: GSE43458 with gene expression profiles of never-smoker (n = 40) and smoker (n = 40) LADC, as well as normal lung tissue (n = 30), also from the BATTLE trial[84]. GSE103512 with gene expression profiles of breast (n = 65), colorectal (n = 55), and non-small-cell lung (n = 60) cancer patients from a Roche dataset was also reanalyzed[85]. Kaplan-Meier analysis was done with the free available KM-plotter (http://www.kmplot.com) analyzing data from LADC patients (n = 720) compared to SCLC (n = 524)[78]. All patients were included and overall survival, all stages and grades were set as parameters[80].

5.7 *In vivo* mice models

5.7.1 Study approval

All mouse experiments were prospectively approved by the Veterinary Administration of Western Greece (approval 276134/14873/2) or by the Bavarian regulatory agency (Regierung von Oberbayern, approval 55.2-1-54-2532-194-2016) and were conducted according to the directive 2010/63/EU.

5.7.2   Mice

All mice were bred at the Patras Center for Animal Models of Disease. Experiments were conducted there. Experimental mice were sex-, weight- (20-30 g), and age- (6-12 weeks) matched; both genders were used. In total, 284 mice were enrolled. 25 *FVB* (21 for tumor experiments, 4 as bone marrow donors), 151 *C57BL/6,* 15 *Cxcr1*^{-/-} (on *C57BL/6* background), 34 *Ccr2*^{-/-} (12 on *C57BL/6* and 18 on *FVB* backgrounds for tumor experiments, 4 on *FVB* background as bone marrow donors), 12 *Cxcr2*^{+/-} (*C57BL/6* background), 32 *Rag2*^{-/-} (*C57BL/6* background), and 15 *Il1b*^{-/-} (*C57BL/6* background) mice were used[80].

5.7.3   *In vivo* tumor formation and drug treatment

For in vivo injections, 10^6 cells were diluted in 50 µl PBS and subcutaneously (sc) injected in the flank. When tumors reached 100 mm^3, drug treatments were initiated and involved daily intraperitoneal (ip) injections with saline 1% DMSO or deltarasin (15 mg/Kg in 100 µL saline 1% DMSO). Tumor dimensions (length, L; width, W; depth, D) were monitored consecutively using calipers and the final volume (V) was calculated with following formula: $V = \pi * L * W * D / 6$. Animals were monitored daily for health status and were euthanized using CO_2 when tumors reached 2-3 cm^3 volume or when in distress, whichever came first. Tumors were extracted and fixed in 4% paraformaldehyde overnight before embedded in paraffin for further analysis[80].

5.7.4   Bone marrow transplantation

FVB wild-type (*WT*) and *Ccr2*^{-/-} mice were used for bone marrow transplants (BMT). *Ccr2*^{-/-} mice were total-body irradiated (900 Rad) before receiving 10x10^6 bone marrow (BM) cells intravenously (iv) 12 hours later[36,41,43]. BM cells were collected from *WT* and *Ccr2*^{-/-} mice by flushing femur and tibia bones using full growth media DMEM (post >F12 back-crossing to the *FVB* background). After irradiation and BM cell receive, mice could recover for full bone marrow reconstitution for 30 days before implanting flank tumors with 10^6 FULA1 cells dissolved in 50

µl PBS and further deltarasin treatment. One mouse per experiment was not engrafted for observation till moribund on day's 5-15 post-irradiation.

5.8   Statistics

Mouse sample size was calculated using G*power (http://www.gpower.hhu.de/)[76]. Significant differences (biologically (> 50%) and statistically (α = 0.05; β = 0.20)) between values from individual mice with SD ~ 30% of mean were analyzed using the two-tailed t-tests, yielding n = 7/group. Experiments with n = 5/group were contemplated in batches, till the achievement of probability (P) < 0.05 with α < 0.05 or P > 0.05 with β < 0.20, whichever came first. Two-way ANOVA was employed to analyze the data. Significant differences in cellular assays were assessed using one-way or two-way ANOVA with Bonferroni post-tests. IC_{50} values were calculated using nonlinear regression analysis comparing data points by extra sum-of-squares F-test. Fisher's exact test for cross-tabulation was performed presenting significance between drug sensitivity and resistance in Kras/$KRAS^{WT/MUT}$ cell lines. Significance was considered when values were < 0.05 (*), < 0.01 (**), and < 0.001 (***). Values are shown as mean ± SD. Sample size (n) states biological replicates. Statistics and plots were done on GraphPad Prism software 5.0 and 6.0 (GraphPad; San Diego, CA)[80].

6. Results

6.1   Primary *in vitro* resistance of KRAS inhibitors

We investigated the cellular response of a panel of murine (*n* = 5 - 7) and human (*n* = 3 - 9) *Kras/KRAS*-mutant (*KRAS*^{MUT} in further text) or *Kras/KRAS*-wildtype (*KRAS*^{WT} in further text) cancer cell lines (Figure 11A, B) to three pre-clinical KRAS inhibitors: The widely used drug deltarasin targeting KRAS transport protein PDEδ, the KRAS^{G12C}-specific inhibitor AA12, and ICMT inhibiting cysmethynil (Figure 3A)[47,49,51]. For this purpose, the most common assays were employed based on literature searches, such as MTT and colony formation assay (Figure 11C). Initially, IC$_{50}$ values were calculated via analysis of cell viability using WST-8 assays after 72 hours of drug treatment as readout (Fig. 12A-D). For this half-log-incremental drug concentrations were applied. We were not able to achieve significant differences regarding *KRAS* mutation status by none of the used inhibitors. Of the 16 cell lines tested, detectable significant differences concerning *KRAS* mutation status were only in four cell lines (LLC (Kras^{G12C}), MC38 (Kras^{G13R}), A549 (KRAS^{G12S}), and H1944 (KRAS^{G13D})) with inhibitor deltarasin and only one cell line (A549) with significant IC$_{50}$ differences after cysmethynil treatment. Importantly, the concentration range to generate *in vitro* efficacy was modest and fluctuated between 1 - 50 µM. In this context a literature research using PUBMED highlighted a massive disparity between FDA-approved tyrosine kinase inhibitors and preclinical inhibitors against KRAS (Figure 11D). While successful inhibitors showed drug doses under 100 nM to achieve efficacy in preclinical *in vitro* assays and did enter the clinic, KRAS inhibitors are only effective with much higher concentrations.
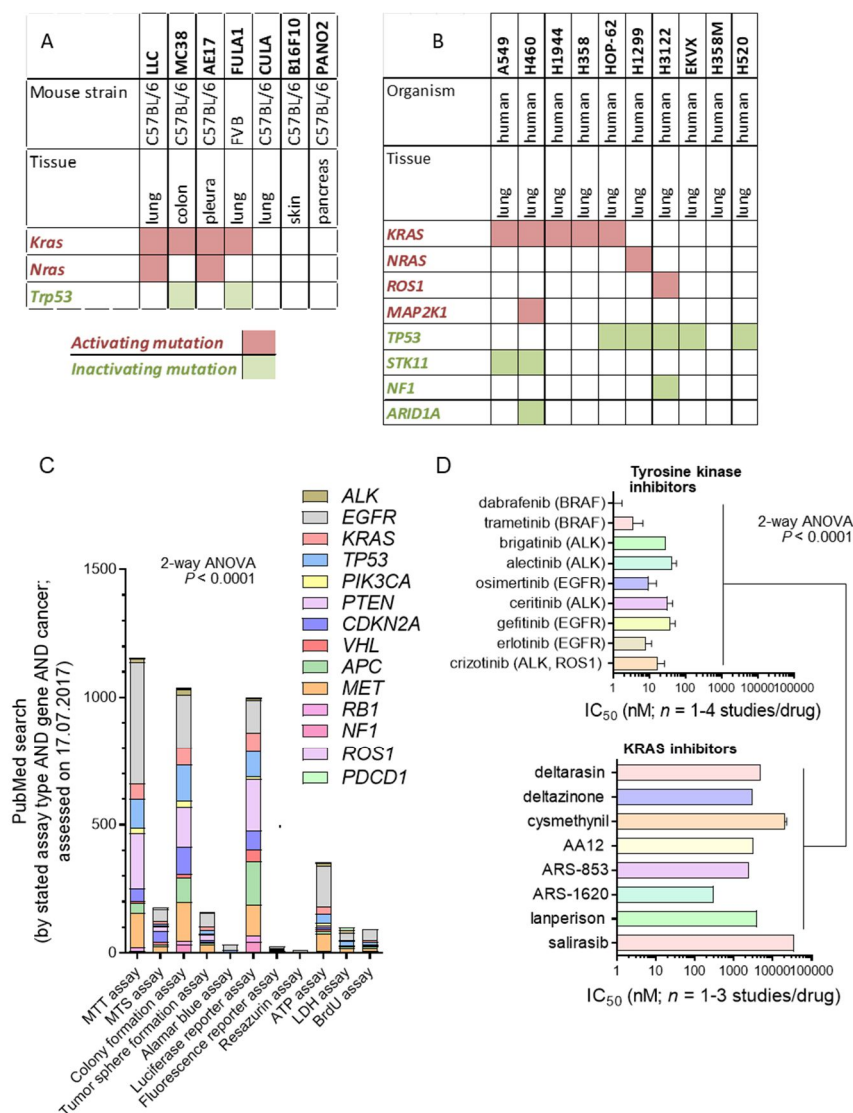
Figure 11: List and information of cell lines used for this dissertation, frequently published *in vitro* assays in cancer research and comparative preclinical efficacy of KRAS versus tyrosine kinase inhibitors (TKI). (A) Mouse cell lines with their syngeneic mouse strain, originated tissue, and mutation status of three genes of interest. Data from reference list under 12.1, S1-S6. (B) Human cell lines and information to mutation status and originated tissue. Data from 12.1, S7. (C) Summary of cellular assays in correspondence to target gene and cancer research. PubMed search done on 17.07.2017 using the terms "assay type" AND "gene" AND "cancer". MTT,3-(4,5-dimethylthiazol-2-yl)-2,5-diphenyltetrazolium bromide; MTS,3-(4,5-dimethylthiazol-2-yl)-5-(3-carboxymethoxyphenyl)-2-(4-sulfophenyl)-2H-tetrazolium); ATP, adenosine triphosphate; LDH, Lactate dehydrogenase; BrdU, bromodeoxyuridine, 5-bromo-2'-deoxyuridine. Data shows number of retrieved publications as readout. (D) Fifty percent inhibitory concentrations (IC$_{50}$) of selected FDA-approved TKI; top) compared to preclinical KRAS inhibitors (bottom). Note the statistically significantly higher IC$_{50}$ of KRAS inhibitors compared with TKI. Data source see supplementary reference list under 12.2, S8-S25. *n* = 1-4 published studies; P, overall probability by 2-way ANOVA. Figure modified from Arendt *et al.*[80].
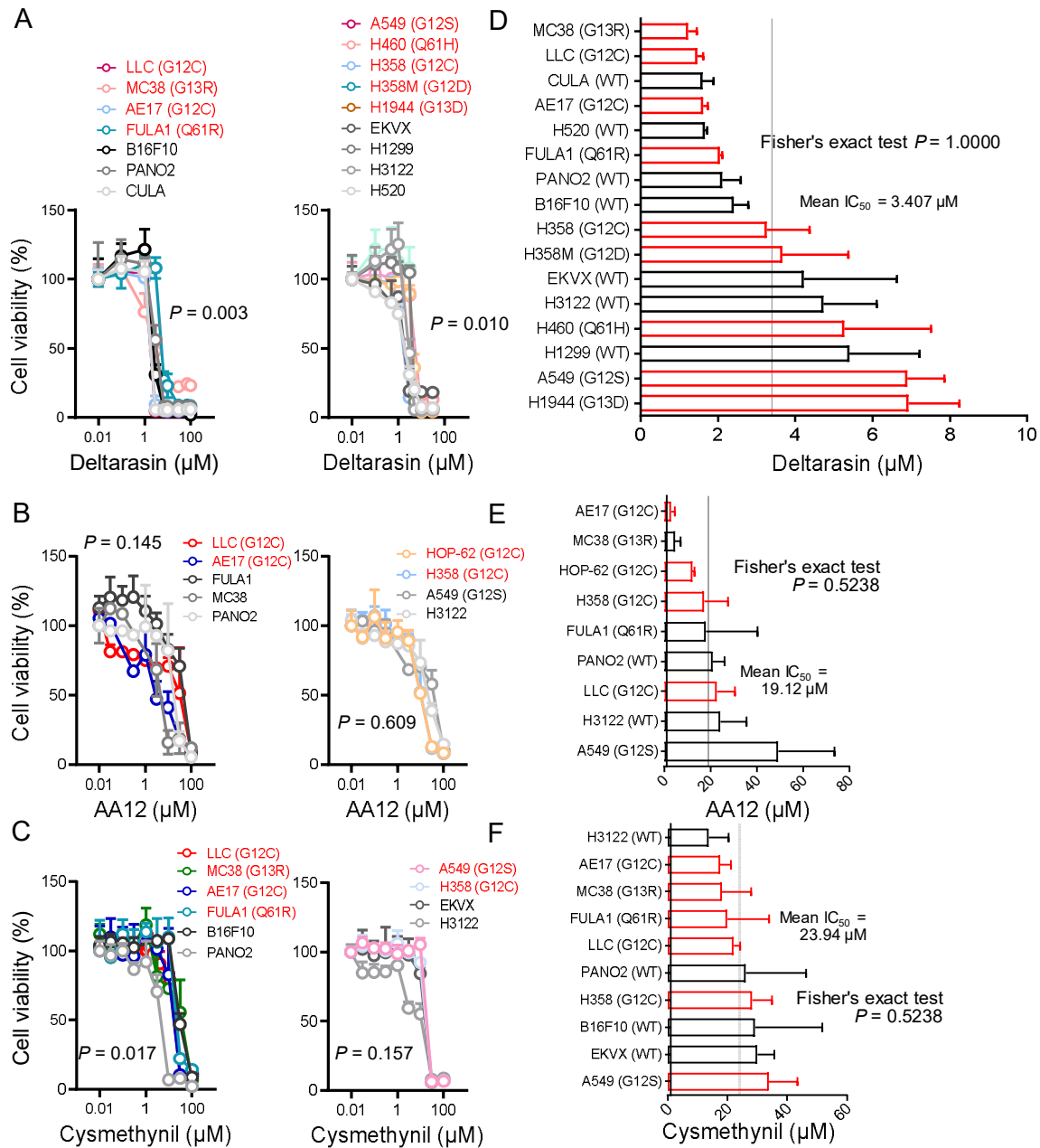
Figure 12: Primary resistance of *KRAS*-mutant tumor cells to *KRAS* inhibitors *in vitro*. Different mouse tumor cell lines (*Kras*[MUT]: LLC, MC38, AE17, FULA1; *Kras*[WT]: B16F10, PANO2) and human tumor cell lines (*Kras*[MUT]: A549, H460, H358, H358M, H1944, HOP-62; *Kras*[WT]: EKVX, H1299, H3122, H520) were assessed for cell viability (determined by WST-8 assay, point mutations are presented in parentheses). n = 3-5/cell line. (A-C) Representative sigmoidal curves of murine (left) and human (right) cell lines treated with increasing doses of deltarasin, AA12, or cysmethynil for 72 hours. n = 3/data point. (D-F) Averages of 50% inhibitory concentrations (IC$_{50}$, μM) of deltarasin, AA12, and cysmethynil on cell viability cancer cell lines. Mean (all cell lines tested), shown in grey lines, was used to separate sensitive and resistant cell lines. Note no significant differences regarding *Kras* mutation status. n = 3-5/data point. Data presented as mean ± SD. P, overall probability by nonlinear fit and extra sum of squares F-test (A-C) or by Fisher's exact test for cross-tabulation of Kras/KRAS mutation status to drug sensitivity/resistance. (D-F). Figure modified from Arendt *et al.*[80].

To solidify the *in vitro* results, we analyzed the response of murine ($n = 4$) and human ($n = 4$) cell lines to IC_{60} values of deltarasin via colony formation assay (Fig. 13A, B). Again, incubation with the KRAS blocker reduced the proliferation and formation of colonies independent of *KRAS* mutation status and not as expected specifically in *KRAS*^{MUT} cell lines (analyzed on basis of counted total colony formation and plating efficiency, supplementary Fig. S1). The human *KRAS*^{WT} cell lines H3122 and EKVX were even stronger inhibited after drug incubation. Since KRAS activates MAPK cascade inducing phosphorylation of ERK, we measured and quantified p-ERK/ GAPDH and t-ERK/ GAPDH via western blot in murine ($n = 6$) and human ($n = 6$) cell lines treated with saline or IC_{60} concentrations of deltarasin for 72h. Unexpectedly, deltarasin achieved an overall downregulation of the p-ERK signal independent from *KRAS* mutation status (Fig. 13C, D, supplementary Fig. S2). Thus, two additional assays strengthened our hypothesis that KRAS drugs fail specific *in vitro* inhibition.
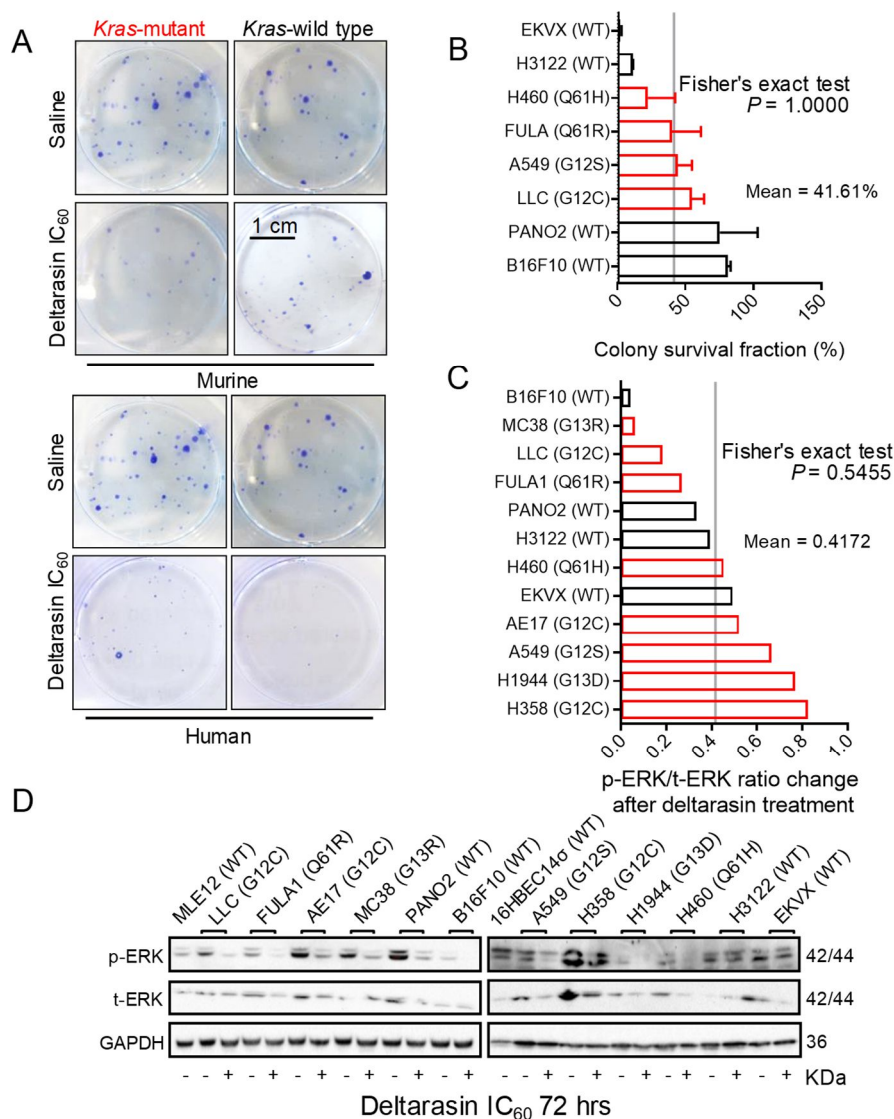
Figure 13: Unspecific response of *Kras/KRAS*[MUT] tumor cells to deltarasin *in vitro*. Multiple mouse and human cancer cell lines with (red) and without (black) *Kras/KRAS* mutations (point mutations shown in parentheses) were evaluated for colony formation by crystal violet (CV) staining and for ERK phosphorylation by phospho (p)- and total (t)-ERK immunoblots after 72 hours treatment with IC$_{60}$ concentrations of deltarasin. *(A)* Representative images of CV stained colonies treated with deltarasin or saline. (B) Colony survival fraction of human and murine cell lines after IC$_{60}$ deltarasin and 3–5 days culture. Values represent data from two independent experiments (*n* = 3/experiment). *(C)* Quantification of normalized p-/t- ERK signal. *(D)* Representative immunoblots of 72 hours treated cell lines with deltarasin or saline and p-ERK, t-ERK and GAPDH signals. Protein lysates pooled from 3 independent treatment experiments. Data presented as mean ± SD. *P*, probability by Fisher's exact test for cross-tabulation of *Kras/KRAS* mutation status to drug sensitivity/resistance. Figure modified from Arendt *et al.*[80].

6.2 Specific *in vivo* results of small molecule KRAS inhibitor deltarasin

In parallel to *in vitro* studies we induced sc tumors in *FVB, C57BL/6,* and *Rag2^{-/-}* mice with *KRAS*[MUT] cell lines LLC (*Kras*[G12C]), FULA1 (*Kras*[Q61R]) or H460 (*KRAS*[Q61H]) and treated mice daily with deltarasin ip (15 mg/Kg) or saline after tumor development (start of treatment: tumor volume ≥ 100 mm^3 and at least 10 days latency post sc injection). The dose was thereby chosen based on literature research and validation done by Zimmermann *et al*[49]. Surprisingly, the drug significantly reduced tumor growth harboring a *KRAS* mutation, but not tumors generated from *KRAS*[WT] cell lines B16F10, PANO2 or EKVX (Fig. 14A, B). Therefore, we hypothesized that deltarasin induced KRAS inhibition depends on an *in vivo* surrounding and is not reproducible in basic cellular assays.
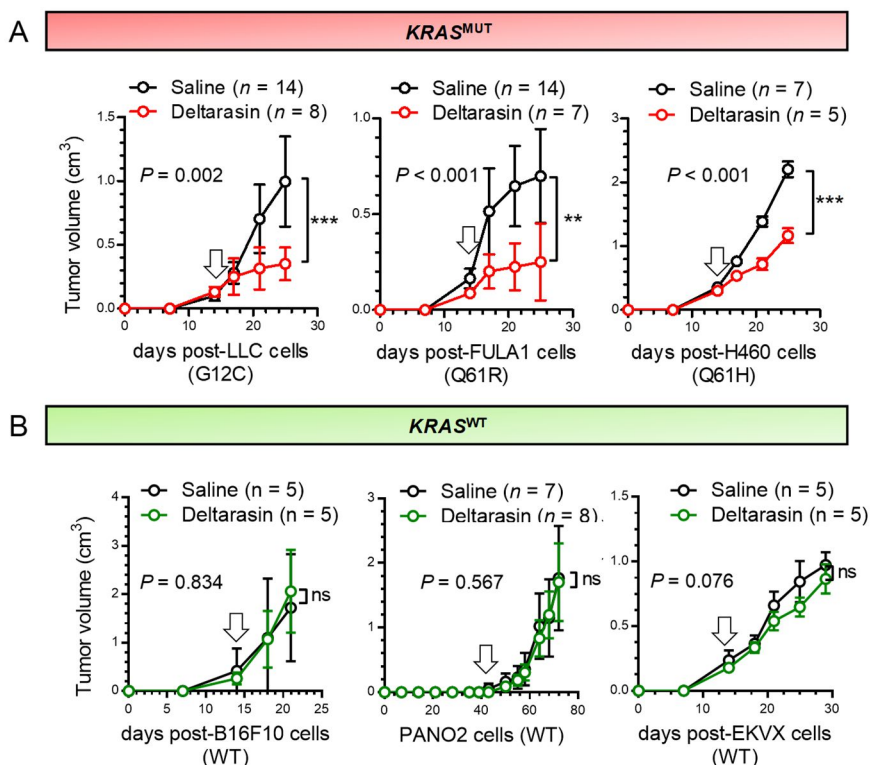
Figure 14: Selective *KRAS* mutation efficacy of deltarasin *in vivo*. Murine and human tumor cell lines with (A; *KRAS*[MUT]: LLC, FULA, H460) or without (B; *KRAS*[WT]: B16F10, PANO2, EKVX) *Kras/KRAS* mutations (codon change in parentheses) were sc injected in the murine flank (10^6 tumor cells) of *C57BL/6, FVB*, or *Rag2^{-/-}* mice. Daily ip injections of saline or 15 mg/Kg deltarasin after tumor development > 100 mm^3 size. Tumor growth is significantly reduced in *KRAS*[MUT] tumors. Data presented as mean ± SD. *n*, sample size stated in the figure; *P*, 2-way ANOVA and Bonferroni post-test; ns, *, **, ***, and ****: *P* > 0.05, *P* < 0.05, *P* < 0.01, *P* < 0.001, and *P* < 0.0001.

6.3 Opposing dependencies *in vitro* and *in vivo* in genetic modified *KRAS* models

To further validate the *in vivo* restricted role of hyperactive KRAS we overexpressed either shRNA (sh*Kras*) in murine *Kras*^{MUT} cell lines or p*Kras*^{G12C} plasmid (plasmid maps see supplementary Fig. S3) in *Kras*^{WT} cell lines[41]. These genetic manipulated cell lines were validated on RNA and protein levels, monitored over 150 hours in culture and studied with MTT reduction assays by colleagues 2017[41]. They showed that mutant KRAS does not affect cell viability *in vitro*. In accord with our inhibitor studies, genetic *Kras* intervention did not achieve a mutation specific effect to deltarasin, determined by IC$_{50}$ value calculation after 72 hours of drug incubation *in vitro,* followed by cell viability assays (Fig. 15A, B). Only one out of six cell lines showed a significant reduction of cell viability, but with opposite effect. Deltarasin was effective in the sh*Kras* MC38 cell line and not in the parental MC38 harboring a *Kras*^{G13R} mutation. Additionally, we used the parental wildtype human cell lines EKVX and H3122 and overexpressed mutant KRAS by transfection of the p*KRAS*^{G12C} plasmid (validation in Supplementary Fig. S4). Transfection did not change the response to different concentrations of deltarasin on cell viability, as expected (Fig. 15A, C). Furthermore, the analysis of ERK phosphorylation revealed no ERK activation after *Kras/KRAS* modulation. Knockdown of hyperactive KRAS with shRNA does show a slight reduction in p-ERK signal, but introduction of p*Kras*^{G12C} does not increase it (Fig. 15D, E; supplementary Fig. S5). In summary, our *in vitro* observations done with three preclinical KRAS inhibitors, and using three different *in vitro* assays showed no consistent KRAS dependency. Of seven genetic modified cell lines only one cell line showed the expected result after deltarasin treatment in the WST-8 assay (MC38 sh*Kras*). Only 36% of the *Kras/KRAS*^{MUT} murine and human cell lines responded to deltarasin and only 17% to cysmethynil. Downregulation of ERK phosphorylation and decrease in colony formation by deltarasin treatment was achieved irrespective of mutant KRAS status in both genetic modified cell lines and parental *Kras/KRAS*^{MUT} or *Kras/KRAS*^{WT} cells. Thus, *in vitro* systems are not optimal to study KRAS and to develop effective inhibitors.

Interestingly, the same genetic modified cell lines showed significant capability to reduce tumor growth *in vivo*: sh*Kras* knockdown in murine cell lines displayed a strong tumor growth decrease over time compared to unmodified cell lines (50-90% biological and statistical ($P <$ 0.001) inhibition). *Vice versa*, introduction of p*Kras*^{G12C} increased the tumor growth rate drastically (Fig. 17A, B). Deltarasin tested in PANO2 p*Kras*^{G12C}- and EKVX p*Kras*^{G12C}-flank tumors had a very good drug response compared to parental cell lines (Fig. 17C). Collectively, these experiments support our findings of inhibiting KRAS pharmacologically. Again, tumor growth seems to be selectively inhibited *in vivo*.
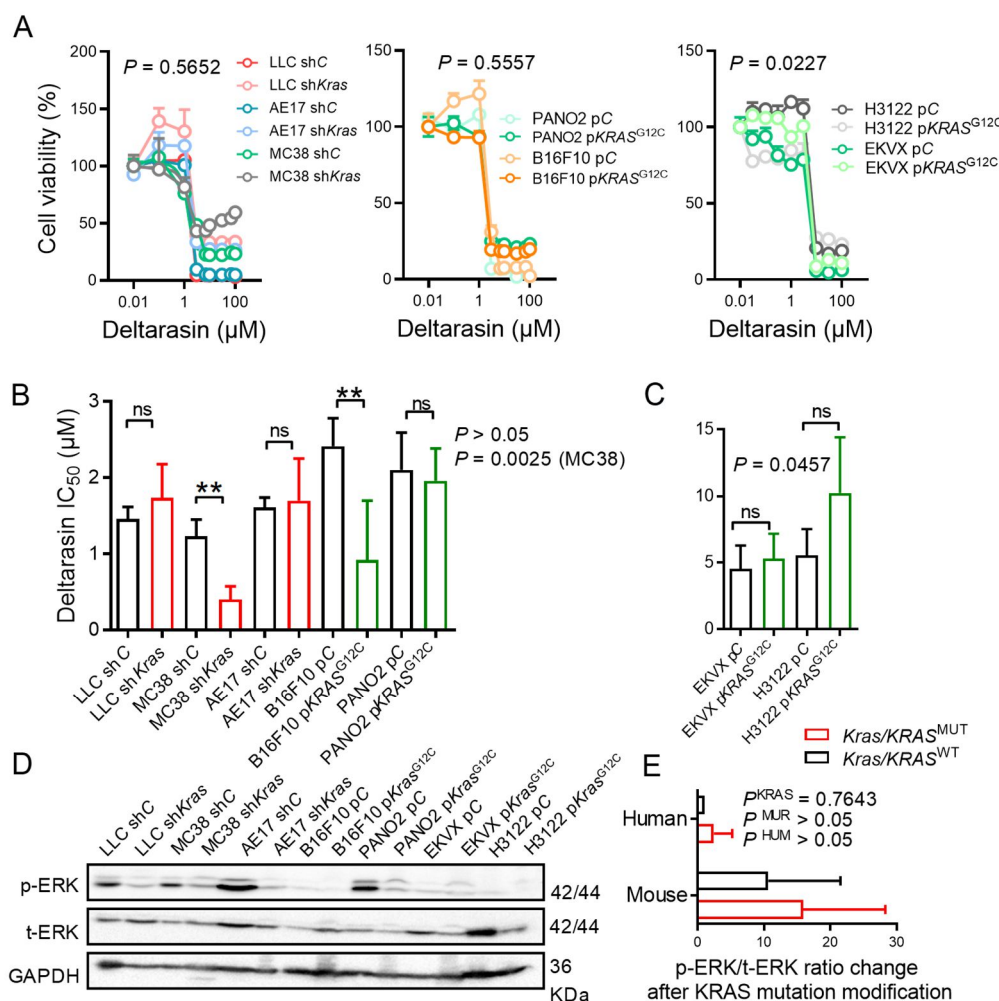
Figure 15: Genetic manipulation of *Kras/KRAS* shows no dependency *in vitro.* (A) Representative sigmoidal curves of different murine and human cell lines with *Kras/KRAS* modification treated with half-log concentrations of deltarasin to assess cell viability after 72 hours of drug treatment. *n* = 3/data point. (B) IC_{50} concentrations of deltarasin treatment in parental (black: stably expression of random shRNA or control plasmid pC) or *Kras*-modified (red: stably expression of sh*Kras* RNA; green: stably expression of mutant $KRAS^{G12C}$ plasmid) tumor cell lines (*n* = 2-4/data point by independent experiments). (C) Human parental (black: stably expression of control plasmid pC) or Kras-modified (green: stably expression of mutant $KRAS^{G12C}$ plasmid) tumor cell lines were assessed for cell viability (determined by WST-8 assay, *n* = 2 - 5/ data-point) after 72 hours of drug treatment. (D) Exemplary immunoblots of cell lines for p-ERK, t-ERK and GAPDH. Protein lysates pooled from 3 independent experiments. (E) Quantification of normalized p-ERK/t-ERK signal after normalization to GAPDH. Individual data points were summarized by mutation status (red: $KRAS^{MUT}$; black: $KRAS^{WT}$) and origin (*n* = 2-3). *P*, overall probability by nonlinear fit and extra sum of squares F-test (A) or one-way (B, C) and two-way (E) ANOVA. ns and **: *P* > 0.05 and *P* < 0.01, respectively, for the indicated comparisons by Bonferroni post-tests. Data are presented as mean ± SD. Figure modified from Arendt *et al.*[80].
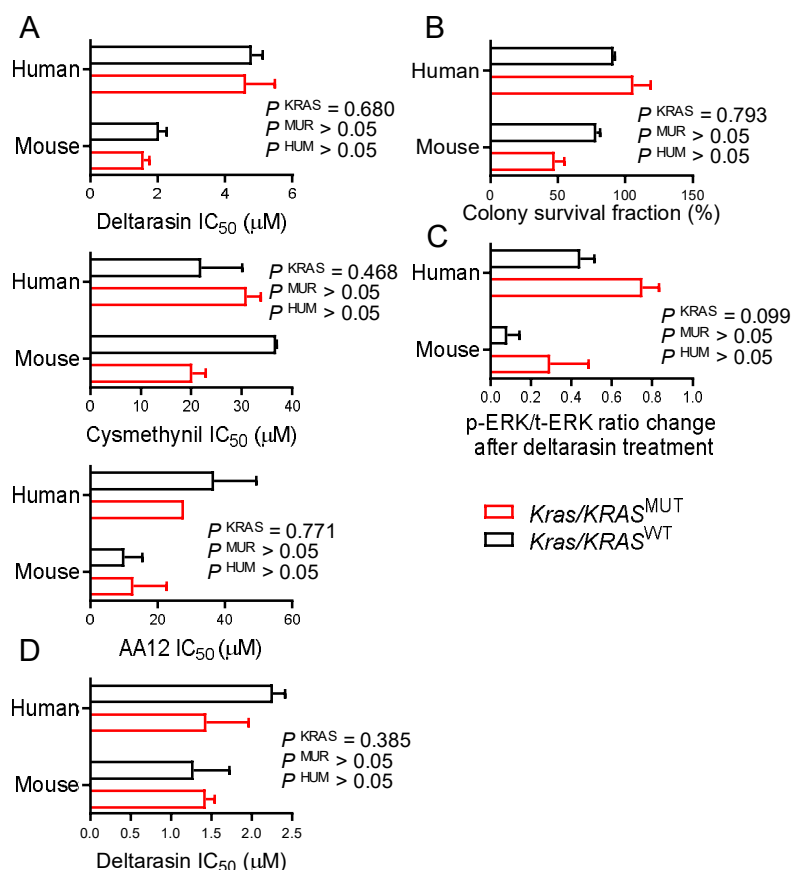
Figure 16: Summary of *in vitro* experiments grouped by species (human and murine) and *Kras/KRAS* mutation status. (A) Summary of IC$_{50}$ values of three KRAS inhibitors deltarasin (n = 3,3; 5,4), AA12 (n = 2,3; 2,2), and cysmethynil (n = 4,2; 2,2) determined by WST-8 assay. (B) Summary of colony formation assay after deltarasin treatment (n = 2,2; 2,2) (C) Summary of western blot analysis and quantification of p-ERK and t-ERK relative to GAPDH (n = 4,2; 4,2). (D) Summary of IC$_{50}$ values of genetic modified cell lines treated with deltarasin and determined by WST-8 assay (n = 5,5; 2,2). P, overall probability by two-way ANOVA. ns: P > 0.05 for the indicated comparisons by Bonferroni post-tests. Data are presented as mean ± SD. n = murine *Kras*^{MUT}, Kras^{WT}; human *KRAS*^{MUT}, *KRAS*^{WT} cell lines.
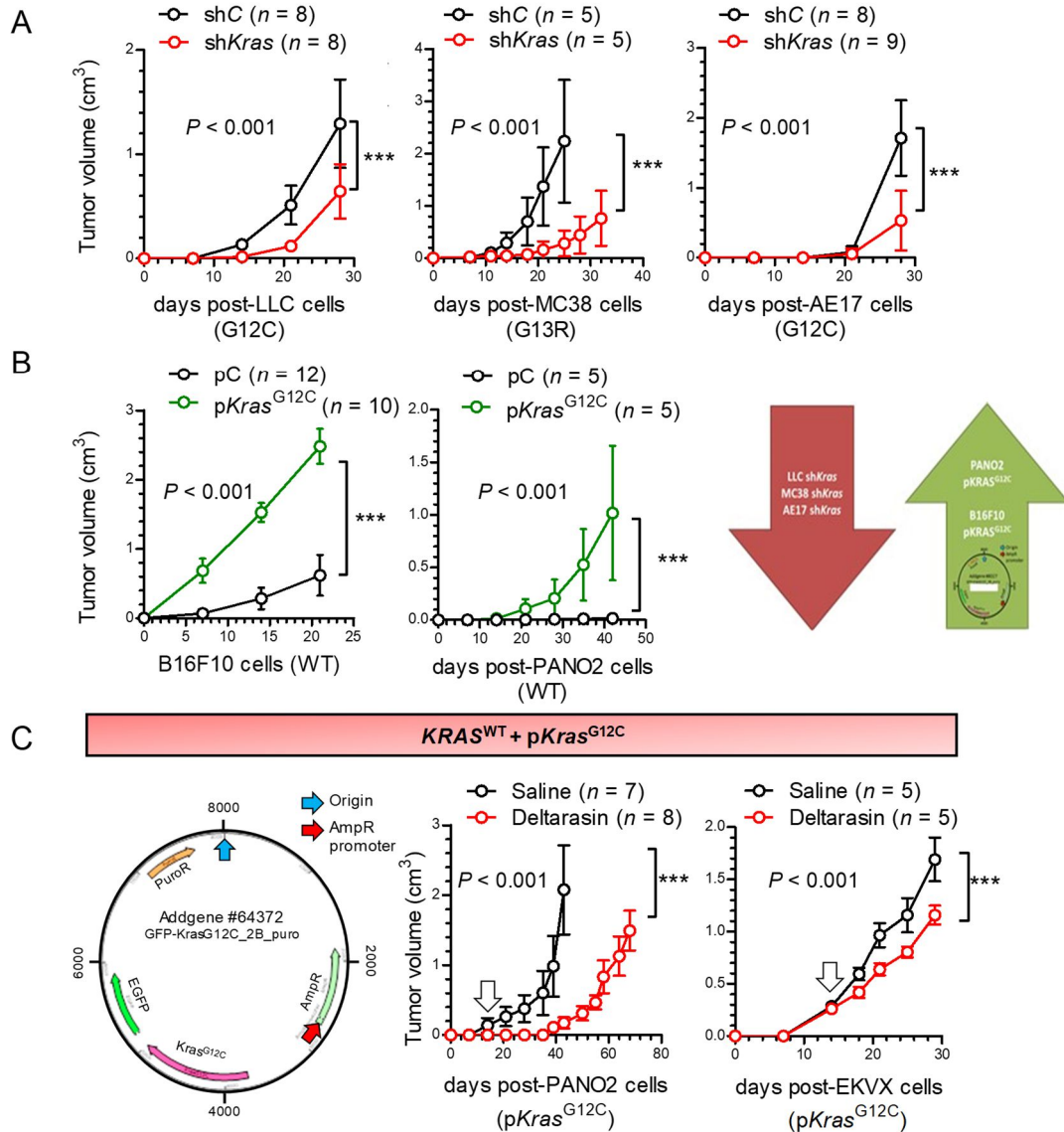
Figure 17: Genetic manipulation of *Kras* shows high dependency *in vivo*. *C57BL/6* mice harboring flank tumors of genetic modified murine cells ((A) sh*Kras*; red, (B) p*Kras*^{G12C}; green) or control cells (sh*C*, p*C*; black) were grown over time and monitored (right: graphic of the effect of genetic *Kras* intervention by shRNA downregulation, red; or plasmid overexpression, green). (C) PANO2 and EKVX overexpressing *Kras* mutant plasmid p*Kras*^{G12C} (Left: graphic of the introduced plasmid containing *KRAS*^{G12C}, *GFP*, and *PUROMYCIN*^{R} sequences), were injected in the murine flank (10^6 tumor cells sc) of either C57BL/6 or Rag2$^{-/-}$ mice. Daily ip injections of saline (black) or 15 mg/kg deltarasin after tumor development > 100 mm^3 size. Data presented as mean ± SD. *n*, sample size stated in the figure; *P*, 2-way ANOVA and Bonferroni post-test; ns, *, **, ***, and ****: *P* > 0.05, *P* < 0.05, *P* < 0.01, *P* < 0.001, and *P* < 0.0001. Figure modified from Arendt *et al.*[80].

6.4 Exclusive *in vivo* development of secondary resistance

A common response of targeted therapy is the development of secondary resistance. We detected these trends in LLC and FULA1 induced flank models post day 28 of daily ip treatment with deltarasin (Fig. 18A). Therefore, we wanted to test the reproducibility of this effect *in vitro* by constantly treating both cell lines with the IC_{60} concentration of the drug over the time of 22 weeks (Fig. 18B). Changes in cell viability were tested at week 1, 12 and 22 via repeating cell viability assays. At all three time points IC_{50} values were in the same range. This indicates an unresponsiveness of monolayer plated cell lines to the drug. We established primary cell lines from flank tumors of LLC and FULA1 from control, sensitive, and resistant mice ($\geq$ 28 days treatment, highlighted by arrows Fig. 18A). These cell lines were isolated and directly tested to their drug response *in vitro*. Expectedly, we were not able to detect similar drug responses in these cell lines, which behaved strongly different *in vivo* (Fig. 18C). These results present the strong mutant specific *in vivo* effect achieved by deltarasin, which vanishes immediately if the *in vivo* setting is lost and cannot be reproduced with basic cellular assays.
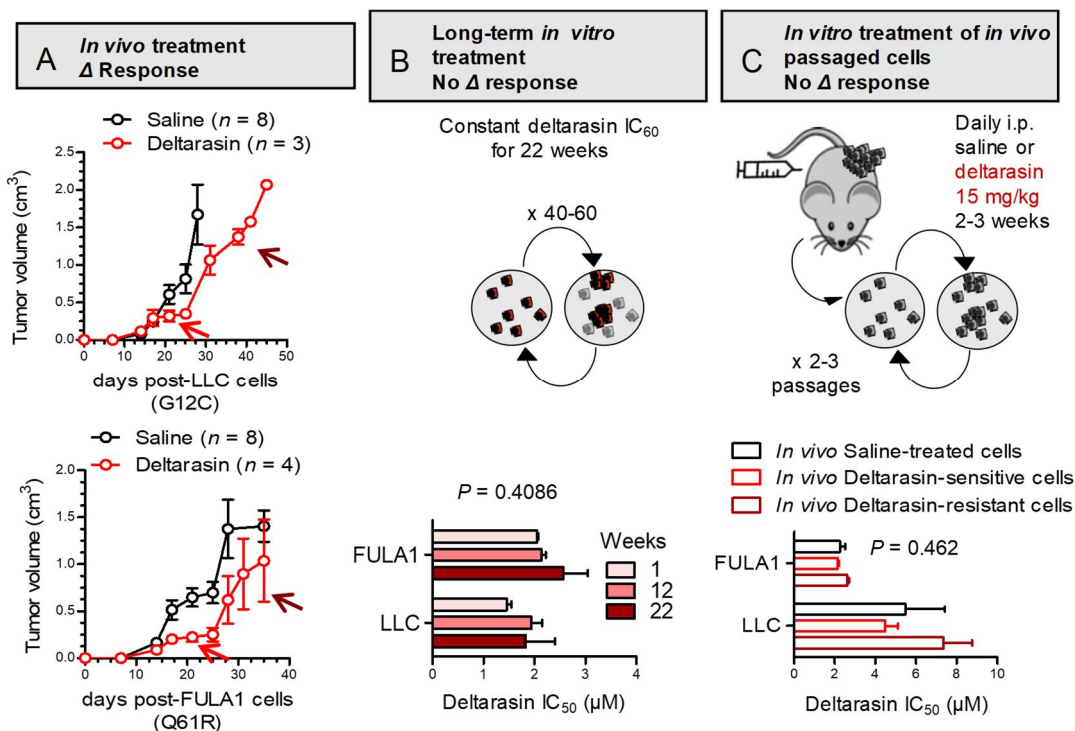
Figure 18: Development of secondary resistance *in vivo* is not reproducible *in vitro*. (A) *C57BL/6* mice with growing flank tumors from 10^6 sc LLC or FULA1 cell injection (*Kras*[MUT]) were treated daily with ip saline or deltarasin (15 mg/kg) and developed secondary resistance on day 25 to 30. Arrows indicate timepoints (red: early drug sensitive state, dark red: late drug resistant state) of extracted tumors for further development of cell lines from different mice (*n* = 1 per state). (B) FULA1 and LLC cells were treated constantly with IC_{60} deltarasin concentrations for 22 weeks and response to the drug was monitored during WST-8 assay on week 1, 12, and 22 (*n* = 3). No altered drug response measurable. (C) Extracted tumor cells were passaged 2-3 times and response to deltarasin was evaluated using WST-8 assay (*n* = 3) of saline treated, deltarasin sensitive and deltarasin resistant tumor cells. Data presented as mean ± SD. *P*, overall probability by two-way ANOVA for the indicated comparisons by Bonferroni post-tests.

6.5   High expression of Ccl2 and Il1r1 in *Kras*-mutant transcriptome profile

Trying to answer the question which mediators are responsible for the *in vivo* only dependency to mutant *Kras*, we analyzed the transcriptome of parental as well as *Kras*-modulated cell lines and benign samples [bone marrow-derived macrophages (BMDM), mast cells (BMMC) whole lungs, and tracheal epithelial cells (TEC)].
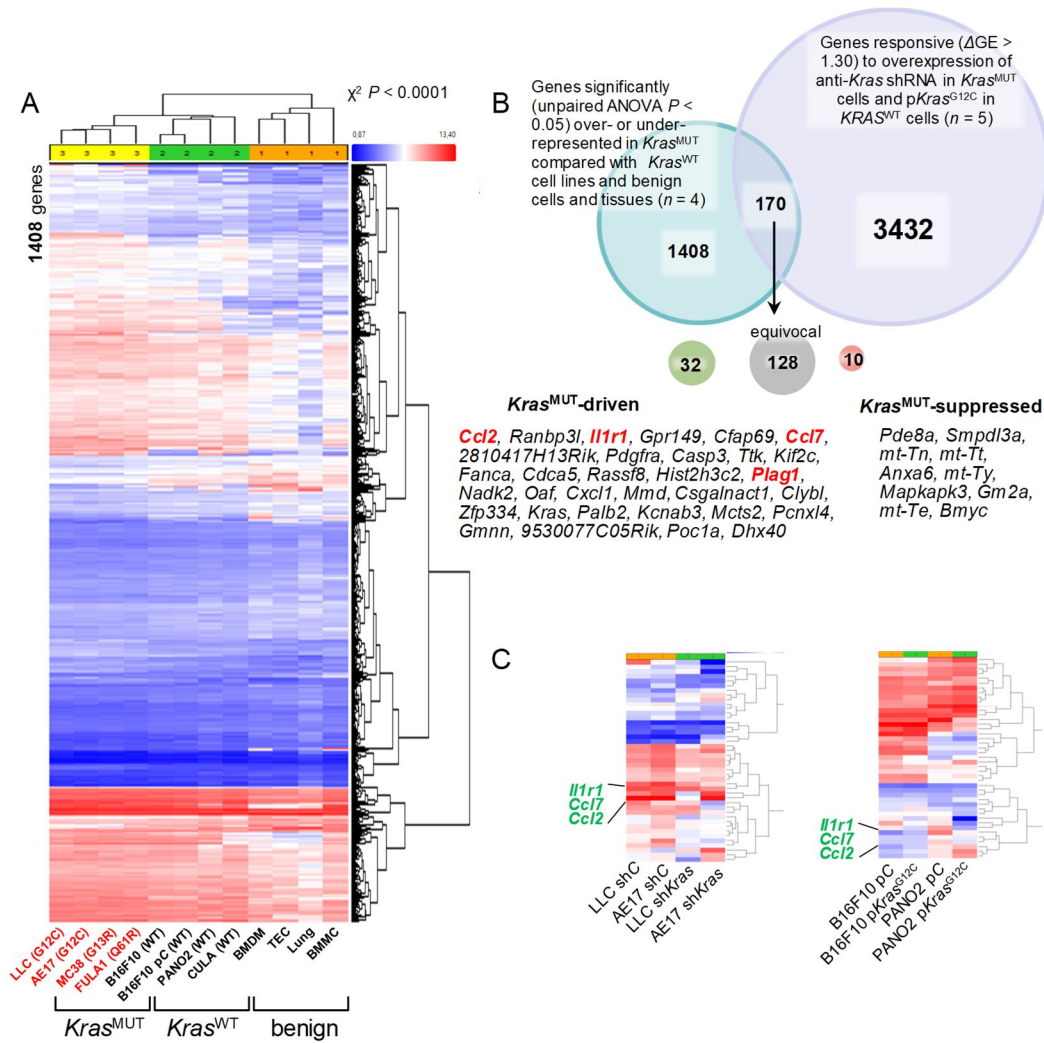
Figure 19: A 42-gene KRAS dependent signature containing inflammatory mediators *Ccl2* and *Il1r1*. (A) Unsupervised hierarchical clustering of gene expression of $Kras^{MUT}$ (n = 4), $Kras^{WT}$ cells (n = 4) and benign cells and tissue (n = 4). (B) Analytical strategy of the transcriptome analysis explained as Venn diagram. (C) Unsupervised hierarchical clustering of gene expression of genetic modified cell line doublets (sh*Kras* versus p*Kras*^{G12C}) reveals correlation of *Il1r1* and *Ccl2*.; P, family-wise error rate probability; n = 2 for every single cell line. Figure modified from Arendt et al.[80].

Unsupervised hierarchical clustering with all parental cell lines showed absolute segregated clustering of $Kras^{MUT}$ cell lines, $Kras^{WT}$ cell lines and benign samples (1408 differentially expressed genes (ΔGE) using an ANOVA P < 0.05 threshold, Fig. 19A). By paired analysis of genetic modified cell lines (LLC, MC38, and AE17 sh*C* versus sh*Kras* and PANO2 and B16F10 p*C* versus p*Kras*^{G12C}) with isogenic cell line doublets, we detected another 3432 *Kras*-responsive transcripts.

Out of 170 transcripts that were present in both gene sets and by excluding every ambiguous gene expression, we ended up with a profile including 32 upregulated genes and 10 downregulated genes regulated by mutant *Kras* (ΔGE > 1.40, Fig. 19B). Interestingly, it contained inflammatory modulators like *Ccl2, Ccl7, Cxcl1*, and *Il1r1* and revealed a tight correlation of these mediators (Fig. 19C). Using WikiPathway analysis and the murine pathway database we found a strong probability of our *Kras*^MUT expression profile in chemokine signaling (Fig. 20A)[75]. To proof the relation to human data, we next translated the murine genes to 37 human orthologues using Orthoretriever (https://www.orthodb.org/and) and run GSEA (http://software.broadinstitute.org/gsea/index.jsp)[74]. A comparison to the Broad institute's 50 hallmark signature including gene sets of angiogenesis, PI3K-AKT-MTOR signaling, and DNA repair, revealed a highly positive enrichment in only one signature, the "inflammatory response" and negative in the "G2M- checkpoint"signature (Fig. 20C, D, supplementary list 12.3 for full hallmark gene list)[86]. Moreover, we used a BATTLE trial dataset consisting of microarray data from 21 *KRAS*^MUT and 17 *EGFR*^MUT NSCLC patient samples (GSE31852), in which the *KRAS*^MUT profile was significantly positive enriched in *KRAS*-mutant LADC only, validating our *Kras*^MUT specific genes in a human cohort (Fig. 20B)[83]. These results led to the assumption that proinflammatory signals are responsible for *in vivo* restricted inhibition of *KRAS*^MUT lung cancer.

6.6 CCR2+ myeloid cells secreting IL-1ß as key players of *in vivo* KRAS-dependence

Next, we wanted to test the importance of CCR2+ IL-1β- secreting myeloid cells for KRAS^MUT tumors. Immunofluorescence staining's of murine and human tumor tissue by immunofluorescence visualized co-existence of IL-1β and CCR2 in the tumor tissue (Fig. 21, 22).
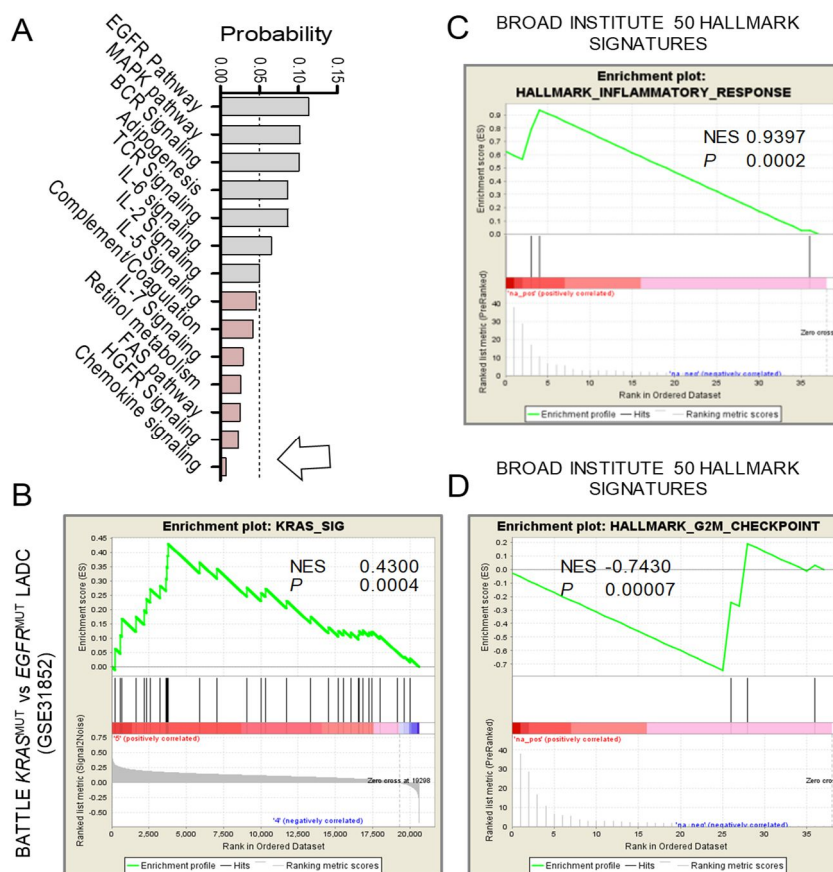
Figure 20: Correlation of 37 human homologs of the *Kras*-specific genes with signaling pathways. (A) Wikipathway analysis showing chemokine signaling overrepresented in the KRAS signature. (B) GSEA analysis of 37 human orthologues against BATTLE dataset containing KRAS^{MUT} (n = 21) and EGFR^{MUT} (n = 17) LADC samples reveals strong correlation to human KRAS^{MUT} signature. (C) Top: GSEA of 37 human orthologues shows more positive enrichment in "inflammatory response" compared to negative enrichment (D) in "G2M checkpoint" (Broad Institute's 50 hallmark signatures). NES, normalized enrichment score; P, family-wise error rate probability. Figure modified from Arendt *et al.*[80].
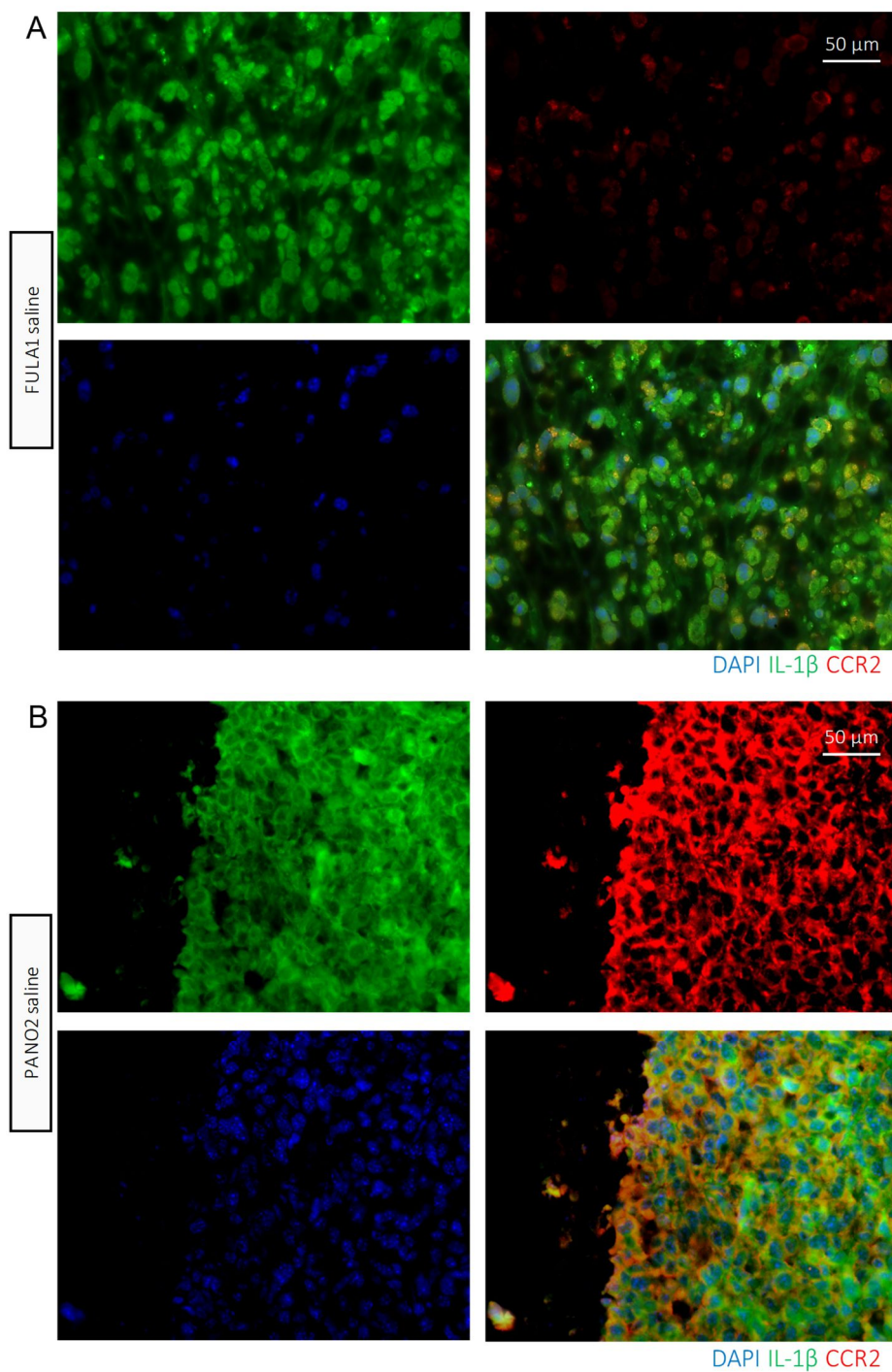
Figure 21: Immunofluorescence images of tumor tissue sections. Murine tumors were established through sc injection of 10^6 tumor cells (FULA1 or PANO2) and extracted from these allograft flank models (*C57BL/6* and *FVB* mice). Immunofluorescence stainings for IL-1β (Alexa488) and CCR2 (Alexa647). Bar = 50 μm. Secondary antibody control stainings see supplementary figure. S7.
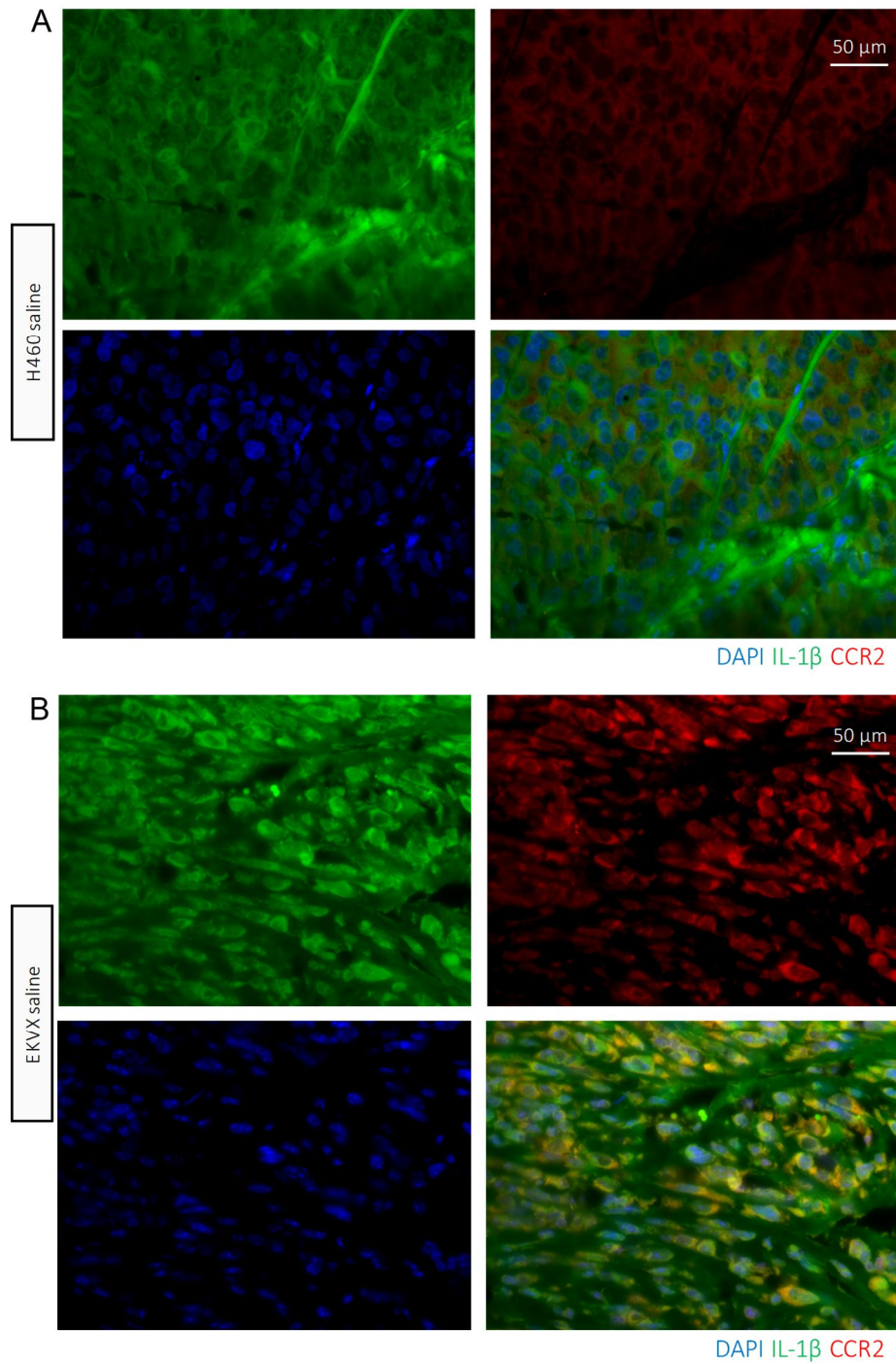
Figure 22: Immunofluorescence images of tumor tissue sections. Human tumors were established through sc injection of 10^6 tumor cells (H460 or EKVX) and extracted from these xenograft flank models (*Rag2*$^{-/-}$ mice). Immunofluorescence stainings for IL-1β (Alexa488) and CCR2 (Alexa647). Bar = 50 μm. Secondary antibody control stainings see supplementary figure S7.

To proof our hypothesis, we used syngeneic *C57BL/6* mice deficient (*Il1b*$^{-/-}$, *Ccr2*$^{-/-}$) in the *Il1b* and *Ccr2* genes or competent (*WT*) mice to induce flank tumors induced with sc injection of LLC cells (*Kras*^{G12C}). Response to daily ip deltarasin (15 mg/Kg) or saline treatment (after tumor size ≥ 100 mm^3) was monitored bi-weekly. As seen before deltarasin was able to reduce statistically and biologically significant tumor growth in WT mice (Fig. 23A). Surprisingly, *Kras*^{MUT}- specific deltarasin effect was completely depleted in *Ccr2*$^{-/-}$ and highly reduced in *Il1b*$^{-/-}$ mice (Fig. 23B). No changes were displayed in chemokine-receptor-knockouts *Cxcr1*$^{-/-}$ and *Cxcr2*$^{+/-}$ mice (Fig. 23C).

To eliminate the option of developmental effects of knockout mice, we used a bone marrow transplant (BMT) experiment using syngeneic FVB mice (*Ccr2*$^{-/-}$ and *WT* mice back-crossed > F12 to the *FVB* strain) and FULA1 cells (*Kras*^{Q61R}). This allowed us to gather results with another cells line and a different *Kras* mutation, as well as broaden the spectrum of mutations closer to human LADC. We next irradiated (900 Rad) *Ccr2*$^{-/-}$ mice to erase all bone marrow (BM) cells. On this background we injected BM from either *WT* or *Ccr2*$^{-/-}$ donors. After recovery time of 30 days FULA1 cells were sc injected and established flank tumors (≥ 100 mm^3) were treated as usual with daily ip deltarasin or saline. Expectedly, *Ccr2*$^{-/-}$ with BM from the same knockout mice did not respond to drug treatment as shown before (Fig. 23B right, 24A right). Instead, *Ccr2*$^{-/-}$ chimeras with *WT* BM reproduced the original statistically and biologically significant drug effect seen in wildtype mice (Fig. 23A, 24A left). Taken together, these results specify that CCR2+ myeloid cell recruitment is required for deltarasin efficacy against *Kras*-mutant tumors *in vivo*. To develop a different tumor model, we transfected FULA1 cells with shRNA against CCL2 to downregulate its expression. Cell clones were selected with puromycin and then picked. Validation was done with ELISA using supernatants of 5 clones (sh*Control* and sh*CCL2*). CCL2 expression is significantly downregulated under sh*CCL2* expression and these cell clones will be used for further experiments in the future Fig. 24B).
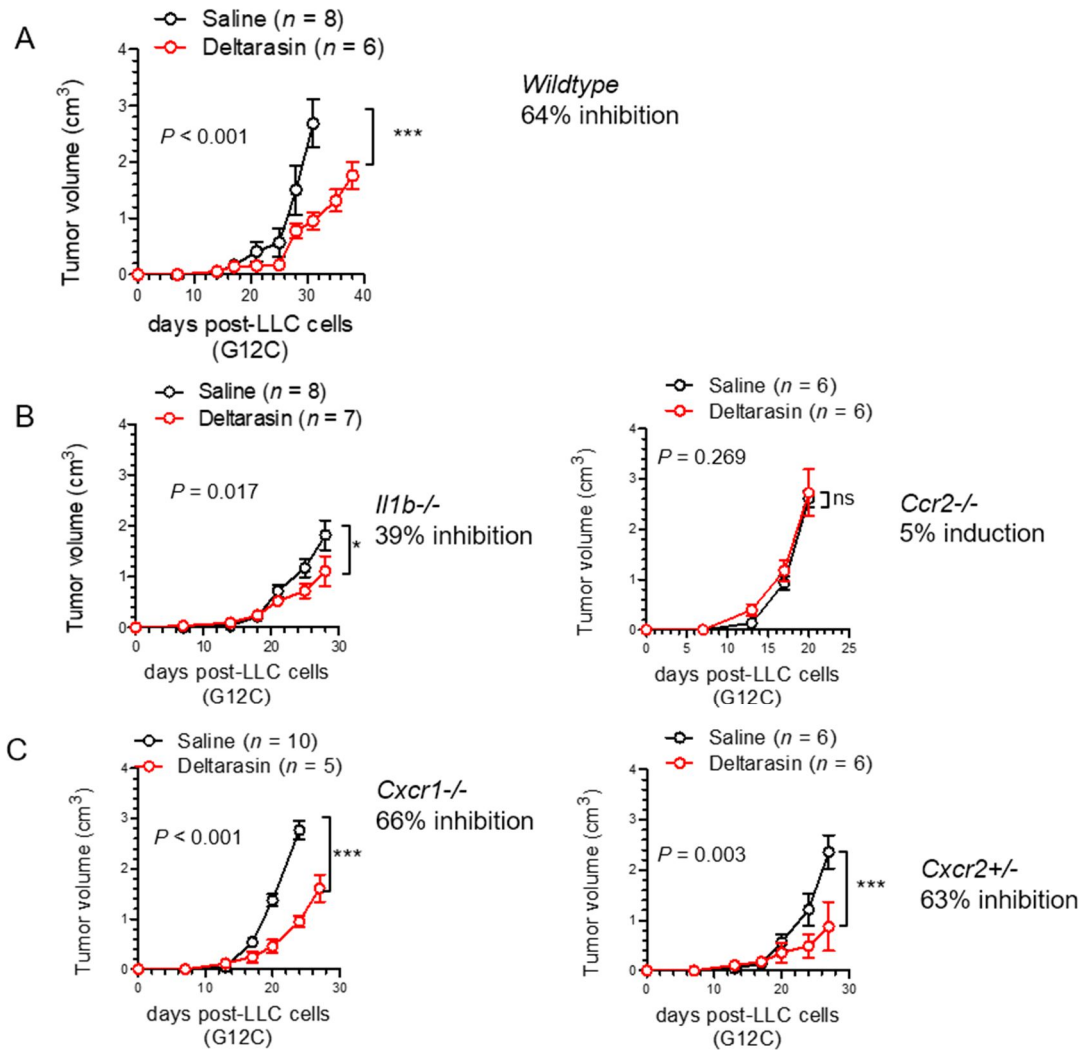
Figure 23: Selective efficacy of the *KRAS* inhibitor deltarasin depends on host CCR2 and IL1B. 10^6 LLC cells (*Kras*^{G12C}) were injected sc for Kras mutant tumor establishment in the rear flank of different knockout mice with *C57BL/6* background. Tumor volume was monitored during daily ip injections of saline (black) or 15 mg/kg deltarasin after tumor development to 100 mm^3 size. (A) Exemplary image of CCR2/IL-1β-co-staining of a *KRAS*-mutant tumor from a *Rag2*$^{-/-}$ mouse presenting co-localization in the tumor stroma. (B) Syngeneic *C57BL/6* wildtype mice with *KRAS*^{MUT} tumors showing efficacy of deltarasin treatment. (C) Il1b$^{-/-}$ and Ccr2$^{-/-}$ deficient mice harboring *KRAS*^{MUT} tumors grew similar in both treatment and saline groups. (D) Deltarasin treatment in Cxcr1$^{-/-}$ and Cxcr2$^{+/-}$ mice with *KRAS*^{MUT} tumors significantly reduced tumor growth alike wildtype *C57BL/6* mice. In brackets: Percentile tumor inhibition by deltarasin compared with saline. *n*, sample size stated in the figure. Data are presented as mean ± SD. *P*, overall probabilities by 2-way ANOVA; ns, *, **, ***, and ****: *P* > 0.05, *P* < 0.05, *P* < 0.01, *P* < 0.001, and *P* < 0.0001.
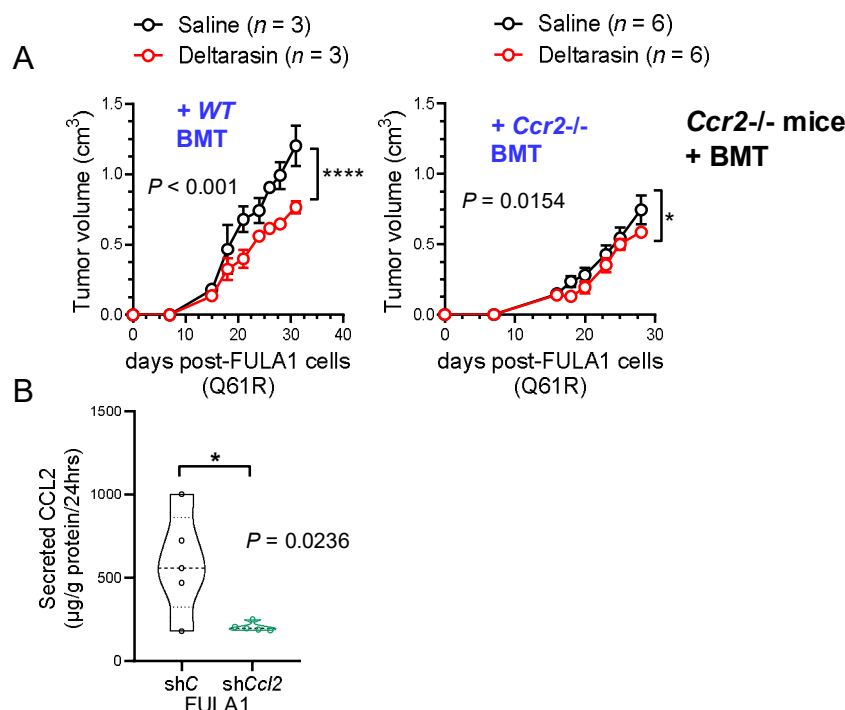
Figure 24: *Kras*-mutant cancer cells require host Ccr2 signaling, which can be disturbed by deltarasin mediated *IL1R1* expression downregulation. (A) *Ccr2*$^{-/-}$ mice were total-body irradiated with 900 Rad before receiving adoptive BMT from *WT* (black, left graph) or *Ccr2*$^{-/-}$ (black, right graph) donors (back-crossed > F12 to the *FVB* strain). One month later both chimera groups received sc 10^6 syngeneic FULA1 cells (*Kras*^{Q61R}). Daily ip saline or deltarasin (15 mg/Kg, red) treatments were started when tumors grow > 100 mm^3. *n*, sample size stated in the figure. Data presented as mean ± SD. *P*, 2-way ANOVA and Bonferroni post-test; ns, *, **, ***, and ****: $P > 0.05$, $P < 0.05$, $P < 0.01$, $P < 0.001$, and $P < 0.0001$. (B) FULA1 cells were transfected with sh*CCL2* or sh*C* mRNA to downregulate CCL2 expression. Validation of positive knockdown done with supernatants of transfected cell lines and ELISA to quantify secreted CCL2 levels. *n* = 5 samples/group; Data presented as mean ± SD. *P*, unpaired t-test. *: $P < 0.05$. Figure modified from Arendt *et al.*[80].

6.7   Deltarasin disrupts IL-1β sensing in *KRAS*-mutant tumor cells

From the microarray-derived *Kras*^{MUT} signature including *Ccl2* and *Il1r1* (Fig. 18B) and previous reports of *KRAS*^{MUT}-mediated *CCL2* and *IL1R1* transcriptional regulation we wanted to investigate the underlying signaling pathway[30,36,79]. To gain these insights in the mechanism of *in vivo* specific deltarasin dependence, we validated the expression of *Il1r1/IL1R1* mRNA and CCL2 protein levels (using LLC, PANO2, H460, EKVX post 72 hours deltarasin treatment) via qPCR and ELISA. Indeed, murine and human *Kras/KRAS*^{MUT} cancer cell lines displayed strikingly increased *Il1r1/IL1R1* mRNA expression related to *Kras/KRAS*^{WT} cell lines.

Furthermore, deltarasin treatment significantly downregulated *Il1r1/IL1R1* transcript levels (Fig. 25A). However, *Kras/KRAS*[MUT] cell lines demonstrated increased and decreased secretion of CCL2 after deltarasin compared with *Kras/KRAS*[WT] cell lines, suggesting that the bulk of *in vivo* deltarasin effect is mediated via downregulation of *Il1r1/IL1R1* expression (Fig. 25B).
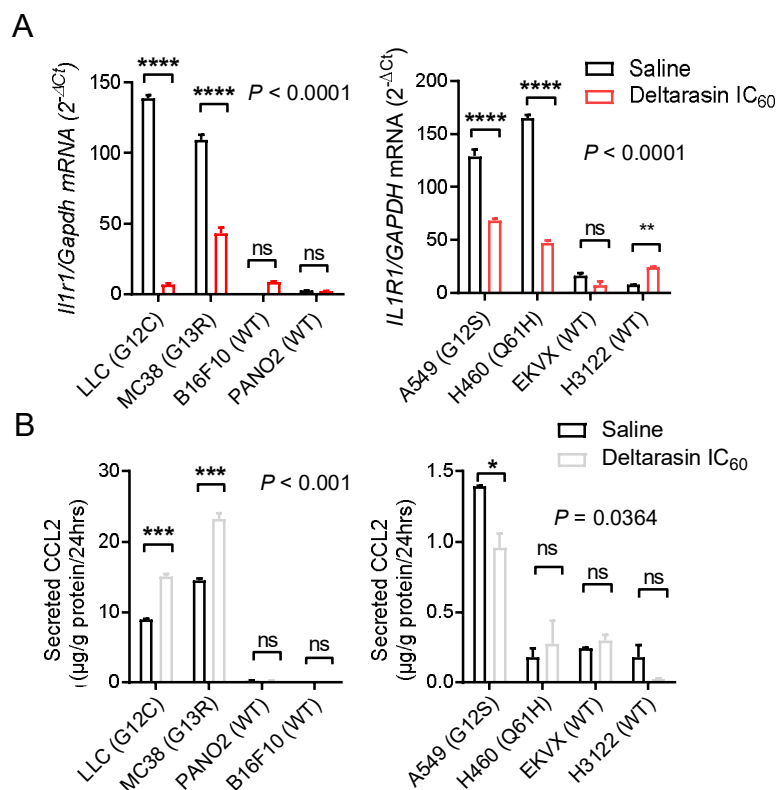

Figure 25: Deltarasin treatment decreases *Il1r1/IL1R1* mRNA expression consistently in *Kras*[MUT] cell lines but has different effects on CCL2 secretion. (A) mRNA expression of *Il1r1/IL1R1* done by qPCR and (B) protein secretion of CCL2 done by ELISA. Mouse (left) and human (right) cancer cell lines were treated for 72 hours with saline or deltarasin IC_{60} concentrations. $n = 3$; data presented as mean ± SD. *P*, overall probabilities by 2-way ANOVA; ns, *, and ***: $P > 0.05$, $P < 0.05$ and $P < 0.001$, respectively, for the indicated comparisons by Bonferroni post-tests. Figure modified from Arendt *et al.*[80].

6.8   KRAS/CCL2/IL1B signature in human cancers

To analyze the significance of our findings to *KRAS*[MUT] human cancers, we evaluated the average gene expression of *KRAS/CCL2/IL1B* in a clinical cohort of smoker LADC ($n = 40$), never-smoker LADC ($n = 40$), and normal lung tissue samples ($n = 30$; GSE43458), public

data of the BATTLE trial[84]. Comparing never-smokers' LADC and normal lung tissue samples with smokers' LADC we found that overall *KRAS/CCL2/IL1B* expression was significantly increased (Figure 26A). In particular, we found higher expression of *IL1B* in smokers versus never-smokers, *CCR2* in smokers versus normal lung tissue and versus never-smokers, and *IL1R1* in smokers versus normal lung tissue. As a fact, *KRAS* mutations occur more frequent in LADC smoker[87]. This finding suggests that, in tumors harboring higher *KRAS* mutation rates the inflammatory signature is overrepresented. This was repeatable in a second dataset including patients with breast (*n* = 65), colorectal (*n* = 55), and lung cancer (*n* = 60; GSE103512), where overall *KRAS/CCL2/IL1B* expression was significantly higher in colorectal and lung cancer, which have high *KRAS* mutation frequencies, compared with breast cancer (Figure 26B)[85].

Assuming, that this inflammatory signaling loop is responsible for the exclusive *in vivo* specific KRAS inhibition, we run online Kaplan-Meier analyses (http://www.kmplot.com) using lung cancer patient data cohorts (Fig. 26C)[78]. Comparing *KRAS/CCL2/IL1B* expression levels in LADC (a tumor type proven to have high KRAS mutation frequency; *n* = 720) and SQCLC (a tumor type proven to have low KRAS mutation frequency; *n* = 520) showed that LADC patients with high expression of the three genes of interest showed poor survival compared to low expressers with a hazard ratio (HR) increase of 1.93. On the contrary, the survival curves of SQCLC were not impacted by the expression levels. When we looked exclusively at smokers only [meaning that looking at even higher *KRAS* mutation frequencies (26.5% versus 33.7%,[88])], HR increased in LADC up to 2.28, whereas patient survival in SQCLC data did not change. These data collectively suggest that human *KRAS*MUT cancers are affected by the KRAS/CCL2/IL1B loop through overexpressing it and thereby controlling survival. Moreover, this shows the clinical relevance of these inflammatory signaling mediators as possible new targets.
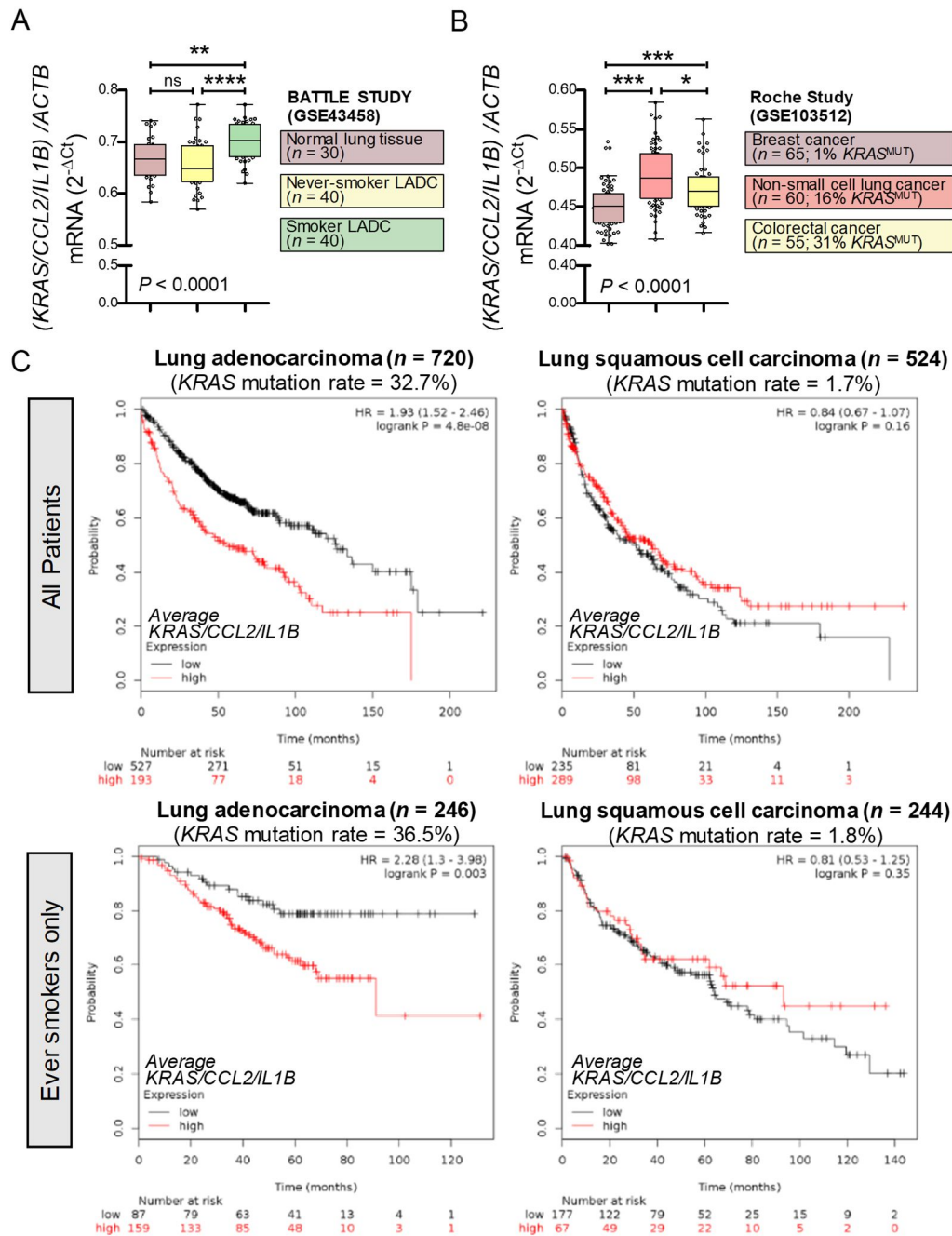
Figure 26: The KRAS/*CCL2/IL1B* axis is overexpressed in *KRAS*[MUT] cancers *and* forecasts poor survival. (A) Average and normalized *KRAS/CCL2/IL1B* expression in LADC patient samples from smokers, never-smokers and normal lung tissue from never-smokers (BATTLE study GSE43458). (B) Normalized *KRAS/CCL2/IL1B* expression in breast, non-small cell lung, and colorectal cancer (ROCHE study GSE103512). *KRAS* mutation frequency numbers are from COSMIC: https://cancer.sanger.ac.uk/cosmic[89]. (C) Kaplan-Meier analyses done on http://www.kmplot.com[78], of lung cancer patients focusing on mean expression of *KRAS, CCL2, and IL1B.* Top: Poorer survival of lung adenocarcinoma patients with high expression shown in red (left, HR = 1.93) compared to SQCLC patients (right, HR = 0.84). Bottom: HR increases in ever- smokers only patients with lung adenocarcinoma while staying the same in SQCLC. *P*, overall probability by one-way ANOVA. ns, *, **, and ***: *P* > 0.05, *P* < 0.05, *P* < 0.01, and *P* < 0.001, respectively, for the indicated comparisons by Bonferroni post-tests. Figure modified from Arendt *et al.*[80].

6.9 Other synthetic lethality partners for KRAS

The transcriptome analysis done with murine $Kras^{WT}$ and $Kras^{MUT}$ cell lines and benign samples revealed not only *Ccl2* and *Ilir1* as possible targets, but also other genes of interest: Ranbp3l, Gpr149, Cfap69, Ccl7, 2810417H13Rik, Pdgfra, Casp3, Ttk, Kif2c, Fanca, Cdca5, Rassf8, Hist2h3c2, Plag1, Nadk2, Oaf, Cxcl1, Mmd, Csgalnact1, Clybl, Zfp334, Kras, Palb2, Kcnab3, Mcts2, Pcnxl4, Gmnn, Poc1a, and Dhx40 were upregulated; Pde8a, Smpdl3a, mt-Tn, mt-Tt, Anxa6, mt-Ty, Mapkapk3, Gm2a, mt-Te, and Bmyc were downregulated. We started validation of Caspase 3 (Casp3), since it is involved in a cancer-specific pathway, the compensatory proliferation, which could explain the *in vivo* only effect of KRAS inhibition. Therefore, we used two Caspase inhibitors, BV6 and Z-DEVD-FMK. The latter is an irreversible Caspase3, -6, -7, -8, and -10 inhibitor. BV6 is an inhibitor of the IAP proteins (inhibitor of apoptosis), which autocatalyzes and activate the downstream effector caspase3. After validating the IC_{50} values of the two inhibitors in 8 cell lines ($Kras^{MUT}$: LLC, FULA1, $KRAS^{MUT}$: A549, H460; $Kras^{WT}$: PANO2, B16F10; $KRAS^{WT}$: H3122, EKVX) with WST-8 assays, a combination of increasing deltarasin concentrations and IC_{25} doses of either BV6 or Z-DEVD-FMK were applied for 72 hours. While Z-DEVD-FMK showed no effect without deltarasin or in combination, the combination with BV6 showed highly significant decrease in cell viability of both wildtype and mutant cell lines (Fig. 27, 28).

A proteomics analysis similar to the transcriptomics analysis was performed using two *Kras*-mutant cell lines (LLC, FULA1) compared to one *Kras*-wildtype cell line (PANO2). The proteome changes induced by deltarasin treatment (IC_{60}, 72h) of the three cell lines were analyzed and compared to deltarasin induced changes in the complement tumor tissue samples gathered from *in vivo* allograft flank models. Strict filtering revealed two proteins upregulated in deltarasin treated $Kras^{MUT}$ cell lines and downregulated in the *in vivo* produced protein lysates: CSN9 and CPT1A. One protein was regulated *vice versa:* K1C16 (Fig. 29A, B). CSN9 and CPT1A showed decreased overall survival in lung cancer patients when the gene of interest is higher expressed (Kaplan-Meier analysis, Fig. 29C).
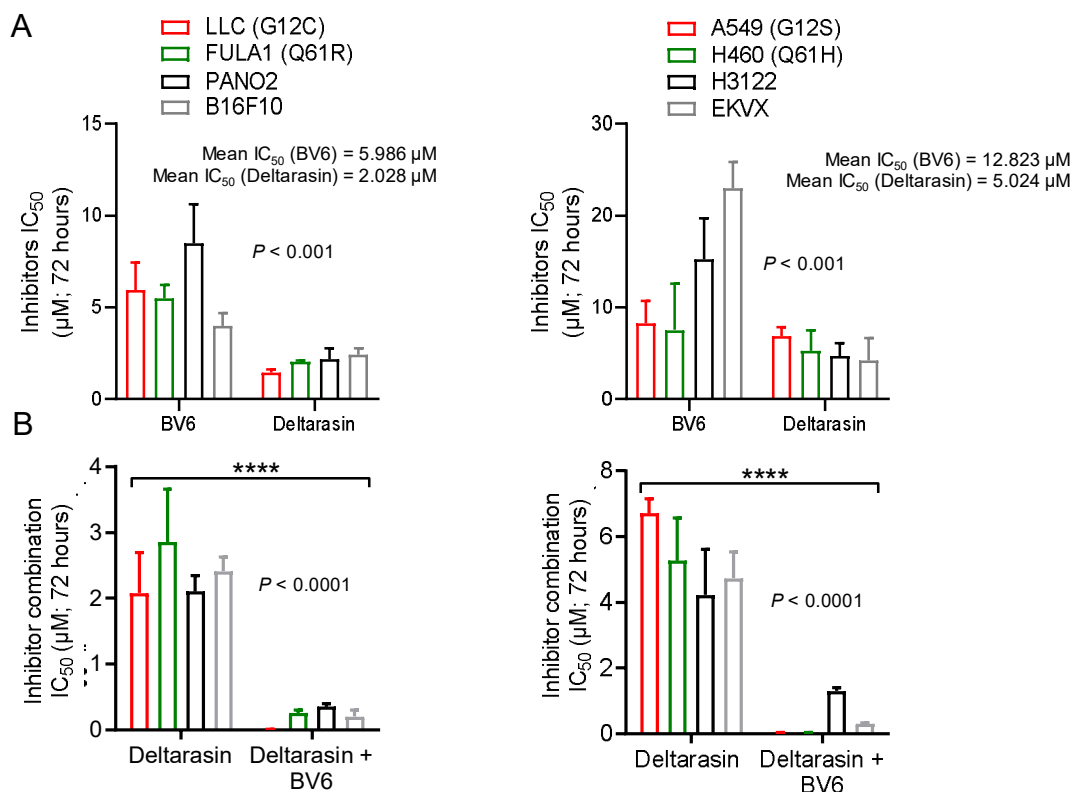
Figure 27: Inhibitor combination of deltarasin (KRAS specific) and BV6 (Caspase specific). (A) IC_{50} values of BV6 compared to deltarasin in murine and human cell lines determined by WST-8 assay, and after 72 h of incubation and accelerating drug combinations. (B) IC_{50} values of BV6 + deltarasin compared to deltarasin in murine and human cell lines determined by WST-8 assay after 72 h of incubation. IC_{25} BV6 doses (3 µM for murine cell lines, 6.5 µM for human cell lines) were added to accelerating deltarasin concentrations. n = 2-5; P, overall probability by one-way ANOVA. ns, *, **, *** and ****: $P > 0.05$, $P < 0.05$, $P < 0.01$, $P < 0.001$, and $P < 0.0001$, respectively, for the indicated comparisons by Bonferroni post-tests. Data are presented as mean ± SD.
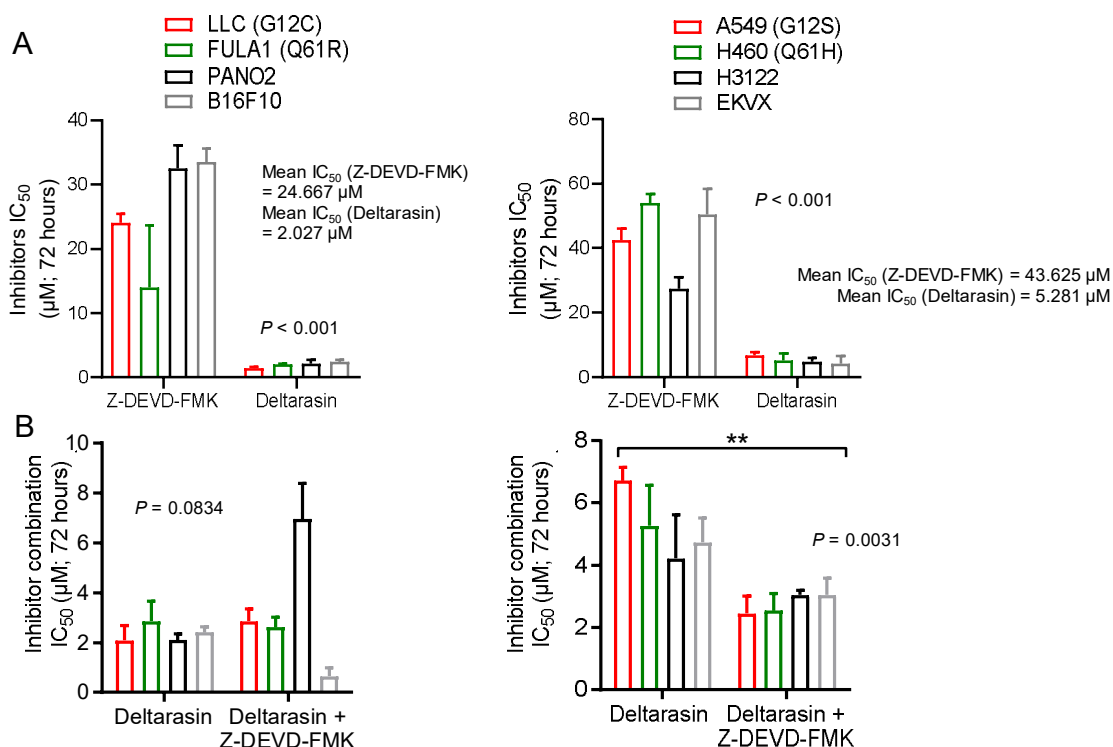
Figure 28: Inhibitor combination of deltarasin (KRAS specific) and Z-DEVD-FMK (Caspase specific). (A) IC_{50} values of Z-DEVD-FMK compared to deltarasin in murine and human cell lines determined by WST-8 assay, and after 72 h of incubation and accelerating deltarasin combinations. (B) IC_{50} values of Z-DEVD-FMK + deltarasin compared to deltarasin alone in murine and human cell lines determined by WST-8 assay after 72 h of incubation. IC_{25} Z-DEVD-FMK doses (12 μM for murine cell lines, 22 μM for human cell lines) were added to accelerating deltarasin concentrations. n = 2-5; P, overall probability by ne-way ANOVA. ns, *, **, *** and ****: $P > 0.05$, $P < 0.05$, $P < 0.01$, $P < 0.001$, and $P < 0.0001$, respectively, for the indicated comparisons by Bonferroni post-tests. Data are presented as mean ± SD.
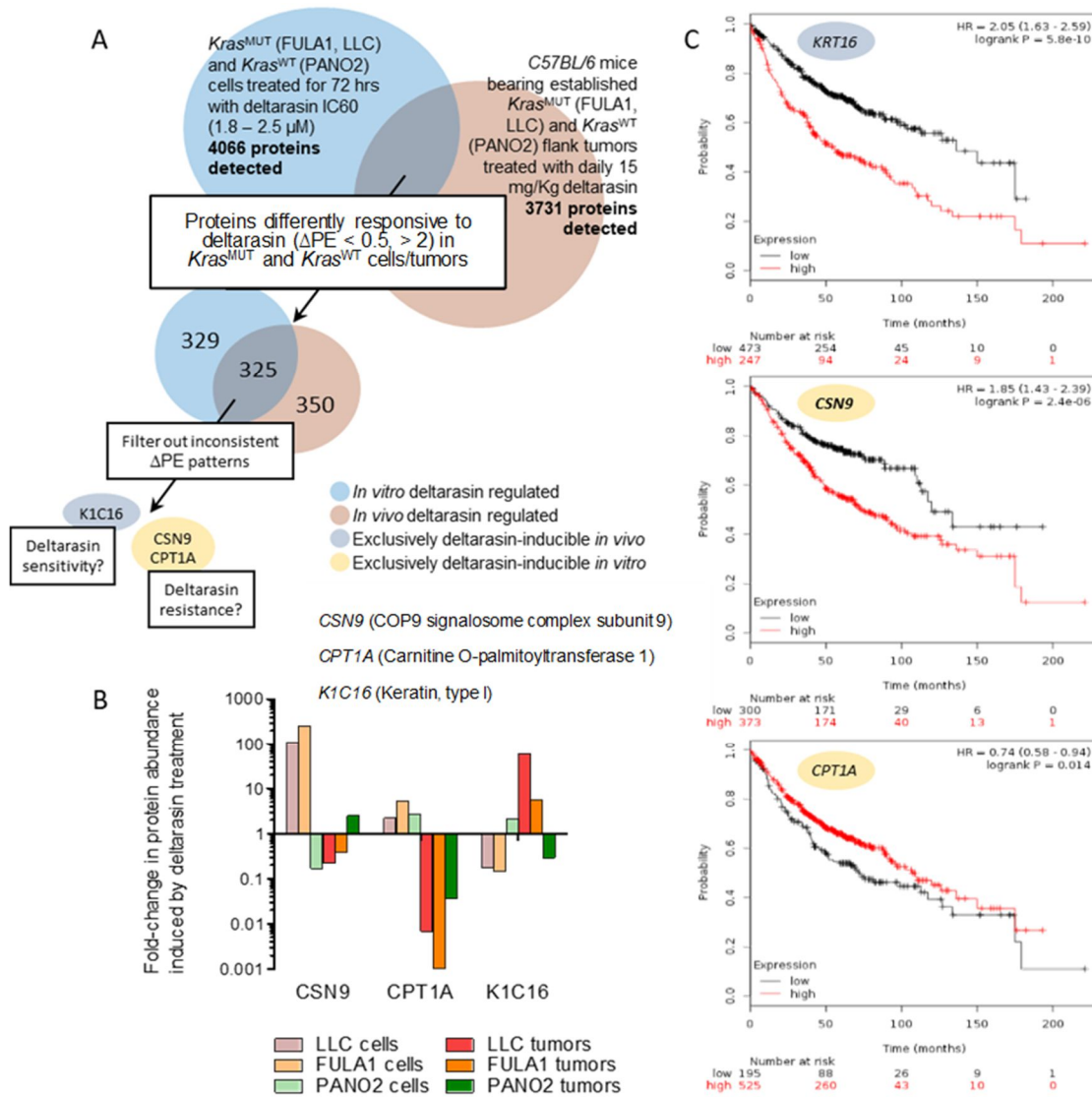
Figure 29: Proteomics analysis of 4 *Kras*^MUT samples (protein lysates of LLC, FULA1 cell lines / murine flank tumors established with LLC/FULA1) and 2 *Kras*^WT protein lysates (PANO2 cell lines/ murine flank tumors established with PANO2. All samples were treated/untreated with deltarasin IC$_{60}$ doses for 72 h. (A) Analytical strategy of the proteome analysis explained as Venn diagram. *n* = 3 for every sample. (B) Analysis revealed 2 proteins upregulated in *Kras*^MUT cell lines after deltarasin induction while downregulated in deltarasin treated tumor samples (CSN9, CPT1A), and 1 protein upregulated in deltarasin treated *Kras*^MUT tumor while downregulated in deltarasin treated *Kras*^MUT cell lines (K1C16). Shown are fold changes in protein abundance ΔPE. (C) Kaplan-Meier analyses done on http://www.kmplot.com[78], of lung cancer patients focusing on low and high expression of the genes of interest.

7. Discussion

The KRAS oncogene, one of the most frequent mutated cancer drivers, is still not druggable, due to its multi-diverse signaling probabilities. We and others hypothesized that hyperactive KRAS controls tumor progression in a cell independent manner and is mainly visible *in vivo*, questioning cellular based assays to find new KRAS drugs. Additionally, we identified main interaction partners, the inflammatory mediators CCL2 and IL-1β. With this we have reason to propose clinical trials aiming to target CCL2, IL-1β, and respective receptors in *KRAS*-mutant tumors.

For this piece of work, 30 human and murine cancer cell lines with diverse mutations and different preclinical KRAS agents were used, tested with various *in vitro* assays. In line with others we detected, that the oncogenicity of KRAS is much stronger in an *in vivo* surrounding. The genetic and pharmacologic KRAS inhibition against *Kras/KRAS*-mutant murine and human tumors was clearly measurable *in vivo*, while conventional *in vitro* studies failed. Using isogenic cell lines, we found a novel mutant *Kras* transcriptome signature including inflammatory mediators *Ccl2* and *Il1r1*. Further research with transgenic mouse strains and adoptive bone marrow transfer experiments revealed a strong *in vivo* dependence to CCR2+ IL-1β-secreting myeloid cells and we prove that the KRAS inhibitor deltarasin functions to decrease *Il1r1/IL1R1* expression in *Kras*/*KRAS*^MUT cancer cells. Additionally, the KRAS/CCL2/IL-1β signature shows an enrichment in human *KRAS*^MUT cancers.
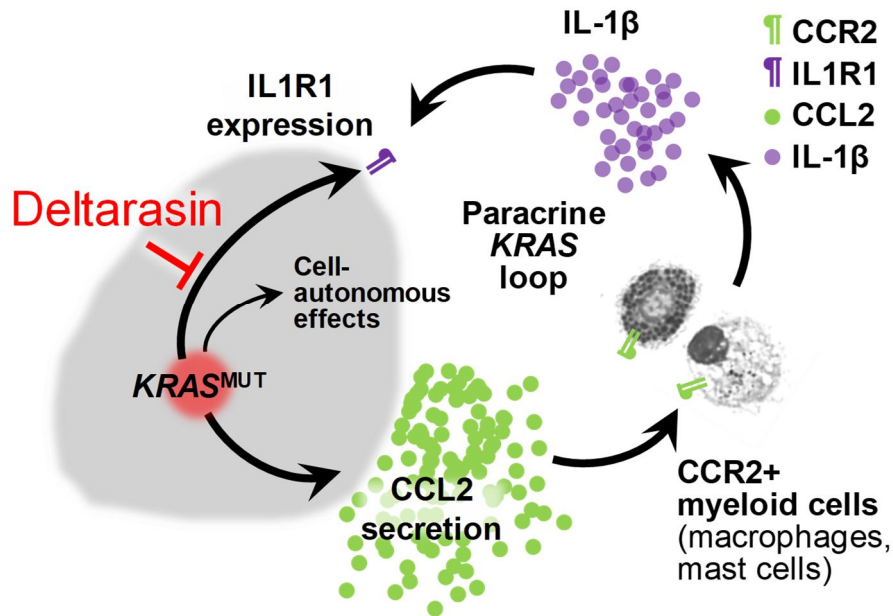
Figure 30: Graphical summary of the proposed mechanism of *in vivo* limited KRAS dependency. *KRAS* mutant cancer cells secrete CCL2 and express IL1R1 in a higher fashion than their wildtype counterparts, thereby recruiting CCR2+ myeloid cells to the tumor environment, subsequently increasing IL-1β levels and activating a positive feedback loop of increased tumor cell proliferation and enhanced inflammatory signaling. Deltarasin can interfere in this loop as KRAS specific inhibitor, decreasing IL1R1 expression and downregulating IL-1β signaling.

7.1   *In vivo* dependency of the KRAS oncogene

The underlying finding that hyperactive KRAS is not influencing cancer cell lines *in vitro* in a consistent fashion, is based on variable cellular assays, tested with three different pre-clinical KRAS agents using a huge set of murine and human cell lines. Unfortunately, reliable and significant differences concerning *KRAS* mutation status were not detectable. Further *in vivo* experiments showing mutation specific tumor growth differences led to the conclusion that KRAS inhibition is largely examinable under *in vivo* conditions. Several points of evidence can be found in the literature, supporting that 2-D cell cultures are suboptimal for the study of KRAS addiction. Singh *et al.* created a "Ras dependency index" (RDI) to classify KRAS dependency by using various human pancreatic and lung cancer cell lines[90]. By using RNAi against *KRAS* they classified cancer cell lines according to their KRAS addiction and consequently created a gene expression signature revealing several synthetic lethality partners. These cell line rankings should be assessed with higher priority in future KRAS target identification and

validation. Another group discusses the issue that synthetic lethal interaction partners for KRAS can never be confirmed across different *KRAS*-mutant tumors. Under the title DRIVE (deep RNAi interrogation of viability effects in cancer), they launched a comprehensive screen using a lentiviral library consisting of > 150000 shRNAs checking 7,837 genes and 398 cancer cell lines. Their data highlights the possibility that no lethal interaction partner for KRAS can be found *in vitro* across commonly used *KRAS* tumor models[91]. Janes *et al.* published their findings about a new KRAS inhibitor, ARS-1620, with the same problematic of high differences between *in vitro* and *in vivo* models. In summary they and others observe less than 50% KRAS addiction of cancer cell lines outside a functioning tumor environment[53]. In the study conducted by Scholl *et al.* identifying STK11 as synthetic lethality partners, 25% of KRAS-independent cell lines did not respond to STK11 suppression[55]. Also, in the publication of Barbie *et al.,* 20% of human $KRAS^{MUT}$ cell lines did not respond to shRNA against TBK1 to decrease cell viability *in vitro*, additionally highlighting the problem of *in vitro* KRAS studies[37]. In this context, we compared effective preclinical drug concentrations of TKIs for lung cancer treatment, among others Erlotinib, Gefitinib, Ceritinib, Crizotinib, and Dabrafenib with respective *in vitro* drug concentrations of different preclinical KRAS inhibitors, all tested in monolayer cell cultures. Interestingly, there is a dissimilarity between these two groups (Fig.11D). Successfully FDA-approved drugs inhibited cancer cell lines in nanomolar concentrations raising optimism for future clinical treatments. Instead, research with preclinical KRAS inhibitors showed efficacy from micromolar concentrations onwards, doses, which are clinically not promising (see supplementary reference list S8-S25). Until now, therapeutic intervention has not yielded any success, although KRAS plays this enormous role in human cancers[92]. The knowledge gained from others and us, of continual failures of KRAS drug development, shifts the focus on *in vivo* restricted mechanisms and its inherent answer to effective KRAS inhibition.

7.2 Targeting inflammatory interaction in KRAS-driven tumorigenesis

There is overwhelming evidence that KRAS-driven carcinogenesis is tightly correlated with tumor promoting inflammation. Activating mutations equip epithelial cells with the ability to survive and expand beyond cell intrinsic mechanism, exploiting cytokines that recruit inflammatory cells, and by this communicating strongly with the tumor environment. This cross-talk can switch the inflammatory response from anti-tumorigenic to pro-tumorigenic. KRAS has the capability of changing the nature of the inflammasome, thereby modulating recruitment, activation, and differentiation of immune cells beyond cell-autonomous effects[41,63,67]. Indeed, organs which are forced to constantly resist negative inflammatory influences or chronic inflammatory diseases, likely develop tumors with high *KRAS* mutation burden[30,68,89].
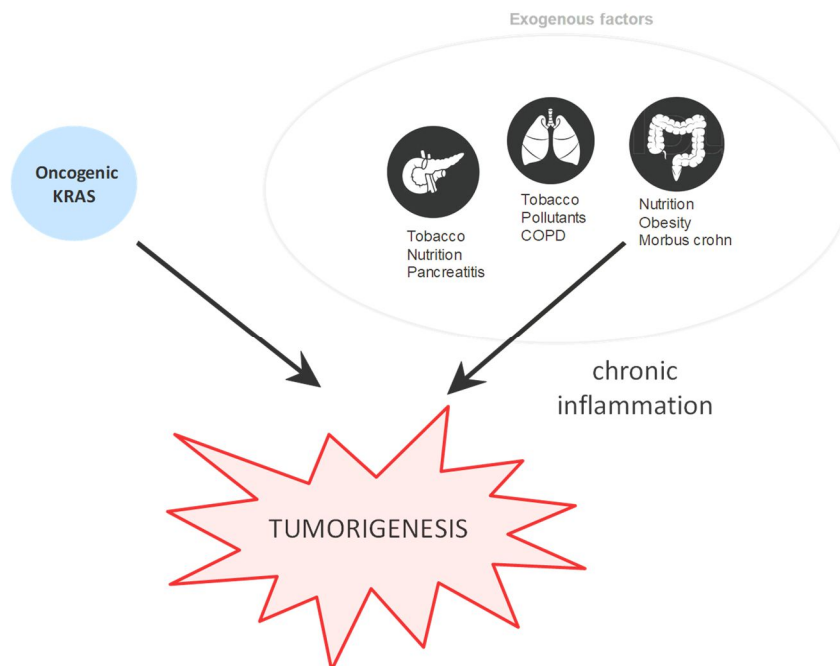

Figure 31: Three cancer types harboring high KRAS mutation rates, lung, pancreas, and colon cancer, often arise through chronic inflammatory processes and diseases in theses organs[30,68,89].

Immune cells communicate via soluble mediators, cytokines, either produced by themselves or the surrounding cancer cells. A pioneering report showed how CXCL8 (IL-8), an angiogenic growth factor, is a transcriptional target of RAS proteins directing paracrine signaling to endothelial cells[44]. This raised the possibility of a specific role in KRAS-driven NSCLC, and IL-

8 was proven to be upregulated in patient samples of KRAS mutated LADC[93]. Using a similar experimental strategy, Ancrile *et al.* identified IL-6 as paracrine signaling molecule of oncogenic RAS, promoting angiogenesis[94]. Later, researchers were able to pin down mutant KRAS as key regulator of IL-6 transcription followed by NF-κB activation and STAT3 expression. The signal transducer and activator of transcription STAT3 is an important transcription factor for tumor growth and angiogenesis, as well as for development of the premalignant state of pancreatic cancer, the acinar-to-ductal metaplasia (ADM)[95,96]. Mutated KRAS is also shown to mediate T-cell recruitment and in turn producing high IL-22 levels, effecting STAT3 and AKT activation[96]. In 2005 Ji *et al.* developed the conditional *Kras^{G12D}* mutant mouse in which the mutated allele is specifically expressed in CC10+ bronchiolar epithelial cells (club cells), and demonstrated the KRAS dependent chemokine production thus recruiting myeloid cells into the tumor[97]. Myeloid cells are studied intensively in context to oncogenic KRAS with specific focus on macrophages and neutrophils. Busch *et al.* were able to assign host immune cells histologically to either SCLC or LADC, showing a lymphocyte dominance in SCLC over myeloid cells (macrophages, neutrophils, and eosinophils) in LADC[98]. These cells infiltrate the KRAS mutant tumor helping it proliferate. They secrete inflammatory mediators which will certainly activate pro-tumorigenic pathways and further contribute to tumor invasiveness. Oncogenic KRAS is known to attract myeloid cells by releasing chemokines, such as CXCL1, CXCL2, and CXCL5 recruiting neutrophils, as well as CCL2, decoying CCR2+ macrophages[41,99]. Another molecule, ICAM-1, was identified as macrophage chemoattractant secreted by KRAS expressing pancreatic cells, which in turn secrete tumor necrosis factors (TNFs) and matrix metalloproteinases (MMPs), well known cancer progressors[100]. This knowledge in mind we analyzed the transcriptome of a panel of *Kras^{MUT}* and *Kras^{WT}* cell lines. Surprisingly, the cell lines did cluster according to their *Kras* mutation status and not to their tissues of origin (Fig. 19A). Our murine *Kras*-specific gene set consisted of multiple inflammatory mediators proving KRAS dependence to the inflammatory tumor microenvironment. It was enriched in human *KRAS^{MUT}* cancers and was linked to poor

survival. Both GSEA and WikiPathways analysis showed some parallels to inflammatory response pathways, proving that the oncogene has proinflammatory functions. The use of syngeneic LADC mice models allowed us to focus on the innate immune response. Most of the murine cell lines used for allograft models were extracted from spontaneously in mice developed tumors or from carcinogen-models, from which cell lines were developed after carcinogen exposure, murine lung tumor development, extraction, cell culturing, and molecular profiling[26,101]. The allograft model has the advantage of an intact host immune system, which is missing in immunocompromised mice. For genetic variation we used two different wildtype mice for our studies, *FVB* and *C57BL/6* mice. Additionally, *Rag2$^{-/-}$* mice, deficient in T- and B-cell differentiation, but expressing intact myeloid cells, were therefore used in this study to work with xenograft models[102]. The measurable drug effect tested in this mice strain supported our theory of an innate inflammatory response that potentiates KRAS inhibition.

7.3 CCL2/CCR2 and IL-1β/IL1R –new targets for KRAS mutant cancer?

Two inflammatory molecules of our gene expression list are found in the literature with similar context, CCL2 and IL1R1. Both play a huge role in tumor development, MPE formation and are specifically upregulated in our *KRAS*-mutant cell lines (Fig. 19)[36,41]. Consequently, we validated both candidates of our *Kras^{MUT}* signature on RNA and Protein level. We narrowed down the drug effectiveness to decrease expression of IL1R1 in *KRAS*-mutant tumor cells and thus stopping the receptivity to IL-1β. CCR2+ myeloid cells were stated as important key players in *KRAS*-mutant tumors and were proven to be mandatory for oncogenic *KRAS* dependence *in vivo,* also shown by their enrichment in tumor tissue (Fig. 21)[36,41,43,79]. This hypothesis was further supported by data from syngeneic mouse models of *Ccr2* and *Il1b* gene knockdown, from BMT experiments with crucial myeloid *Ccr2* reconstitution, and by xenograft experiments in *Rag2$^{-/-}$* mice (intact myeloid cells, but B- and T-cell function deficient) using human cancer cell lines[102]. Compared to effective deltarasin in *FVB* mice, slowing down tumor growth statistically, the drug lost its efficacy in *Ccr2* knockdown strains completely and in parts

in *Il1b* knockdown strains. In summary, we were able to show how deltarasin functions to inhibit a mutant *KRAS*-initiated inflammatory loop of tumor-secreted CCL2 and myeloid-derived IL-1β. The lesser effect in *Il1b* knockdown mice can be explained due to present IL-1α with redundant effects[103]. The chemokine CCL2 (MCP-1), produced from bone marrow, stroma and tumor, plays a huge role in guiding the infiltration of myeloid cells to the tumor microenvironment due to its chemoattractant function[36,41,104,105]. Ninety percent of its surface receptor CCR2 is expressed by monocytes and NK cells. The CCL2-CCR2 axis is a well-studied subject concerning pro-tumorigenic function, cancer metastasis, migration, pathological inflammation, and angiogenesis. CCL2 and its receptor control and recruit monocytes from the bone marrow into the bloodstream to sites of inflammation and tumor environment. The chemokine can turn them in tumor associated macrophages (TAM). TAMs are limiting the effect of anti-tumorigenic immune responses, in favor of progression and chemoresistance[106]. The activation can increase expression of metalloproteinases like MMP2 and MMP9 in cancer cells and thereby increase invasion and metastatic potential destroying healthy ECM. In breast, colon, and prostate cancer, CCL2 blockade with murine or humane neutralizing antibodies were highly effective in reducing tumor burden, macrophages infiltration, tumor associated vascularity, and metastasis[105]. In a breast cancer chemoresistance study of 2012 it was shown how CCR2+ myeloid cells contribute to resistance development to Doxorubicin and Cisplatin, well known chemotherapeutics. In *Ccr2* null host mice Doxorubicin effect was prolonged by inhibiting resistance development. They and others suggest treatment combination of chemotherapy with agents changing the inflammatory signaling, in particular CCR2 or CCL2 inhibitors[107].

Increased IL-1 levels have been connected to the pathogenesis of acute and chronic (i.e. atherosclerosis, rheumatoid arthritis) inflammatory diseases[108]. In cancer excessive IL-1 concentrations are tumor growth promotors and poor prognostic factors for patients. Thereby, IL-1β and IL-1α play distinct and similar roles[109]. An important difference is IL-1β's regulation by acute inflammatory signaling, while Il-1α is ubiquitous expressed and homeostatic present

within the cell[108]. Krelin *et al.* published their studies with different IL-1 knockout mice (IL-1α^{-/-}, IL-1β^{-/-}, IL-1α/β[-/-], IL-1Ra^{-/-}) and 3-methylcholanthrene (3-MCA), a strong carcinogen, in which they named IL-1β as main tumor progressor and potentiator of inflammatory response. In IL-1β^{-/-} and IL-1α/β[-/-] mice, tumor development was significantly slowed down after 3-MCA treatment compared to the other null mice (≥ 110 days)[108,110]. The tumor microenvironment derived interleukin can activate complex downstream signaling pathways in cancer cells, such as activation of NF-kB, which induces transcription of inflammatory mediators like CCL2 and IL-1 itself, and thereby tumor growth[36,41]. Agalioti *et al.* studied paracrine CCL2 signaling to CCR2+ myeloid cells (mononuclear and mast cells) in dependence to oncogenic KRAS. This progresses malignant pleural effusion by induction of vascular permeability and angiogenesis. It was druggable both with deltarasin and CCL2 neutralizing antibody[41]. Subsequently, CCR2+ myeloid cells secreted IL-1β, which was found to selectively elevate non-canonical IKKα-mediated NF-κB activity, thereby enhancing tumor progression, MPE formation and drug resistance. The signaling culminates in enhanced CXCL1/PPBP expression which escalates tumor-associated inflammation. In this study, Marazioti *et al.* analyzed the origin of host IL-1β and eliminated the possibility of cancer cell producing IL-1β[36]. Both studies elucidate the mechanism of KRAS function to recruit immune cells to the tumor environment. Unfortunately, clinical trials of therapeutics like the anti-human CCL2 antibody carlumab (CNTO888) were disappointing by limited drug efficacy and tolerability. Still, CCL2 neutralizing antibodies yield good preclinical results in cancer models, and the axis seems to be a relevant target in our findings[104,105,111–114]. In addition to CCL2/CCR2, blockade of IL-1β/IL1R1 in cancer therapy is a promising and well-studied research subject[115]. Targeting IL-1β with the monoclonal antibody canakinumab, which is in clinical trials, raises enthusiasm in cancer therapy. In this context, Ridker *et al.* published an exploratory evaluation of the CANTOS trial (Canakinumab anti-inflammatory thrombosis outcome study). This study included 10061 patients with atherosclerosis, 129 of which had lung cancer[115,116]. They confirmed as second aim, if low (50 mg), medium (150 mg), or high (300 mg)-dose canakinumab (*sc* every three months) might

change cancer frequency. Treatment with the high-dose canakinumab decreased the total cancer mortality significantly (*n* = 77) by 51%, which was astonishing. The incidence of lung cancer decreased by 39% in the medium-dose and in the high-dose group by 67%, while the mortality of lung cancer decreased by 77%. The *KRAS* mutation status of these patients would be of tremendous value to analyze and answer the question of context. Our results suggest canakinumab as possible selective anti-KRAS drug. These research findings together with the present work, highlight CCL2, IL-1β, and their receptors as important inflammatory addiction partners, and make them highly interesting in clinical context.

7.4   Other synthetical lethality partners of KRAS

The Kras^{MUT} gene expression list of our cell line panel includes other synthetic lethality partners of KRAS. Besides *Kras*, *Ccl2*, and *Il1r1,* the signature contains signal transducers *Gpr149, Rassf8*, and *Ranbp3l*, inflammatory mediators *Cxcl1, Ccl7*, and *Casp3*, cell surface receptors *Ttk* and *Pdgfra*, and tumor suppressors and cell cycle genes *Plag1, Cdca5*, *Fanca*, *Hist2h3c2*, and *Gmnn*, among others. CXCL1 is proven to be a downstream effector of mutant KRAS. KRAS mutant tumor cells activate non-canonical NF-κB pathway via IKKα in response to high concentration of host derived IL-1β. This leads to enhanced transcription of this chemokine and subsequent progression of malignant pleural effusion[36]. CXCL1 is also correlated with lymph node and peritoneal metastasis, and lymphatic venous malignant invasion[117]. Geminin DNA Replication Inhibitor (Gmnn) was recently identified as a tumor suppressor in colon and lung cancer[118]. The cysteine protease Casp3 is not just an apoptosis effector caspase, but also central signal molecule of rapid tumor-repopulation and radiotherapy resistance induced via apoptosis[119]. Caspase-3 can thereby activate calcium independent phospholipase A2 (iPLA$_2$) which further activates prostaglandin E$_2$ (PGE$_2$) synthesis. This increases stem cell proliferation and leads to compensatory tumor repopulation. Apoptosis can thereby actively promote cell survival of the surrounding cells by the dual role of the Caspase-3. It was shown, that high expression of Caspase-3 is linked to shorter survival rates in cancer patient samples

making it a negative prognostic biomarker[119]. The induced inflammatory response mechanism via deltarasin could mask these survival signals of this compensatory proliferation pathway (Fig. 30). In *in vitro* experiments this non-cell-autonomous survival effect is not existing, therefore KRAS inhibitors are not specifically effective. Nevertheless, results with the caspase inhibitor Z-DEVD-FMK did not show an effect, but since the inhibitor has an overall caspase inhibition effect, pro-survival effects could be stronger and targeting apoptosis pathways needs to be carefully evaluated[120]. The inhibitor of apoptosis (IAP) antagonist BV6 in combination with deltarasin showed promising effects. The drug, a SMAC-mimetic (SMAC, second mitochondrial derived activator of caspases; human natural IAP antagonist) targets IAP proteins, which control the cleavage and activation of Caspase-3[121]. Inhibition of IAP proteins also affect downregulation of NF-kB and MAPK pathways, highly supportive effects to inhibit tumor growth, especially for KRAS- mutant cancer types. Thereby the inflammatory response via cytokine induction and proinflammatory gene regulation is decreased by the IAP inhibitor. Since IAP proteins demonstrate a good target for cancer treatments several antagonists have entered clinical trials[122]. Our proteomics analysis revealed another candidate which was higher expressed in KRAS-mutant cell lines and lower in KRAS-mutant tumor samples, both expression levels valuated after longer deltarasin treatment, the COP9 signalosome complex subunit 9 (CSN9). The complex is strongly involved in innate immune signaling and proteasome activation, as well as prediction of better survival if lower expressed. By controlling the ubiquitin-proteasome system (UPS) it can thereby indirectly regulate tumor suppressors like p53, transcription factors, or oncogenes. The clinical value of this axis is proven by the use of proteasome inhibitors such as bortezomib. That makes COP9 as regulatory element of the UPS therapeutically interesting in the treatment of cancer[123,124].
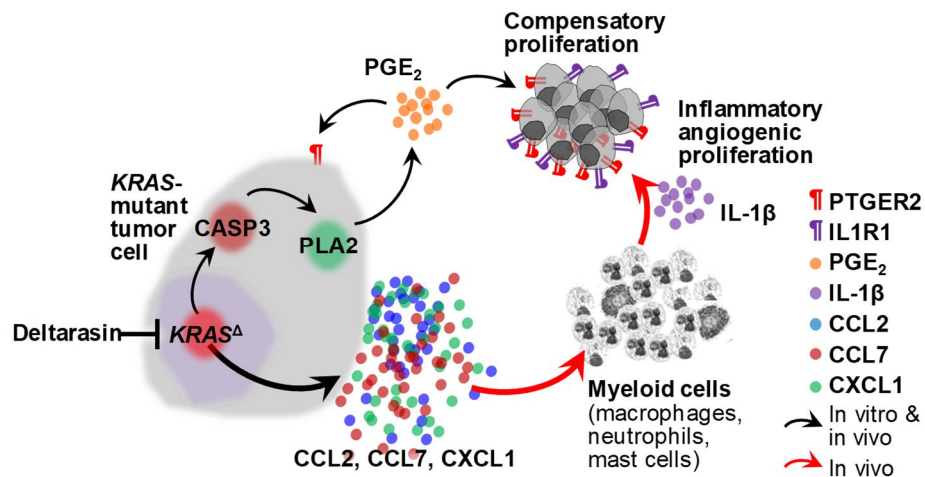
Figure 32: A compensatory proliferation mechanism activated through KRAS-mediated high expression of caspase-3. Activation of caspase-3 will increase PGE_2 synthesis via PLA_2 thereby activation a tumor-specific pro-survival mechanism of compensatory proliferation. This can be inhibited via deltarasin *in vivo* by recruitment of inflammatory cells to the tumor microenvironment. PTGER2, prostaglandin E receptor 2; PGE2, prostaglandin E2; PLA2, Phospholipase A2.

7.5 Conclusion

In summary, we show that KRAS^{MUT} cancer cells act highly diverse depending on the given surrounding. Our work is in line with others claiming a change in drug development process for finding KRAS inhibitors. We identify an underlying mechanism of KRAS action beyond intrinsic cell-autonomous signaling and show that cancer with oncogenic *KRAS* overexpresses CCL2 and IL1R1 to recruit CCR2+ IL-1β-expressing myeloid cells to feed an inflammatory signaling loop. In our studies using deltarasin we found an underlying mechanism of action, which is targeting IL1R1 expression. In addition, we were able to show the relation of murine based research to human patient data. The KRAS/CCL2/IL-1β axis is essential for KRAS-dependent tumor growth and blockade and can be used in the future to design clinical trials for KRAS mutant cancers.

New findings:

- Extensive proof for the discrepancy between *in vitro* and *in vivo* findings related to KRAS inhibition.
- Identification and validation of the mechanism for the *in vivo*-restricted efficacy of KRAS inhibitors.
- Determination of the requirement for the KRAS/CCL2/IL-1β axis for successful KRAS inhibition.
- Proof-of-concept human data supporting the existence of the proposed mechanism in human cancer.
- A novel KRAS signature containing candidate KRAS addiction partners for future research

8. References

1. Cao, M. & Chen, W. Epidemiology of lung cancer in China. *Thoracic cancer* **10,** 3–7; 10.1111/1759-7714.12916 (2019).

2. Giopanou, I., Arendt, K. A. M. & Stathopoulos, G. T. Lung carcinogenesis and fibrosis taken together: just coincidence? *Current opinion in pulmonary medicine* **23,** 290–297; 10.1097/MCP.0000000000000390 (2017).

3. Husain, M. J., English, L. M. & Ramanandraibe, N. An overview of tobacco control and prevention policy status in Africa. *Preventive medicine* **91S,** S16-S22; 10.1016/j.ypmed.2016.02.017 (2016).

4. Alberg, A. J., Brock, M. V., Ford, J. G., Samet, J. M. & Spivack, S. D. Epidemiology of lung cancer: Diagnosis and management of lung cancer, 3rd ed: American College of Chest Physicians evidence-based clinical practice guidelines. *Chest* **143,** e1S-e29S; 10.1378/chest.12-2345 (2013).

5. Walser, T. *et al.* Smoking and lung cancer: the role of inflammation. *Proceedings of the American Thoracic Society* **5,** 811–815; 10.1513/pats.200809-100TH (2008).

6. Inamura, K. Lung Cancer: Understanding Its Molecular Pathology and the 2015 WHO Classification. *Frontiers in oncology* **7,** 193; 10.3389/fonc.2017.00193 (2017).

7. cancer genome atlas research network. Comprehensive molecular profiling of lung adenocarcinoma. *Nature* **511,** 543–550; 10.1038/nature13385. (2014).

8. Kempf, E., Rousseau, B., Besse, B. & Paz-Ares, L. KRAS oncogene in lung cancer: focus on molecularly driven clinical trials. *European respiratory review : an official journal of the European Respiratory Society* **25,** 71–76; 10.1183/16000617.0071-2015 (2016).

9. Nussinov, R. & Tsai, C.-J. 'Latent drivers' expand the cancer mutational landscape. *Current opinion in structural biology* **32,** 25–32; 10.1016/j.sbi.2015.01.004 (2015).

10. Detterbeck, F. C., Boffa, D. J., Kim, A. W. & Tanoue, L. T. The Eighth Edition Lung Cancer Stage Classification. *Chest* **151,** 193–203; 10.1016/j.chest.2016.10.010 (2017).

11. Collins, L. G., Haines, C., Perkel, R. & Enck, R. E. Lung cancer: diagnosis and management. *American family physician* **75,** 56–63 (2007).

12. Molina, J. R., Yang, P., Cassivi, S. D., Schild, S. E. & Adjei, A. A. Non-small cell lung cancer: epidemiology, risk factors, treatment, and survivorship. *Mayo Clinic proceedings* **83,** 584–594; 10.4065/83.5.584 (2008).

13. Mok, T. S. *et al.* Osimertinib or Platinum-Pemetrexed in EGFR T790M-Positive Lung Cancer. *The New England journal of medicine* **376,** 629–640; 10.1056/NEJMoa1612674 (2017).

14. Nguyen, K.-S. H., Neal, J. W. & Wakelee, H. Review of the current targeted therapies for non-small-cell lung cancer. *World journal of clinical oncology* **5,** 576–587; 10.5306/wjco.v5.i4.576 (2014).

15. Friday, B. B. & Adjei, A. A. K-ras as a target for cancer therapy. *Biochimica et biophysica acta* **1756,** 127–144; 10.1016/j.bbcan.2005.08.001 (2005).

16. Nogrady, B. Immunotherapy: Chemical tricks. *Nature* **513,** S10-S11; 10.1038/513S10a (2014).

17. Haigis, K. M. KRAS Alleles: The Devil Is in the Detail. *Trends in cancer* **3,** 686–697; 10.1016/j.trecan.2017.08.006. (2017).

18. Cox, A. D. & Der, C. J. Ras history: The saga continues. *Small GTPases* **1,** 2–27; 10.4161/sgtp.1.1.12178 (2010).

19. Ryan, M. B. & Corcoran, R. B. Therapeutic strategies to target RAS-mutant cancers. *Nature reviews. Clinical oncology* **15,** 709–720; 10.1038/s41571-018-0105-0 (2018).

20. Wang, Y., Kaiser, C. E., Frett, B. & Li, H.-Y. Targeting mutant KRAS for anticancer therapeutics: a review of novel small molecule modulators. *Journal of medicinal chemistry* **56,** 5219–5230; 10.1021/jm3017706 (2013).

21. Vasan, N., Boyer, J. L. & Herbst, R. S. A RAS renaissance: emerging targeted therapies for KRAS-mutated non-small cell lung cancer. *Clinical cancer research : an official journal of the American Association for Cancer Research* **20,** 3921–3930; 10.1158/1078-0432.CCR-13-1762 (2014).

22. Leung, K. F., Baron, R., Ali, B. R., Magee, A. I. & Seabra, M. C. Rab GTPases containing a CAAX motif are processed post-geranylgeranylation by proteolysis and methylation. *The Journal of biological chemistry* **282,** 1487–1497; 10.1074/jbc.M605557200 (2007).

23. Nussinov, R., Tsai, C.-J. & Jang, H. Oncogenic Ras Isoforms Signaling Specificity at the Membrane. *Cancer research* **78,** 593–602; 10.1158/0008-5472.CAN-17-2727 (2018).

24. Pylayeva-Gupta, Y., Grabocka, E. & Bar-Sagi, D. RAS oncogenes: weaving a tumorigenic web. *Nature reviews. Cancer* **11,** 761–774; 10.1038/nrc3106 (2011).

25. Nussinov, R., Tsai, C.-J., Chakrabarti, M. & Jang, H. A New View of Ras Isoforms in Cancers. *Cancer research* **76,** 18–23; 10.1158/0008-5472.CAN-15-1536 (2016).

26. Kanellakis, N. I. *et al.* Tobacco chemical-induced mouse lung adenocarcinoma cell lines pin the prolactin orthologue proliferin as a lung tumour promoter. *Carcinogenesis*; 10.1093/carcin/bgz047 (2019).

27. Castelletti, N. *et al.* Risk of lung adenocarcinoma from smoking and radiation arises in distinct molecular pathways. *Carcinogenesis*; 10.1093/carcin/bgz036 (2019).

28. Kessler, D. *et al.* Drugging an undruggable pocket on KRAS. *Proceedings of the National Academy of Sciences of the United States of America*; 10.1073/pnas.1904529116 (2019).

29. Quinlan, M. P., Quatela, S. E., Philips, M. R. & Settleman, J. Activated Kras, but not Hras or Nras, may initiate tumors of endodermal origin via stem cell expansion. *Molecular and cellular biology* **28,** 2659–2674; 10.1128/MCB.01661-07 (2008).

30. Spella, M., Marazioti, A., Arendt, K. A. M. & Stathopoulos, G. T. RAS oncogenes direct metastasis. *Molecular & cellular oncology* **4,** e1345711; 10.1080/23723556.2017.1345711 (2017).

31. Collins, M. A. & Di Pasca Magliano, M. Kras as a key oncogene and therapeutic target in pancreatic cancer. *Frontiers in physiology* **4,** 407; 10.3389/fphys.2013.00407 (2013).

32. Nussinov, R., Tsai, C.-J. & Jang, H. Independent and core pathways in oncogenic KRAS signaling. *Expert review of proteomics* **13,** 711–716; 10.1080/14789450.2016.1209417 (2016).

33. Singh, A. & Settleman, J. Oncogenic K-ras "addiction" and synthetic lethality. *Cell cycle (Georgetown, Tex.)* **8,** 2676–2677; 10.4161/cc.8.17.9336 (2009).

34. Cheng, H. *et al.* Targeting the PI3K/AKT/mTOR pathway: potential for lung cancer treatment. *Lung cancer management* **3,** 67–75; 10.2217/lmt.13.72 (2014).

35. Park, M. H. & Hong, J. T. Roles of NF-κB in Cancer and Inflammatory Diseases and Their Therapeutic Approaches. *Cells* **5**; 10.3390/cells5020015 (2016).

36. Marazioti, A. *et al.* Myeloid-derived interleukin-1β drives oncogenic KRAS-NF-κB addiction in malignant pleural effusion. *Nature communications* **9,** 672; 10.1038/s41467-018-03051-z (2018).

37. Barbie, D. A. *et al.* Systematic RNA interference reveals that oncogenic KRAS-driven cancers require TBK1. *Nature* **462,** 108–112; 10.1038/nature08460 (2009).

38. Bassères, D. S., Ebbs, A., Cogswell, P. C. & Baldwin, A. S. IKK is a therapeutic target in KRAS-Induced lung cancer with disrupted p53 activity. *Genes & cancer* **5,** 41–55; 10.18632/genesandcancer.5 (2014).

39. Vreka, M. *et al.* IκB Kinase α Is Required for Development and Progression of KRAS-Mutant Lung Adenocarcinoma. *Cancer research* **78,** 2939–2951; 10.1158/0008-5472.CAN-17-1944 (2018).

40. Ballin, M., Gomez, D. E., Sinha, C. C. & Thorgeirsson, U. P. Ras oncogene mediated induction of a 92 kDa metalloproteinase; strong correlation with the malignant phenotype. *Biochemical and biophysical research communications* **154,** 832–838; 10.1016/0006-291x(88)90215-x (1988).

41. Agalioti, T. *et al.* Mutant KRAS promotes malignant pleural effusion formation. *Nature communications* **8,** 15205; 10.1038/ncomms15205 (2017).

42. Downward, J. Targeting RAS signalling pathways in cancer therapy. *Nature reviews. Cancer* **3,** 11–22; 10.1038/nrc969 (2003).

43. Giannou, A. D. *et al.* Mast cells mediate malignant pleural effusion formation. *The Journal of clinical investigation* **125,** 2317–2334; 10.1172/JCI79840 (2015).

44. Sparmann, A. & Bar-Sagi, D. Ras-induced interleukin-8 expression plays a critical role in tumor growth and angiogenesis. *Cancer cell* **6,** 447–458; 10.1016/j.ccr.2004.09.028 (2004).

45. Yang, P. Epidemiology of lung cancer prognosis: quantity and quality of life. *Methods in molecular biology (Clifton, N.J.)* **471,** 469–486; 10.1007/978-1-59745-416-2_24 (2009).

46. Baker, N. M. & Der, C. J. Cancer: Drug for an 'undruggable' protein. *Nature* **497,** 577–578; 10.1038/nature12248 (2013).

47. Winter-Vann, A. M. *et al.* A small-molecule inhibitor of isoprenylcysteine carboxyl methyltransferase with antitumor activity in cancer cells. *Proceedings of the National Academy of Sciences of the United States of America* **102,** 4336–4341; 10.1073/pnas.0408107102 (2005).

48. Wang, M. *et al.* Inhibition of isoprenylcysteine carboxylmethyltransferase induces autophagic-dependent apoptosis and impairs tumor growth. *Oncogene* **29,** 4959–4970; 10.1038/onc.2010.247 (2010).

49. Zimmermann, G. *et al.* Small molecule inhibition of the KRAS-PDEδ interaction impairs oncogenic KRAS signalling. *Nature* **497,** 638–642; 10.1038/nature12205 (2013).

50. Rotblat, B., Ehrlich, M., Haklai, R. & Kloog, Y. The Ras inhibitor farnesylthiosalicylic acid (Salirasib) disrupts the spatiotemporal localization of active Ras: a potential treatment for cancer. *Methods in enzymology* **439,** 467–489; 10.1016/S0076-6879(07)00432-6 (2008).

51. Ostrem, J. M., Peters, U., Sos, M. L., Wells, J. A. & Shokat, K. M. K-Ras(G12C) inhibitors allosterically control GTP affinity and effector interactions. *Nature* **503,** 548–551; 10.1038/nature12796 (2013).

52. Lito, P., Solomon, M., Li, L.-S., Hansen, R. & Rosen, N. Allele-specific inhibitors inactivate mutant KRAS G12C by a trapping mechanism. *Science (New York, N.Y.)* **351,** 604–608; 10.1126/science.aad6204 (2016).

53. Janes, M. R. *et al.* Targeting KRAS Mutant Cancers with a Covalent G12C-Specific Inhibitor. *Cell* **172,** 578-589.e17; 10.1016/j.cell.2018.01.006 (2018).

54. AMG 510 First to Inhibit "Undruggable" KRAS. *Cancer discovery*; 10.1158/2159-8290.CD-NB2019-073 (2019).

55. Scholl, C. *et al.* Synthetic lethal interaction between oncogenic KRAS dependency and STK33 suppression in human cancer cells. *Cell* **137,** 821–834; 10.1016/j.cell.2009.03.017. (2009).

56. Puyol, M. *et al.* A synthetic lethal interaction between K-Ras oncogenes and Cdk4 unveils a therapeutic strategy for non-small cell lung carcinoma. *Cancer cell* **18,** 63–73; 10.1016/j.ccr.2010.05.025 (2010).

57. Stephen, A. G., Esposito, D., Bagni, R. K. & McCormick, F. Dragging ras back in the ring. *Cancer cell* **25,** 272–281; 10.1016/j.ccr.2014.02.017 (2014).

58. Matikas, A., Mistriotis, D., Georgoulias, V. & Kotsakis, A. Targeting KRAS mutated non-small cell lung cancer: A history of failures and a future of hope for a diverse entity. *Critical reviews in oncology/hematology* **110,** 1–12; 10.1016/j.critrevonc.2016.12.005 (2017).

59. Downward, J. RAS's cloak of invincibility slips at last? *Cancer cell* **25,** 5–6; 10.1016/j.ccr.2013.12.016 (2014).

60. Chen, P.-Y. *et al.* Adaptive and Reversible Resistance to Kras Inhibition in Pancreatic Cancer Cells. *Cancer research* **78,** 985–1002; 10.1158/0008-5472.CAN-17-2129 (2018).

61. McCormick, F. Progress in targeting RAS with small molecule drugs. *The Biochemical journal* **476,** 365–374; 10.1042/BCJ20170441 (2019).

62. Hanahan, D. & Weinberg, R. A. The hallmarks of cancer. *Cell* **100,** 57–70 (2000).

63. Hanahan, D. & Weinberg, R. A. Hallmarks of cancer: the next generation. *Cell* **144,** 646–674; 10.1016/j.cell.2011.02.013 (2011).

64. Virchow, R. L. K. *Cellular pathology as based upon physiological and pathological histology … / by Rudolf Virchow. Translated from the 2d ed. of the original by Frank*

Chance. With notes and numerous emendations, principally from MS. notes of the author (J. B. Lippincott, Philadelphia, 1863).

65. Schreiber, R. D., Old, L. J. & Smyth, M. J. Cancer immunoediting: integrating immunity's roles in cancer suppression and promotion. *Science (New York, N.Y.)* **331,** 1565–1570; 10.1126/science.1203486 (2011).

66. Dranoff, G. Cytokines in cancer pathogenesis and cancer therapy. *Nature reviews. Cancer* **4,** 11–22; 10.1038/nrc1252 (2004).

67. Chaplin, D. D. Overview of the immune response. *The Journal of allergy and clinical immunology* **125,** S3-23; 10.1016/j.jaci.2009.12.980. (2010).

68. Korniluk, A., Koper, O., Kemona, H. & Dymicka-Piekarska, V. From inflammation to cancer. *Irish journal of medical science* **186,** 57–62; 10.1007/s11845-016-1464-0 (2017).

69. Parkin, J. & Cohen, B. An overview of the immune system. *The Lancet* **357,** 1777–1789; 10.1016/S0140-6736(00)04904-7 (2001).

70. Medzhitov, R. & Janeway, C. Innate immunity. *The New England journal of medicine* **343,** 338–344; 10.1056/nejm200008033430506 (2000).

71. Dvorak, H. F. Tumors: wounds that do not heal. Similarities between tumor stroma generation and wound healing. *The New England journal of medicine* **315,** 1650–1659; 10.1056/NEJM198612253152606 (1986).

72. Grivennikov, S. I., Greten, F. R. & Karin, M. Immunity, inflammation, and cancer. *Cell* **140,** 883–899; 10.1016/j.cell.2010.01.025 (2010).

73. Mantovani, A., Allavena, P., Sica, A. & Balkwill, F. Cancer-related inflammation. *Nature* **454,** 436–444; 10.1038/nature07205. (2008).

74. Subramanian, A. *et al.* Gene set enrichment analysis: a knowledge-based approach for interpreting genome-wide expression profiles. *Proceedings of the National Academy of Sciences of the United States of America* **102,** 15545–15550; 10.1073/pnas.0506580102 (2005).

75. Pico, A. R. *et al.* WikiPathways: pathway editing for the people. *PLoS biology* **6,** e184; 10.1371/journal.pbio.0060184 (2008).

76. Faul, F., Erdfelder, E., Lang, A.-G. & Buchner, A. G*Power 3: a flexible statistical power analysis program for the social, behavioral, and biomedical sciences. *Behavior research methods* **39,** 175–191 (2007).

77. Kriventseva, E. V. *et al.* OrthoDB v10: sampling the diversity of animal, plant, fungal, protist, bacterial and viral genomes for evolutionary and functional annotations of orthologs. *Nucleic acids research* **47,** D807-D811; 10.1093/nar/gky1053. (2019).

78. Győrffy, B., Surowiak, P., Budczies, J. & Lánczky, A. Online survival analysis software to assess the prognostic value of biomarkers using transcriptomic data in non-small-cell lung cancer. *PloS one* **8,** e82241; 10.1371/journal.pone.0082241 (2013).

79. Giannou, A. D. *et al.* NRAS destines tumor cells to the lungs. *EMBO molecular medicine* **9,** 672–686; 10.15252/emmm.201606978 (2017).

80. Arendt, K. A.M. *et al. An in vivo inflammatory loop potentiates KRAS blockade* (2019).

81. Ginouves, M., Carme, B., Couppie, P. & Prevot, G. Comparison of tetrazolium salt assays for evaluation of drug activity against Leishmania spp. *Journal of clinical microbiology* **52,** 2131–2138; 10.1128/JCM.00201-14 (2014).

82. Hauck, S. M. *et al.* Deciphering membrane-associated molecular processes in target tissue of autoimmune uveitis by label-free quantitative mass spectrometry. *Molecular & cellular proteomics : MCP* **9,** 2292–2305; 10.1074/mcp.M110.001073 (2010).

83. Kim, E. S. *et al.* The BATTLE trial: personalizing therapy for lung cancer. *Cancer discovery* **1,** 44–53; 10.1158/2159-8274.CD-10-0010 (2011).

84. Kabbout, M. *et al.* ETS2 mediated tumor suppressive function and MET oncogene inhibition in human non-small cell lung cancer. *Clinical cancer research : an official journal of the American Association for Cancer Research* **19,** 3383–3395; 10.1158/1078-0432.CCR-13-0341 (2013).

85. Brouwer-Visser, J. *et al.* Regulatory T-cell Genes Drive Altered Immune Microenvironment in Adult Solid Cancers and Allow for Immune Contextual Patient Subtyping. *Cancer epidemiology, biomarkers & prevention : a publication of the American Association for Cancer Research, cosponsored by the American Society of Preventive Oncology* **27,** 103–112; 10.1158/1055-9965.EPI-17-0461 (2018).

86. Liberzon, A. *et al.* The Molecular Signatures Database (MSigDB) hallmark gene set collection. *Cell systems* **1,** 417–425; 10.1016/j.cels.2015.12.004 (2015).

87. Campbell, J. D. *et al.* Distinct patterns of somatic genome alterations in lung adenocarcinomas and squamous cell carcinomas. *Nature genetics* **48,** 607–616; 10.1038/ng.3564 (2016).

88. Ahrendt, S. A. *et al.* Cigarette smoking is strongly associated with mutation of the K-ras gene in patients with primary adenocarcinoma of the lung. *Cancer* **92,** 1525–1530; 10.1002/1097-0142(20010915)92:6<1525::aid-cncr1478>3.0.co;2-h (2001).

89. Tate, J. G. *et al.* COSMIC: the Catalogue Of Somatic Mutations In Cancer. *Nucleic acids research* **47,** D941-D947; 10.1093/nar/gky1015 (2019).

90. Singh, A. *et al.* A gene expression signature associated with "K-Ras addiction" reveals regulators of EMT and tumor cell survival. *Cancer cell* **15,** 489–500; 10.1016/j.ccr.2009.03.022 (2009).

91. McDonald, E. R. *et al.* Project DRIVE: A Compendium of Cancer Dependencies and Synthetic Lethal Relationships Uncovered by Large-Scale, Deep RNAi Screening. *Cell* **170,** 577-592.e10; 10.1016/j.cell.2017.07.005 (2017).

92. McCormick, F. KRAS as a Therapeutic Target. *Clinical cancer research : an official journal of the American Association for Cancer Research* **21,** 1797–1801; 10.1158/1078-0432.CCR-14-2662 (2015).

93. Sunaga, N. *et al.* Oncogenic KRAS-induced interleukin-8 overexpression promotes cell growth and migration and contributes to aggressive phenotypes of non-small cell lung cancer. *International journal of cancer* **130,** 1733–1744; 10.1002/ijc.26164 (2012).

94. Ancrile, B., Lim, K.-H. & Counter, C. M. Oncogenic Ras-induced secretion of IL6 is required for tumorigenesis. *Genes & development* **21,** 1714–1719; 10.1101/gad.1549407 (2007).

95. Corcoran, R. B. *et al.* STAT3 plays a critical role in KRAS-induced pancreatic tumorigenesis. *Cancer research* **71,** 5020–5029; 10.1158/0008-5472.CAN-11-0908 (2011).

96. Khosravi, N. *et al.* IL22 Promotes Kras-Mutant Lung Cancer by Induction of a Protumor Immune Response and Protection of Stemness Properties. *Cancer immunology research* **6,** 788–797; 10.1158/2326-6066.CIR-17-0655 (2018).

97. Ji, H. *et al.* K-ras activation generates an inflammatory response in lung tumors. *Oncogene* **25,** 2105–2112; 10.1038/sj.onc.1209237 (2006).

98. Busch, S. E. *et al.* Lung Cancer Subtypes Generate Unique Immune Responses. *Journal of immunology (Baltimore, Md. : 1950)* **197,** 4493–4503; 10.4049/jimmunol.1600576 (2016).

99. Dias Carvalho, P. *et al.* KRAS Oncogenic Signaling Extends beyond Cancer Cells to Orchestrate the Microenvironment. *Cancer research* **78,** 7–14; 10.1158/0008-5472.CAN-17-2084 (2018).

100. Liou, G.-Y. *et al.* Mutant KRAS-induced expression of ICAM-1 in pancreatic acinar cells causes attraction of macrophages to expedite the formation of precancerous lesions. *Cancer discovery* **5,** 52–63; 10.1158/2159-8290.CD-14-0474 (2015).

101. Bertram, J. S. & Janik, P. Establishment of a cloned line of Lewis Lung Carcinoma cells adapted to cell culture. *Cancer letters* **11,** 63–73 (1980).

102. Hao, Z. & Rajewsky, K. Homeostasis of peripheral B cells in the absence of B cell influx from the bone marrow. *The Journal of experimental medicine* **194,** 1151–1164; 10.1084/jem.194.8.1151 (2001).

103. Apte, R. N. *et al.* The involvement of IL-1 in tumorigenesis, tumor invasiveness, metastasis and tumor-host interactions. *Cancer metastasis reviews* **25,** 387–408; 10.1007/s10555-006-9004-4 (2006).

104. Qian, B.-Z. *et al.* CCL2 recruits inflammatory monocytes to facilitate breast-tumour metastasis. *Nature* **475,** 222–225; 10.1038/nature10138 (2011).

105. Lim, S. Y., Yuzhalin, A. E., Gordon-Weeks, A. N. & Muschel, R. J. Targeting the CCL2-CCR2 signaling axis in cancer metastasis. *Oncotarget* **7,** 28697–28710; 10.18632/oncotarget.7376 (2016).

106. Nywening, T. M. *et al.* Targeting tumour-associated macrophages with CCR2 inhibition in combination with FOLFIRINOX in patients with borderline resectable and locally advanced pancreatic cancer: a single-centre, open-label, dose-finding, non-randomised, phase 1b trial. *The Lancet. Oncology* **17,** 651–662; 10.1016/S1470-2045(16)00078-4 (2016).

107.   Nakasone, E. S. *et al.* Imaging tumor-stroma interactions during chemotherapy reveals contributions of the microenvironment to resistance. *Cancer cell* **21,** 488–503; 10.1016/j.ccr.2012.02.017 (2012).

108.   Apte, R. N. & Voronov, E. Is interleukin-1 a good or bad 'guy' in tumor immunobiology and immunotherapy? *Immunological reviews* **222,** 222–241; 10.1111/j.1600-065X.2008.00615.x (2008).

109.   Marazioti, A. *et al.* Beneficial impact of CCL2 and CCL12 neutralization on experimental malignant pleural effusion. *PloS one* **8,** e71207; 10.1371/journal.pone.0071207 (2013).

110.   Krelin, Y. *et al.* Interleukin-1beta-driven inflammation promotes the development and invasiveness of chemical carcinogen-induced tumors. *Cancer research* **67,** 1062–1071; 10.1158/0008-5472.CAN-06-2956 (2007).

111.   Fridlender, Z. G. *et al.* CCL2 blockade augments cancer immunotherapy. *Cancer research* **70,** 109–118; 10.1158/0008-5472.CAN-09-2326 (2010).

112.   Loberg, R. D. *et al.* Targeting CCL2 with systemic delivery of neutralizing antibodies induces prostate cancer tumor regression in vivo. *Cancer research* **67,** 9417–9424; 10.1158/0008-5472.CAN-07-1286 (2007).

113.   Sandhu, S. K. *et al.* A first-in-human, first-in-class, phase I study of carlumab (CNTO 888), a human monoclonal antibody against CC-chemokine ligand 2 in patients with solid tumors. *Cancer chemotherapy and pharmacology* **71,** 1041–1050; 10.1007/s00280-013-2099-8 (2013).

114.   Brana, I. *et al.* Carlumab, an anti-C-C chemokine ligand 2 monoclonal antibody, in combination with four chemotherapy regimens for the treatment of patients with solid

tumors: an open-label, multicenter phase 1b study. *Targeted oncology* **10,** 111–123; 10.1007/s11523-014-0320-2 (2015).

115.   Ridker, P. M. *et al.* Effect of interleukin-1β inhibition with canakinumab on incident lung cancer in patients with atherosclerosis: exploratory results from a randomised, double-blind, placebo-controlled trial. *Lancet (London, England)* **390,** 1833–1842; 10.1016/S0140-6736(17)32247-X (2017).

116.   Ridker, P. M. *et al.* Antiinflammatory Therapy with Canakinumab for Atherosclerotic Disease. *The New England journal of medicine* **377,** 1119–1131; 10.1056/NEJMoa1707914 (2017).

117.   Kasashima, H. *et al.* Clinicopathologic significance of the CXCL1-CXCR2 axis in the tumor microenvironment of gastric carcinoma. *PloS one* **12,** e0178635; 10.1371/journal.pone.0178635 (2017).

118.   Champeris Tsaniras, S. *et al.* Geminin ablation in vivo enhances tumorigenesis through increased genomic instability. *The Journal of pathology* **246,** 134–140; 10.1002/path.5128 (2018).

119.   Huang, Q. *et al.* Caspase 3-mediated stimulation of tumor cell repopulation during cancer radiotherapy. *Nature medicine* **17,** 860–866; 10.1038/nm.2385 (2011).

120.   Zhang, J. *et al.* P62 regulates resveratrol-mediated Fas/Cav-1 complex formation and transition from autophagy to apoptosis. *Oncotarget* **6,** 789–801; 10.18632/oncotarget.2733 (2015).

121.   Kavanagh, E., Rodhe, J., Burguillos, M. A., Venero, J. L. & Joseph, B. Regulation of caspase-3 processing by cIAP2 controls the switch between pro-inflammatory activation and cell death in microglia. *Cell death & disease* **5,** e1565; 10.1038/cddis.2014.514 (2014).

122. Almagro, M. C. de & Vucic, D. The inhibitor of apoptosis (IAP) proteins are critical regulators of signaling pathways and targets for anti-cancer therapy. *Experimental oncology* **34,** 200–211 (2012).

123. Lee, M.-H., Zhao, R., Phan, L. & Yeung, S.-C. J. Roles of COP9 signalosome in cancer. *Cell cycle (Georgetown, Tex.)* **10,** 3057–3066; 10.4161/cc.10.18.17320 (2011).

124. Schlierf, A. *et al.* Targeted inhibition of the COP9 signalosome for treatment of cancer. *Nature communications* **7,** 13166; 10.1038/ncomms13166 (2016).

9. Abbreviations

9.1 List of acronyms and abbreviations

AA	amino acid
ABTS	2,2'-Azinobis [3-ethylbenzothiazoline-6-sulfonic acid]-diammonium salt
ATP	adenosine triphosphate
BM	bone marrow
BMT	bone marrow transplantation
BSA	bovine serum albumin
BrdU	bromodeoxyuridine, 5-bromo-2'-deoxyuridine
CRC	colorectal cancer
DMEM	dulbecco's modified eagle medium
DMSO	dimethylsulfoxide
DRIVE	deep RNAi interrogation of viability effects in cancer
e.g.	exempli gratia, for example
ELISA	enzyme-linked immunosorbent assay
GdmCL	guanidine hydrochloride
GSEA	gene set enrichment analysis
GTP	guanosine triphosphate
HR	hazard ratio
ip	intraperitoneal
iv	intravenous
IU	international units
Kras/KRAS^{MUT}	Kras/KRAS mutant
Kras/KRAS^{WT}	Kras/KRAS wildtype
LADC	lung adenocarcinoma
LC	lung cancer

ml	milliliter
MPE	malignant pleural effusion
MTT	3-(4,5-dimethylthiazol-2-yl)-2,5-diphenyltetrazolium bromide
MTS	3-(4,5-dimethylthiazol-2-yl)-5-(3-carboxymethoxyphenyl)-2-(4-sulfophenyl)-2H-tetrazolium)
NAD/NADH	nicotinamide adenine dinucleotide
NADP/NADPH	nicotinamide adenine dinucleotide phosphate
nm	nanometer
NSCLC	non-small-cell lung cancer
PBS	phosphate-buffered saline
PDAC	pancreatic ductal adenocarcinoma
PMS	5-methylphenazinium methyl sulfate
RIPA	radioimmunoprecipitation assay
RPMI	roswell park memorial institute
sc	subcutan
SCID mice	Severe combined immunodeficient mice
SCLC	small-cell lung cancer
SDS	sodiumdodecylsulfate
SDS-PAGE	SDS-polyacrylamide gel electrophoresis
sh	short hairpin
SQCLC	squamous cell lung cancer
TAE	Tris-acetate-EDTA
TCGA	the cancer genome atlas
TKI	tyrosine-kinase-inhibitor
WT	wild-type
WST-8	tetrazolium-1[2-(4-iodophenyl)-3-(4-nitrophenyl)-5-(2,4-disulphophenyl)-2H-teterazolium
µg	microgramm

9.2   List of gene/protein description

AKT	Protein Kinase B
ALK	Anaplastic Lymphoma Receptor Tyrosine Kinase
ARID1A	AT-Rich Interaction Domain 1A
BAD	Bcl-2-Antagonist of Cell Death
BCL-2	B-cell Lymphoma 2
BRAF	B-Raf Proto-Oncogene
CCL2	C-C motif Chemokine Ligand 2
CCR2	C-C motif Chemokine Receptor 2
CDK4	Cyclin Dependent Kinase 4
CDKN2A	Cyclin Dependent Kinase Inhibitor 2A
CXCL1	Chemokine (C-X-C motif) Ligand 1
CXCR1	Chemokine (C-X-C motif) Receptor 1
EGFR	Epidermal Growth Factor Receptor
ERK	Extracellular-Signal-Regulated Kinase
FT	Farnesyltransferase
GAP	GTPase Activating Protein
GAPDH	Glyceraldehyde 3-Phosphate Dehydrogenase
GEF	Guanine Nucleotide Exchange Factor
GGT	Geranylgeranytransferase
Gmnn	Geminin DNA Replication Inhibitor
GRB2	Growth Factor Receptor Bound 2
HRAS	HRas Proto-Oncogene; Harvey Rat Sarcoma (historical name)
HRP	Horseradish Peroxidase
ICMT	Isoprenylcysteine Carboxylmethyltransferase
IKKα/β	IκB Kinase alpha/beta
IκB	NF-kappa-B inhibitor alpha
IL1B	Interleukin 1 beta
IL1R	Interleukin 1 Receptor
iPLA2	Calcium Independent Phospholipase A2

KEAP	Kelch Like ECH Associated Protein 1
KRAS	KRAS proto-oncogene GTPase; Kirsten Rat Sarcoma (historical name)
LDH	Lactate Dehydrogenase
MAPK	Mitogen-Activated Protein Kinase
MCP-1	Monocyte Chemotactic Protein 1
MEK	Mitogen-activated Protein Kinase Kinase (MAPKK)
MET	MET Proto-Oncogene
mTOR	Mammalian Target of Rapamycin
NF-κB	Nuclear Factor κ light-chain Enhancer of Activated B Cells
NF1	Neurofibromin-1
NRAS	NRAS Proto-Oncogene; Neuroblastoma Rat Sarcoma (historical name)
PD-1	Programmed Cell Death 1
PD-L1	Programmed Cell Death-Ligand 1
PDEδ	Phosphodiesterase δ
PDK1	Pyruvate Dehydrogenase Kinase 1
PIK3CA	Phosphatidylinositol-4,5-Bisphosphate 3-Kinase Catalytic Subunit Alpha
PI3K	Phosphatidylinositol 3-Kinase
PLK1	Polo Like Kinase 1
PTEN	Phosphatase and Tensin Homolog
p-ERK	Phospho- Extracellular-Signal Regulated Kinase
RAG2	Recombination Activating Gene 2
RAF	Rapidly Accelerated Fibrosarcoma
RAS	Ras Sarcoma
RCE1	Ras-Converting Enzyme 1
RTK	Receptor Tyrosine Kinase
ROS1	ROS Proto-Oncogene 1
SHC	SHC Adaptor Protein
SH3	Sarcoma Homology 3
SMAC	Second Mitochondrial Derived Activator of Caspases
SMARCA4	SWI/SNF Related, Matrix Associated, Actin Dependent Regulator Of Chromatin, Subfamily A, Member 4

SOS	Son of Sevenless
STK11	Serine/Threonine Kinase 11
TBK1	TANK Binding Kinase 1
t-ERK	Total- Extracellular-Signal Regulated Kinase
TP53	Tumor Protein P53

10. List of figures

11.   List of tables

12. Appendix

12.1 Supplementary figures

Supplementary figure. S1: Response of KRAS-mutant cancer cell lines to deltarasin IC_{60} concentrations for 72 hours and analysis by colony formation assay. Diverse mouse (A; $Kras^{MUT}$: LLC, FULA1; $Kras^{WT}$: B16F10, PANO2) and human (B; $KRAS^{MUT}$: A549, H460; $KRAS^{WT}$: EKVX, H3122) tumor cell lines were evaluated for colony formation ($n = 3$/ data-point). Data presented as mean ± SD. P, overall probability by one-way ANOVA. ns, *, **, ***, and ****: P > 0.05, P < 0.05, P < 0.01, P < 0.001, and P < 0.0001 respectively, for the presented comparisons by Bonferroni post-tests. Shown are total number of colonies formed (A, B), plating efficiency of 300 cells/well at experiment start (C, D), and survival fraction of single cells given as ratio treatment/ no treatment (E, F). Figure modified from Arendt *et al.*[80].
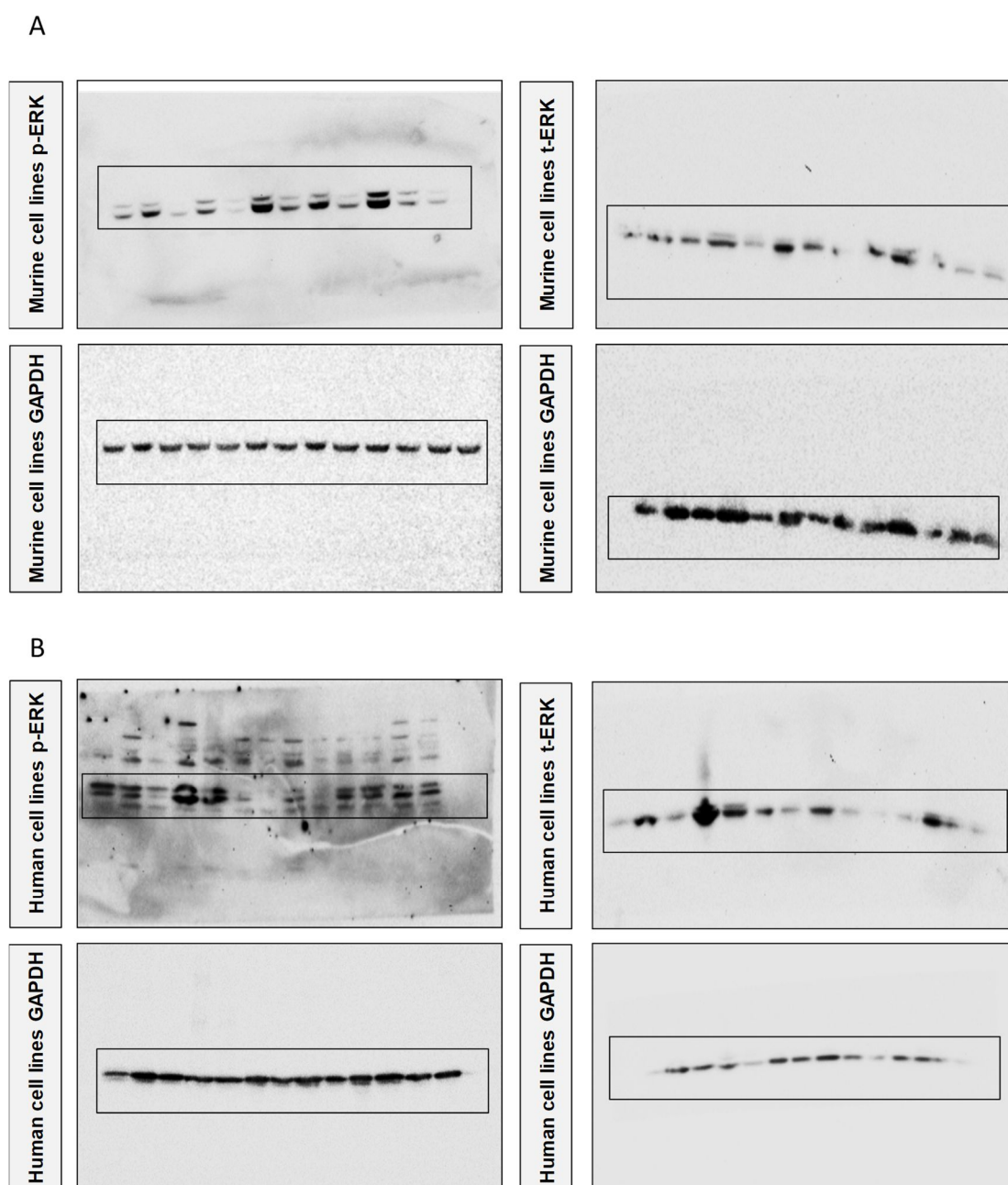
Supplementary figure. S2: Full pictures of Western blot analysis for figure 12D. (A) Murine cell line protein extracts of untreated and treated samples with deltarasin (72 hours; IC$_{60}$). Left, p-ERK, right t-ERK; below, belonging GAPDH lanes. (B) Human cell line protein extracts of untreated and treated samples with deltarasin (72 hours; IC$_{60}$). Left, p-ERK, right t-ERK; below, belonging GAPDH lanes. Black boxes highlight areas of the blots shown in main figure. Figure modified from Arendt *et al.*[80]*.
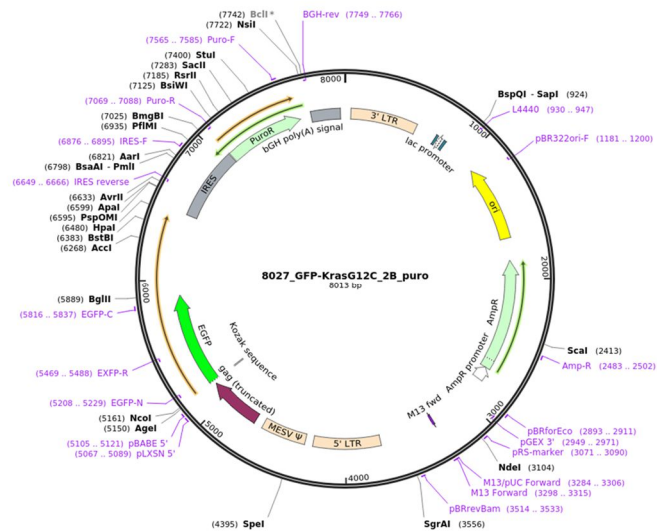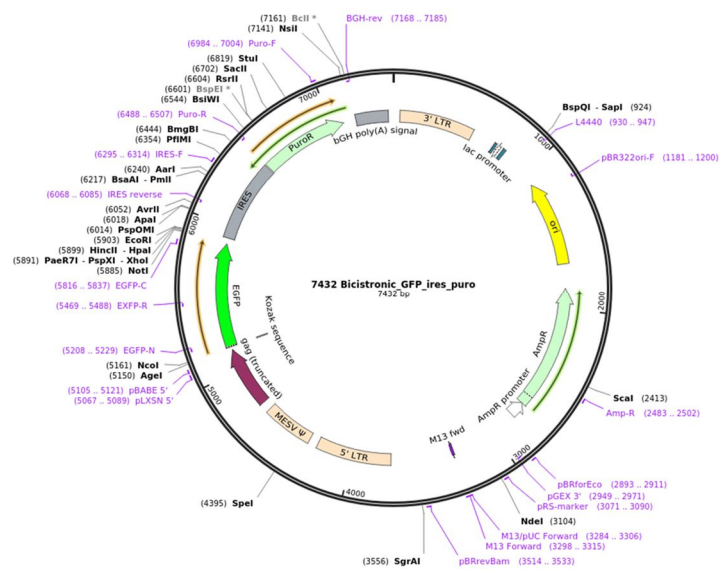
Supplementary figure. S3: Vector maps of GFP-Kras^{G12C} plasmid. Overexpression of mutant KRAS (A) and control plasmid with only GFP (B). Vector maps from http://www.addgene.com. Plasmids are purchased through the Addgene website.
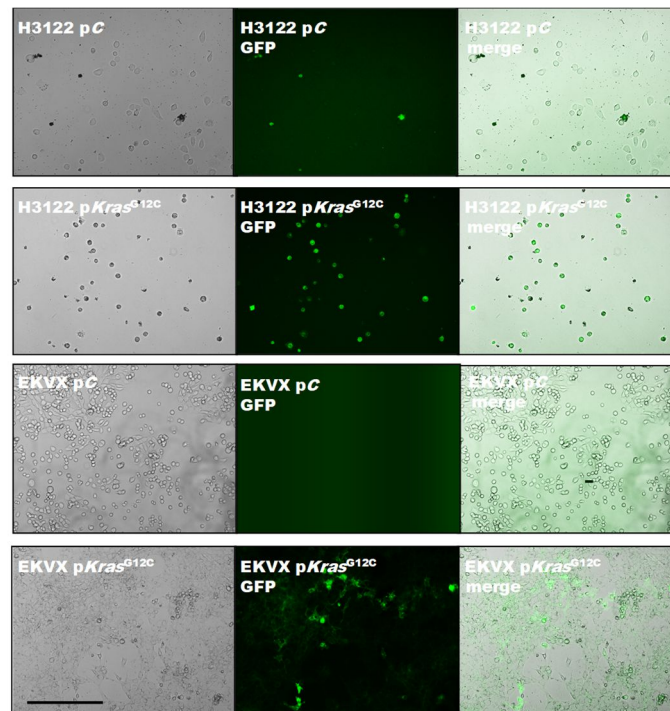
Supplementary figure. S4: Transduction of pKras[G12C] in human cell lines H3122 and EKVX was validated via immunofluorescence. The pKras[G12C] plasmid includes GFP and puromycin resistance genes. Representative microscopy images of p*C* control or pKras[G12C] transfected cell lines. Left, brightfield images; middle, green fluorescent images; right, merged images. A confocal microscope LCI510 (Zeiss; Jena, Germany) was used. Figure modified from Arendt *et al.*[80].

Supplementary figure. S5: Full pictures of Western blot analysis for figure 15D. Murine and human cell line protein extracts with or without *Kras/KRAS* genetic modification were used for this experiment. Left, p-ERK, right, t-ERK; below, belonging GAPDH lanes. Black boxes are the area of the blots presented in the main figure. Figure modified from Arendt *et al.*[80].
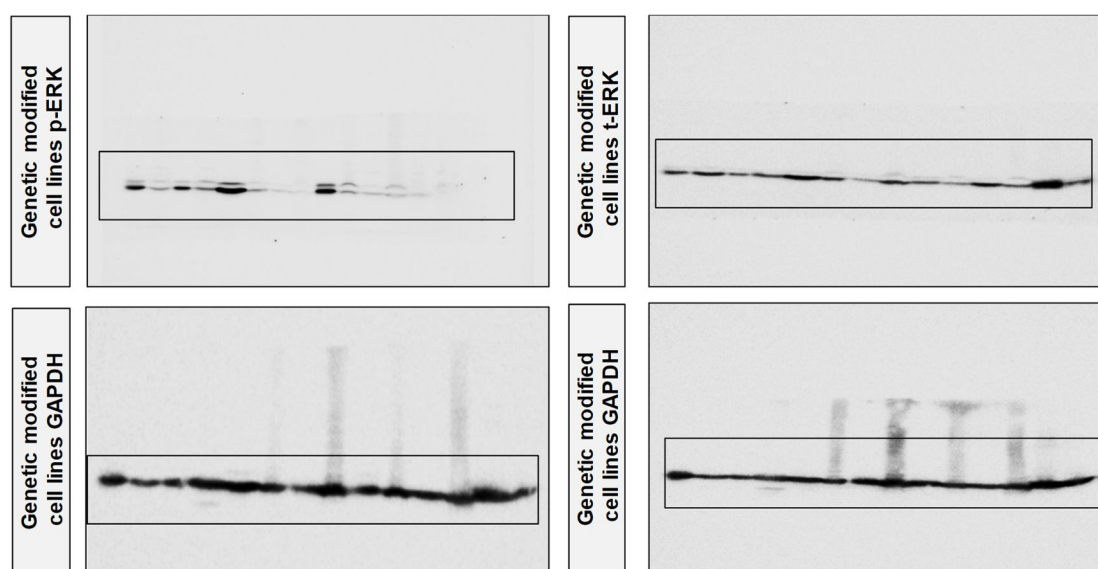
1408 genes
significantly (P < 0.05) over- or under-represented in
KRAS-mutant cell lines (LLC, AE17, MC38, FULA1) over both *KRAS*-WT cell lines (B16F10, B16F10 pC, PANO2, CULA) and benign samples (TEC, BMDM, BMMC, Lungs)

116 genes
over-represented in *KRAS*-mutant cells, silenced by *KRAS*-shRNA, and induced by *KRAS*-overexpression

33 genes
under-represented in *KRAS*-mutant cells, induced by *KRAS*-shRNA, and suppressed by *KRAS*-overexpression

55 genes
with equivocal changes

204 common genes

3432 genes
responsive (ΔGE > 1.4) to both
KRAS-shRNA in *KRAS*-mutant cell lines (LLC and AE17) and to *KRAS*-overexpression in *KRAS*-WT cell lines (B16F10 and PANO2)

Filtering MC38 manual

32 genes
over-represented in *KRAS*-mutant cells, silenced by *KRAS*-shRNA, and induced by *KRAS*-overexpression

10 genes
under-represented in *KRAS*-mutant cells, induced by *KRAS*-shRNA, and suppressed by *KRAS*-overexpression

128 genes
with equivocal changes

170 common genes

Supplementary figure. S6: Detailed overview of the analysis of the transcriptomics data of murine cell lines. MC38 was filtered manually since data was produced on a different GeneChip (Mouse Gene 1.0 ST array). All the other samples were hybridized to GeneChip MoGene 2.0 ST arrays (Affymetrix, St. Clara, CA). For analysis TAC software was used and differential gene expression was filtered for a final mutant *Kras*-specific gene list.
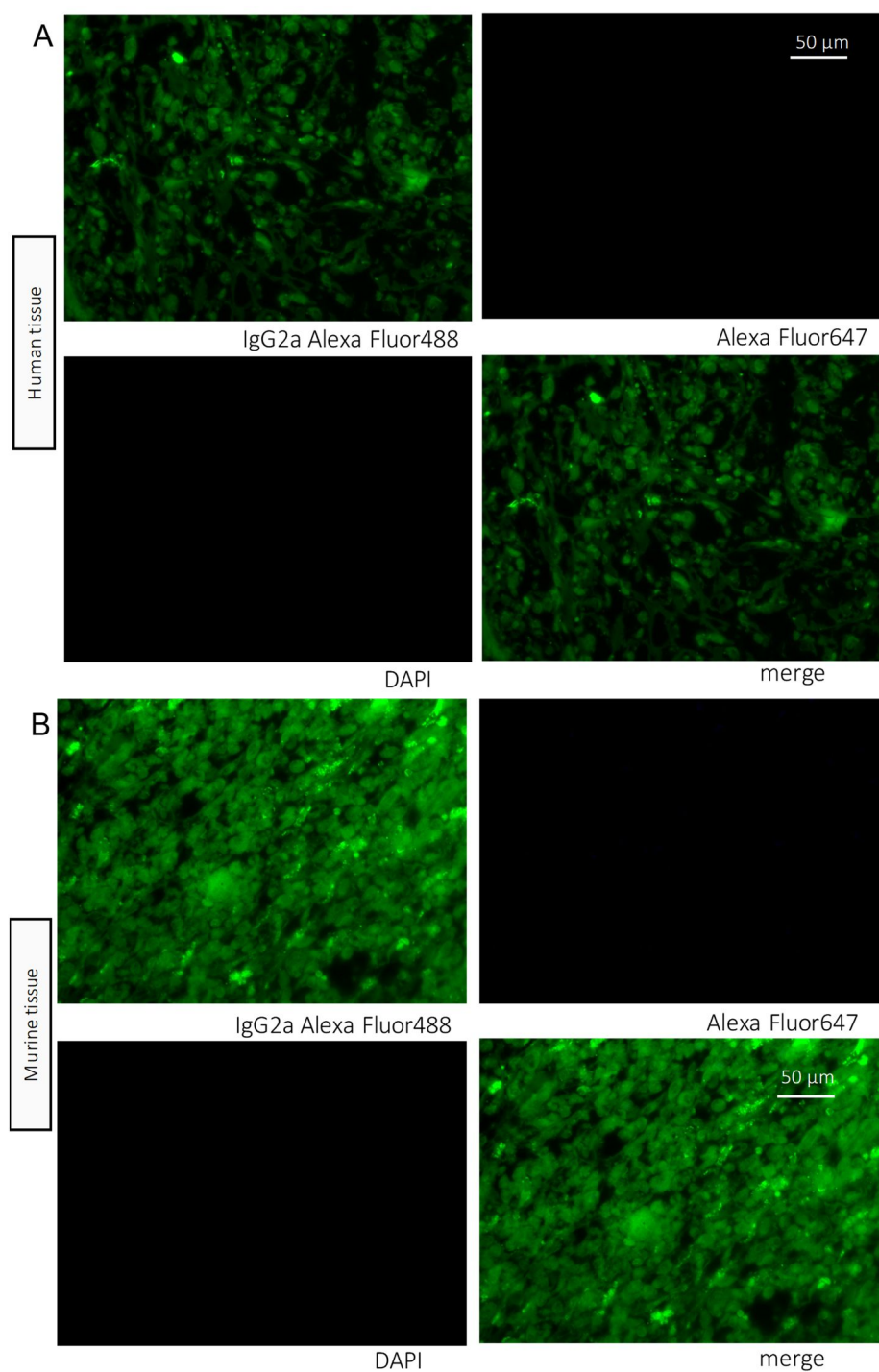
Supplementary figure. S7: Immunofluorescence images of tumor tissue sections. Human and murine tumors were established through sc injection of 10^6 tumor cells (FULA1, PANO2; H460, EKVX) and extracted from these xenograft flank models (*FVB, C57BL/6; Rag2$^{-/-}$ mice*). Antibody control stainings for IL-1β (IgG2a Alexa Fluor488) and CCR2 (Alexa Fluor647). Bar = 50 µm.

12.2   Supplementary tables

Supplementary table S1: Deltarasin effects tested in murine and human cancer cell lines.

Originating oganism	Cell line	Tissue origin	*KRAS* mutation	IC$_{50}$ (µM, mean±SD)[a]	*n*
C57BL/6 mouse	LLC	Lewis lung carcinoma	G12C	1.46 ± 0.16	3
C57BL/6 mouse	MC38	Colon adenocarcinoma	G13R	1.23 ± 0.22	3
C57BL/6 mouse	AE17	Malignant pleural mesothelioma	G12C	1.61 ± 0.13	3
FVB mouse	FULA	Urethane-induced lung adenocarcinoma	Q61R	2.10 ± 0.06	3
C57BL/6 mouse	B16F10	Malignant skin melanoma	None	2.41 ± 0.37	3
C57BL/6 mouse	PANO2	Pancreatic adenocarcinoma	None	2.10 ± 0.49	4
C57BL/6 mouse	CULA	Urethane-induced lung adenocarcinoma	None	1.59 ± 0.29	3
Human	A549	Lung adenocarcinoma	G12S	6.90 ± 0.96	3
Human	H460	Lung large cell carcinoma	Q61H	5.27 ± 2.24	3
Human	H358	NSCLC	G12C	3.27 ±1.10	3
Human	H358M	Bronchiolo-alveolar carcinoma	G12D	3.67 ± 1.70	3
Human	H1944	NSCLC	G13D	6.93 ± 1.32	3
Human	H520	Squamous cell carcinoma	None	1.67 ± 0.06	3
Human	EKVX	Lung adenocarcinoma	None	4.22 ± 2.41	3
Human	H1299	NSCLC	None	5.40 ± 1.81	3
Human	H3122	NSCLC	None	4.73 ± 1.38	3

a IC$_{50}$, 50% inhibitory concentration by WST-8 assay (Bimake); SD, standard deviation; *n*, sample size; NSCLC, non-small cell lung cancer.

Supplementary table S2: AA12 effects tested in murine and human cancer cell lines.

Originating oganism	Cell line	Tissue origin	*KRAS* mutation	IC$_{50}$ (μM, mean±SD)[a]	*n*
C57BL/6 mouse	LLC	Lewis lung carcinoma	G12C	22.69 ± 7.95	3
C57BL/6 mouse	MC38	Colon adenocarcinoma	G13R	4.59 ± 2.45	2
C57BL/6 mouse	AE17	Malignant pleural mesothelioma	G12C	3.06 ± 1.39	2
FVB mouse	FULA1	Urethane-induced lung adenocarcinoma	Q61R	4.97 ± 2.28	2
C57BL/6 mouse	PANO2	Pancreatic adenocarcinoma	None	20.85 ± 5.11	2
Human	A549	Lung adenocarcinoma	G12S	49.30 ± 24.31	3
Human	HOP-62	Lung adenocarcinoma	G12C		3
Human	H358	NSCLC	G12C	27.85 ± 4.41	2
Human	H3122	NSCLC	None	24.24 ± 11.41	3

a IC$_{50}$, 50% inhibitory concentration by WST-8 assay (Bimake); SD, standard deviation; *n*, sample size; NSCLC, non-small cell lung cancer.

Supplementary table S3: Cysmethynil effects tested in murine and human cancer cell lines.

Originating oganism	Cell line	Tissue origin	*KRAS* mutation	IC$_{50}$ (µM, mean±SD)[a]	*n*
C57BL/6 mouse	LLC	Lewis lung carcinoma	G12C	22.11 ± 2.19	2
C57BL/6 mouse	MC38	Colon adenocarcinoma	G13R	18.13 ± 9.92	2
C57BL/6 mouse	AE17	Malignant pleural mesothelioma	G12C	17.62 ± 3.57	3
FVB mouse	FULA1	Urethane-induced lung adenocarcinoma	Q61R	27.37 ± 7.78	2
C57BL/6 mouse	B16F10	Malignant skin melanoma	None	19.61 ± 13.27	3
C57BL/6 mouse	PANO2	Pancreatic adenocarcinoma	None	16.92 ± 17.22	2
Human	A549	Lung adenocarcinoma	G12S	30.84 ± 9.10	3
Human	H358	NSCLC	G12C	28.32 ± 6.57	3
Human	EKVX	Lung adenocarcinoma	None	30.05 ± 5.66	3
Human	H3122	NSCLC	None	10.95 ± 3.77	3

a IC$_{50}$, 50% inhibitory concentration by WST-8 assay (Biomake); SD, standard deviation; *n*, sample size; NSCLC, non-small cell lung cancer.

Supplementary table S4: Deltarasin in combination with IC_{25} BV6 (murine: 3 µM, human: 6.5 µM) effects tested in murine and human cancer cell lines.

Originating oganism	Cellline	Tissue origin	*KRAS* mutation	IC_{50} (µM, mean±SD)[a]	*n*
C57BL/6 mouse	LLC	Lewis lung carcinoma	G12C	0.004 ± 0.01	2
FVB mouse	FULA1	Urethane-induced lung adenocarcinoma	Q61R	0.25 ± 0.07	2
C57BL/6 mouse	B16F10	Malignant skin melanoma	None	0.2 ± 0.14	2
C57BL/6 mouse	PANO2	Pancreatic adenocarcinoma	None	0.35 ± 0.07	2
Human	A549	Lung adenocarcinoma	G12S	0.03 ± 0.01	2
Human	H460	Lung large cell carcinoma	Q61H	0.01 ± 0.003	2
Human	EKVX	Lung adenocarcinoma	None	1.31 ± 0.14	2
Human	H3122	NSCLC	None	0.31 ± 0.02	2

a IC_{50}, 50% inhibitory concentration by WST-8 assay (Bimake); SD, standard deviation; *n*, sample size; NSCLC, non-small cell lung cancer.

Supplementary table S5: Deltarasin in combination with IC_{25} Z-DEVD-FMK (murine: 12 µM, human: 22 µM) effects tested in murine and human cancer cell lines.

Originating oganism	Cell line	Tissue origin	*KRAS* mutation	IC_{50} (µM, mean±SD)[a]	*n*
C57BL/6 mouse	LLC	Lewis lung carcinoma	G12C	2.86 ± 0.68	2
FVB mouse	FULA1	Urethane-induced lung adenocarcinoma	Q61R	2.61 ± 0.58	2
C57BL/6 mouse	B16F10	Malignant skin melanoma	None	0.65 ± 0.49	2
C57BL/6 mouse	PANO2	Pancreatic adenocarcinoma	None	6.95 ± 2.05	2
Human	A549	Lung adenocarcinoma	G12S	2.45 ± 0.78	2
Human	H460	Lung large cell carcinoma	Q61H	2.55 ± 0.77	2
Human	EKVX	Lung adenocarcinoma	None	3.05 ± 0.21	2
Human	H3122	NSCLC	None	2.99 ± 0.69	2

a IC_{50}, 50% inhibitory concentration by WST-8 assay (Bimakel); SD, standard deviation; *n*, sample size; NSCLC, non-small cell lung cancer.

Supplementary table S6: Microarray analysis was performed and created a 42-gene mutant *Kras* signature after analysis of significant genes (P < 0.05 by unpaired ANOVA with bonferroni post-tests). For identification, *Kras*-mutant tumor cells compared with *Kras*-wild-type tumor cells and benign cells and tissues were tested, as well as >30% response to modulation of *Kras* expression five tumor cell line doublets tested (AE17, LLC, and MC38 cells expressing sh*C* versus sh*Kras* and B16F10 and PANO2 cells expressing pC versus p*Kras*[G12C]). Table modified from Arendt *et al.*[80].

Gene Symbol	Description	*Kras*[WTa]	*Kras*[MUTb]	% *Kras*[Rc]
Ccl2	chemokine (C-C motif) ligand 2	0.82	37.79	56.29
Ranbp3l	RAN binding protein 3-like	0.93	35.26	78.33
Il1r1	interleukin 1 receptor, type I	2.39	25.63	36.71
Gpr149	G protein-coupled receptor 149	0.80	22.94	55.68
Cfap69	cilia and flagella associated protein 69	4.50	20.11	40.29
Ccl7	chemokine (C-C motif) ligand 7	0.96	16.11	50.14
2810417H13Rik	RIKEN cDNA 2810417H13 gene	11.39	12.64	42.33
Pdgfra	platelet derived growth factor receptor α	1.89	12.38	41.60
Casp3	caspase 3	4.20	10.48	30.74
Ttk	Ttk protein kinase	7.94	9.58	45.13
Kif2c	kinesin family member 2C	5.98	7.78	45.06
Fanca	Fanconi anemia, complementation group A	4.00	5.58	46.78
Cdca5	cell division cycle associated 5	3.56	5.43	47.15
Rassf8	Ras association (RalGDS/AF-6) domain family (N-terminal) member 8	2.46	5.35	32.08
Hist2h3c2	histone cluster 2, H3c2	1.20	4.69	38.87
Plag1	pleiomorphic adenoma gene 1	0.78	4.53	53.15
Nadk2	NAD kinase 2, mitochondrial	1.58	4.50	50.89
Oaf	OAF homolog (Drosophila)	2.39	4.23	31.03
Cxcl1	chemokine (C-X-C motif) ligand 1	1.56	4.23	73.09
Mmd	monocyte to macrophage differentiation-associated	2.93	4.06	35.92
Csgalnact1	chondroitin sulfate N-acetylgalactosaminyltransferase 1	0.74	3.97	50.96

Clybl	citrate lyase beta like	1.72	3.76	42.33
Zfp334	zinc finger protein 334	1.04	3.68	58.59
Kras	v-Ki-ras2 Kirsten rat sarcoma viral oncogene homolog	2.08	2.60	39.71
Palb2	partner and localizer of BRCA2	2.39	2.57	30.55
Kcnab3	potassium voltage-gated channel, shaker-related subfamily, beta member 3	1.25	2.55	49.23
Mcts2	malignant T cell amplified sequence 2	1.45	2.36	30.65
Pcnxl4	pecanex-like 4 (Drosophila)	1.38	2.19	39.54
Gmnn	geminin	1.39	2.04	34.57
9530077C05Rik	RIKEN cDNA 9530077C05 gene	1.17	1.88	30.46
Poc1a	POC1 centriolar protein homolog A	1.46	1.68	36.71
Dhx40	DEAH (Asp-Glu-Ala-His) box polypeptide 40	1.28	1.67	31.03
Pde8a	phosphodiesterase 8A	1.54	0.23	-181.67
mt-Tt	mitochondriallyencoded tRNA theonine	0.78	0.22	-95.34
Mapkapk3	mitogen-activated protein kinase-activated protein kinase 3	0.60	0.20	-96.43
Anxa6	annexin A6	0.69	0.19	-76.05
mt-Te	mitochondrially encoded tRNA glutamic acid	0.33	0.16	-49.69
mt-Ty	mitochondriallyencoded tRNA tyrosine	0.22	0.15	-77.77
Bmyc	brain expressed myelocytomatosis oncogene	1.42	0.15	-71.71
Gm2a	GM2 ganglioside activator protein	0.40	0.12	-70.05
Smpdl3a	sphingomyelin phosphodiesterase, acid-like 3A	1.21	0.11	-123.77
mt-Tn	mitochondriallyencoded tRNA asparagine	0.33	0.11	-105.91

a   Normalized mRNA expression levels of *Kras*-wild-type (WT) cell lines (B16F10, B16F10 p*C*, CULA, and PANO2) presented as ratios to expression of benign cells (bone marrow-derived macrophages BMDM and mast cells BMMC, tracheal epithelial cells TEC) and lungs (n = 4/group).

b   Normalized mRNA expression levels of *Kras*-mutant (MUT) cell lines (AE17, FULA1, LLC, and MC38) presented as ratios to expression of benign cells (BMDM, BMMC, and TEC) and lungs (n = 4/group).

c   Percentile mean response (R) of mRNA expression to *Kras* modulation, including *Kras* silencing of *Kras*-mutant cell lines (AE17, LLC, and MC38) and overexpression of mutant Kras[G12C] plasmid in

Kras-wildtype cells (B16F10 and PANO2). Positive responses specify suppression by *Kras* silencing and induction by overexpression of mutant Kras[G12C] plasmid. Negative responses specify induction by *Kras* silencing and suppression by overexpression of mutant Kras[G12C] plasmid.

LLC, C57BL/6 Lewis lung carcinoma; MC38, C57BL/6 colon adenocarcinoma; AE17, C57BL/6 malignant pleural mesothelioma; FULA, FVB urethane-induced lung adenocarcinoma; B16F10, C57BL/6 malignant skin melanoma; PANO2, C57BL/6 pancreatic adenocarcinoma; CULA, C57BL/6 urethane-induced lung adenocarcinoma.

12.3   Supplementary list: Hallmark gene set, Broad institute[86]

- HALLMARK_ADIPOGENESIS
- HALLMARK_ALLOGRAFT_REJECTION
- HALLMARK_ANDROGEN_RESPONSE
- HALLMARK_ANGIOGENESIS
- HALLMARK_APICAL_JUNCTION
- HALLMARK_APICAL_SURFACE
- HALLMARK_APOPTOSIS
- HALLMARK_BILE_ACID_METABOLISM
- HALLMARK_CHOLESTEROL_HOMEOSTASIS
- HALLMARK_COAGULATION
- HALLMARK_COMPLEMENT
- HALLMARK_DNA_REPAIR
- HALLMARK_E2F_TARGETS
- HALLMARK_EPITHELIAL_MESENCHYMAL_TRANSITION
- HALLMARK_ESTROGEN_RESPONSE_EARLY
- HALLMARK_ESTROGEN_RESPONSE_LATE
- HALLMARK_FATTY_ACID_METABOLISM
- HALLMARK_G2M_CHECKPOINT
- HALLMARK_GLYCOLYSIS
- HALLMARK_HEDGEHOG_SIGNALING
- HALLMARK_HEME_METABOLISM
- HALLMARK_HYPOXIA
- HALLMARK_IL2_STAT5_SIGNALING
- HALLMARK_IL6_JAK_STAT3_SIGNALING
- HALLMARK_INFLAMMATORY_RESPONSE
- HALLMARK_INTERFERON_ALPHA_RESPONSE
- HALLMARK_INTERFERON_GAMMA_RESPONSE
- HALLMARK_KRAS_SIGNALING_DN
- HALLMARK_KRAS_SIGNALING_UP
- HALLMARK_MITOTIC_SPINDLE
- HALLMARK_MTORC1_SIGNALING
- HALLMARK_MYC_TARGETS_V1
- HALLMARK_MYC_TARGETS_V2
- HALLMARK_MYOGENESIS
- HALLMARK_NOTCH_SIGNALING
- HALLMARK_OXIDATIVE_PHOSPHORYLATION

- – HALLMARK_P53_PATHWAY
- – HALLMARK_PANCREAS_BETA_CELLS
- – HALLMARK_PEROXISOME
- – HALLMARK_PI3K_AKT_MTOR_SIGNALING
- – HALLMARK_PROTEIN_SECRETION
- – HALLMARK_REACTIVE_OXIGEN_SPECIES_PATHWAY
- – HALLMARK_SPERMATOGENESIS
- – HALLMARK_TGF_BETA_SIGNALING
- – HALLMARK_TNFA_SIGNALING_VIA_NFKB
- – HALLMARK_UNFOLDED_PROTEIN_RESPONSE
- – HALLMARK_UV_RESPONSE_DN
- – HALLMARK_UV_RESPONSE_UP
- – HALLMARK_WNT_BETA_CATENIN_SIGNALING
- – HALLMARK_XENOBIOTIC_METABOLISM

12.4 Supplementary references for Fig. 11D

S1.   Agalioti T, Giannou AD, Krontira AC, Kanellakis NI, Kati D, Vreka M, et al. Mutant KRAS promotes malignant pleural effusion formation. Nat Commun 2017;8:15205.

S2.   Marazioti A, Lilis I, Vreka M, Apostolopoulou H, Kalogeropoulou A, Giopanou I,et al. Myeloid-derived IL-1ß drives oncogenic KRAS-NF-kB addiction in malignant pleural effusion. Nat Commun 2018; 9:672.

S3.   Giannou AD, Marazioti A, Kanellakis NI, Giopanou I, Lilis I, Zazara DE, et al. NRAS destines tumor cells to the lungs. EMBO Mol Med2017;9:672–686.

S4.   Giopanou I, Lilis I, Papaleonidopoulos V, Agalioti T, Kanellakis NI, Spiropoulou N, et al. Tumor–derived osteopontin isoforms cooperate with TRP53 and CCL2 to promote lung metastasis. Oncoimmunology 2017;6:e1256528.

S5.   Kanellakis NI, Giannou AD, Pepe MA, Agalioti T, Zazara DE, Giopanou I, et al. Tobacco chemical-induced mouse lung adenocarcinoma cell lines pin the prolactin orthologue proliferin as a lung tumour promoter. Carcinogenesis 2019 Mar 4. pii: bgz047. doi: 10.1093/carcin/bgz047.

S6.   Giannou AD, Marazioti A, Spella M, Kanellakis NI, Apostolopoulou H, Psallidas I, et al. Mast cells mediate malignant pleural effusion formation. J Clin Invest 2015;125:2317–34.

S7.   Tate JG, Bamford S, Jubb HC, Sondka Z, Beare DM, Bindal N, et al. COSMIC: the Catalogue Of Somatic Mutations In Cancer. Nucleic Acids Res 2019;47:D941–D947.

S8.   Hong S, Hong S, Han SB. Overcoming metastatic melanoma with BRAF inhibitors. Arch Pharm Res 2011;34:699-701.

S9.   Yamaguchi T, Kakefuda R, Tajima N, Sowa Y, Sakai T. Antitumor activities of JTP-74057 (GSK1120212), a novel MEK1/2 inhibitor, on colorectal cancer cell lines in vitro and in vivo. Int J Oncol 2011;39:23-31.

S10.   Hirano T, Yasuda H, Tani T, Hamamoto J, Oashi A, Ishioka K, et al. In vitro modeling to determine mutation specificity of EGFR tyrosine kinase inhibitors against clinically relevant EGFR mutants in non-small-cell lung cancer. Oncotarget2015;6:38789-803.

S11.   Sakamoto H, Tsukaguchi T, Hiroshima S, Kodama T, Kobayashi T, Fukami TA, et al. CH5424802, a selective ALK inhibitor capable of blocking the resistant gatekeeper mutant. Cancer Cell 2011;19:679-90.

S12.   Huang WS, Liu S, Zou D, Thomas M, Wang Y, Zhou T, et al. Discovery of Brigatinib (AP26113), a Phosphine Oxide-Containing, Potent, Orally Active Inhibitor of Anaplastic Lymphoma Kinase. J Med Chem 2016;59:4948-64.

S13.   Chen J, Jiang C, Wang S. LDK378: a promising anaplastic lymphoma kinase (ALK) inhibitor. J Med Chem 2013;56:5673-4.

S14.   Prahallad A, Sun C, Huang S, Di Nicolantonio F, Salazar R, Zecchin D, et al. Unresponsiveness of colon cancer to BRAF(V600E) inhibition through feedback activation of EGFR. Nature 2012;483:100-3.

S15.   Wilson TR, Fridlyand J, Yan Y, Penuel E, Burton L, Chan E, et al. Widespread potential for growth-factor-driven resistance to anticancer kinase inhibitors. Nature 2012;487:505-9.

S16.   Zhang Z, Lee JC, Lin L, Olivas V, Au V, LaFramboise T, et al. Activation of the AXL kinase causes resistance to EGFR–targeted therapy in lung cancer. Nat Genet 2012;44:852–60.

S17.   Zhang F, Cheong JK. The renewed battle against RAS-mutant cancers. Cell Mol Life Sci 2016;73:1845-58.

S18.   Lito P, Solomon M, Li LS, Hansen R, Rosen N. Allele-specific inhibitors inactivate mutant KRAS G12C by a trapping mechanism. Science 2016;351:604-8.

S19.   Ostrem JM, Peters U, Sos ML, Wells JA, Shokat KM. K-Ras(G12C) inhibitors allosterically control GTP affinity and effector interactions. Nature 2013;503:548–51.

S20.   Winter–Vann AM, Baron RA, Wong W, dela Cruz J, York JD, Gooden DM, et al. A small–molecule inhibitor of isoprenylcysteine carboxyl methyltransferase with antitumor activity in cancer cells. Proc Natl Acad Sci U S A 2005;102:4336–41

S21.   Wang M, Hossain MS, Tan W, Coolman B, Zhou J, Liu S, et al. Inhibition of isoprenylcysteine carboxylmethyltransferase induces autophagic–dependent apoptosis and impairs tumor growth. Oncogene 2010;29:4959–70.

S22.   Weisz B, Giehl K, Gana-Weisz M, Egozi Y, Ben-Baruch G, Marciano D, et al. A new functional Ras antagonist inhibits human pancreatic tumor growth in nude mice. Oncogene 1999;18:2579-88.

S23.   Zimmermann G, Papke B, Ismail S, Vartak N, Chandra A, Hoffmann M, et al. Small molecule inhibition of the KRAS-PDEδ interaction impairs oncogenic KRAS signalling. Nature 2013;497:638–42.

S24.   Shaw AT, Winslow MM, Magendantz M, Ouyang C, Dowdle J, Subramanian A, et al. Selective killing of K-ras mutant cancer cells by small molecule inducers of oxidative stress. Proc Natl Acad Sci U S A 2011;108:8773-8.

S25.   Papke B, Murarka S, Vogel HA, Martín-Gago P, Kovacevic M, Truxius DC, et al. Identification of pyrazolopyridazinones as PDEδ inhibitors. Nat Commun 2016;7:11360.

13.   Personal information

13.1   Publications

Dissertation

Arendt Kristina Anna Maria (KAM), 2019. An in vivo inflammatory loop potentiates

KRAS blockade. Helmholtz Center and Medical Faculty LMU Munich

First author publication

Arendt KAM, Ntaliarda G, Armenis V, Kati D, Henning C, Giotopoulou GA, Pepe MA, Klotz

LV, Lamort AS, Hatz RA, Kobold S, Stathopoulos GT. An in vivo inflammatory loop potentiates

KRAS blockade. 2019, under review, *

Co-author publications

Spella M, Lilis I, Pepe MA, Chen Y, Armaka M, Lamort AS, Zazara DE, Roumelioti F, Vreka M, Kanellakis NI, Wagner DE, Giannou AD, Armenis V, **Arendt KAM**, Klotz LV, Toumpanakis D, Karavana V, Zakynthinos SG, Giopanou I, Marazioti A, Aidinis V, Sotillo R, Stathopoulos GT. *Club cells form lung adenocarcinomas and maintain the alveoli of adult mice.* Elife. 2019 May 29;8.

Klotz LV, Courty Y, Lindner M, Petit-Courty A, Stowasser A, Koch I, Eichhorn ME, Lilis I, Morresi-Hauf A, **Arendt KAM**, Pepe M, Giopanou I, Ntaliarda G, Behrend SJ, Oplopoiou M, Gissot V, Guyetant S, Marchand-Adam S, Behr J, Kaiser JC, Hatz RA, Lamort AS, Stathopoulos GT. *Comprehensive clinical profiling of the Gauting locoregional lung adenocarcinoma donors.* Cancer Med. 2019 Apr;8(4):1486-1499.

Kanellakis NI, Giannou AD, Pepe MA, Agalioti T, Zazara DE, Giopanou I, Psallidas I, Spella M, Marazioti A, **Arendt KAM**, Lamort AS, Tsaniras SC, Taraviras S, Papadaki H, Lilis I, Stathopoulos GT. *Tobacco chemical-induced mouse lung adenocarcinoma cell*

lines pin the prolactin orthologue proliferin as a lung tumour promoter. Carcinogenesis. 2019 Mar 4. pii: bgz047.

Voigt C1, May P, Gottschlich A, Markota A, Wenk D, Gerlach I, Voigt S, Stathopoulos GT, **Arendt KAM**, Heise C, Rataj F, Janssen KP, Königshoff M, Winter H, Himsl I, Thasler WE, Schnurr M, Rothenfußer S, Endres S, Kobold S. *Cancer cells induce interleukin-22 production from memory CD4+ T cells via interleukin-1 to promote tumor growth.* Proc Natl Acad Sci U S A. 2017 Dec 5;114(49):12994-12999.

Reviews

Giopanou I, **Arendt KAM**, Stathopoulos GT. *Lung carcinogenesis and fibrosis taken together: just co-incidence?* Curr Opin Pulm Med. 2017 Jul;23(4):290-297.

Spella M, Marazioti A, **Arendt KAM**, Stathopoulos GT. *RAS oncogenes direct metastasis.* Mol Cell Oncol. 2017 Jul 5;4(5): e1345711.

* publication for dissertation

13.2   Conferences

09/2019   World Conference on Lung Cancer (**WCLC**), Barcelona, Spain.

09/2018   European Association of Cancer Research (**EACR**) Conference, Berlin, Germany.

03/2018   Lung Science Conference of European Respiratory Society (**ERS**), Estoril, Portugal.

02/2018   Deutsches Zentrum Lungenforschung (**DZL**) Annual Meeting, Bad Nauheim, Germany.

11/2017   **DZL** Lung Cancer Retreat, Bad Nauheim, Germany.

11/2016   **DZL** Lung Cancer Retreat, Heidelberg, Germany.

14. Acknowledgement

I started in an empty lab, but with great people on my side, who gave me support and confidence. We overcame many boundaries and this thesis is proof that we made it work. I learned many lessons on this way, about work, life, people, and of course science. My supervisor was very supportive during this time and without him I would have not made it this far. Thanks to my wonderful colleagues Laura Klotz, Malamati Vreka, Laura Mattner, Salome Rehm, Aditi Mehta, Stephanie Weiß, Jessica Götzfried, Larissa Mößmer, Max Strunz, Sabine Behrend, Georgia Giotopoulou, Caroline Hackl and many more. They made the time at the CPC very special. Thanks to the Greek research group in Patras who supported the project and me from far away. I also want to thank Doreen Franke and Claudia Staab-Weijnitz for their mental support during the rollercoaster called PhD life. A special thanks to my TAC members, who gave their critical input and their time to improve and evaluate this PhD project.